UNIVERSITÀ DEGLI STUDI DI PALERMO

Dottorato in Energia e Tecnologie dell'Informazione
Dipartimento di Energia, Ingegneria dell'Informazione e Modelli Matematici (DEIM)
Settore Scientifico Disciplinare: ING-INF/01

THE SILICON PHOTOMULTIPLIER:
A PROMISING PHOTODETECTOR FOR BIOSENSING APPLICATIONS

<div style="display:flex">

LA DOTTORESSA
Maria Francesca Santangelo

IL COORDINATORE
Ch.ma Prof.sa Maria Stella Mongiovì

</div>

IL TUTOR
Ch.mo Prof. Alessandro Busacca

CO TUTOR
Dott.sa Sebania Libertino

CICLO XXIX
ANNO 2017

"If a man will begin with certainties, he shall end in doubts; but if he will be content to begin with doubts, he shall end in certainties."

Francis Bacon

UNIVERSITY OF PALERMO

Abstract

PhD Course in Energy ant Information Technologies

Department of Energy, Information engineering and Mathematical models (DEIM)

Doctor of Philosophy

The Silicon Photomultiplier: A promising photodetector for biosensing applications

by Maria Francesca Santangelo

The Silicon Photomultiplier (SiPM) is a solid state photodetector based on an array of single photon avalanche diodes (SPAD) connected in series with an individual quenching resistor. It is biased above the breakdown voltage (BV), that is, each pixel is operated in Geiger mode. SiPMs are an emerging technology, with promising applications in the field of sensors for their unique properties: high quantum efficiency, low operating voltage, high speed, high gain, insensitivity to magnetic fields and single photon sensitivity. Due to its high sensitivity and speed, such device may be used in low level light detection, e.g. in biochemical and biotechnological analysis where the goal is to minimize the analyte concentration.

The importance of biosensors is currently growing exponentially and is driving the scientific community to generate versatile platforms, which can be used for a variety of applications and which can be mass-produced at low cost. Silicon-based devices, compatible with CMOS (Complementary Metal Oxide Semiconductor) technology, are still among the best candidates to fulfil all requirements for large market opportunities. The possibility of fabricating sensors directly in Si facilitates miniaturisation and low cost (for large volumes), thanks to the well-established semiconductor industry. This enables the fabrication of lightweight devices which are both small and can operate with very low volumes of sample (DNA, proteins, etc.). Moreover, interfacing the sensor to complex circuits is simplified due to the common base materials used. All these characteristics make Si-based biosensors the best candidate for consumer technology. The design of a sensor includes two fundamental elements: the transductor and the sensitive element, and both depend on the type of measurement to be made. The sensing molecules (biological) must be immobilised in the sensing system, without altering their biochemical properties and without damaging the inorganic board or electronic component. Among the different fields of biosensor applications, the biomedical sector attracts a special attention due to the countless needs to measure disease-related parameters, especially in aggressive diseases and to monitor the parameters associated with the maintenance of health.

The reasons that drive the research to develop embedded and portable systems for biomedical applications are manifold. Firstly, the strong requirement of medical tools able to monitor vital signs or diagnostic markers in portable Point-of-Care (PoC) format have encouraged to develop solution for miniaturized systems at low cost, easy to use in order to allow patient self-monitoring. Among the diagnostic tools, if genetic analyses are required, DNA microarray and the Real Time- Polymerase Chain Reaction (PCR) are suggested, but they can be performed only by highly specialized laboratories. The first technique is a biological method to measure the expression level of a large number of genes simultaneously. The second is used in molecular biology to amplify and simultaneously detect or quantify a targeted DNA sequence. These analyses require large equipment and laborious protocols. The presence on the market of low cost and easy to use systems would enable genetic screening on the entire population.

Optical transduction is certainly the most used detection method in biomedical field and, usually, it is used to detect the fluorescence emitted by specific fluorescent molecules, called markers, used to label fragments of DNA in DNA microarray and Real Time PCR applications. However, this method allows detecting the bioluminescence emitted by living organisms. Bioluminescence is the result of chemical processes, where the energy produced is released as visible light. Common applications of bioluminescence detection include in vivo studies of infection (with bioluminescent pathogens), cancer progression (using a bioluminescent cancer cell line), and reconstitution kinetics (using bioluminescent stem cells). This technology allows to the researchers to improve cancer investigation in several systems such as blood, brain, breast, fibrosarcoma, melanoma, pancreatic, prostate, colorectal.

The main purpose of this thesis is to develop compact systems for DNA analysis (DNA microarray and Real Time PCR) and to measure the bioluminescence emitted by adenosine triphosphate (ATP, the key element for intracellular energy transfer) and genetic reporter (e.g. luciferase bioluminescent) for studying gene expression and cellular events, coupled to gene expression.

In this Thesis, I performed an electrical and optical analysis of a novel class of SiPMs in the CW regime.

Chapter 1 describes the operating principle of SiPM and its most important characteristics. Moreover, a brief comparison between traditional photomultipliers and SiPM is reported.

In **Chapter 2** more details about the SiPM used in this work and its electric-optical characterization are reported. Moreover, two different experimental setup for Lifetime and Photon counting measurements are described.

After the brief introduction about SiPM history, some biosensor applications studied in this thesis are discussed. In particular, in **Chapter 3**, SiPM application to DNA microarray technology is described. I present results of DNA fragments characterization and discuss the great potentialities of a DNA microarray system based on SiPM technology.

Chapter 4 introduces the SiPM application to Real Time PCR technology. I present the results obtained by using two different fluorophores, fully characterized and I show the ability of SiPM to

detect very weak signals carried out by the excitation of small concentration of analyte in the sample.

In **Chapter 5**, a brief introduction of bioluminescence is presented. This approach is widely used for several biosensing applications, where ATP and luciferase bioluminescence are measured. I present the results obtained and discuss the potentialities of a system based on SiPM technology as a miniaturized, cost-effective approach for detecting bioluminescence to study gene expression of cancer cells.

The results of this work show a new approach to investigate the SiPM capabilities, the CW regime, demonstrating its outstanding performances and showing its use in innovative biosensing applications.

This work was carried out in collaboration with the researchers of the "Sensor Lab" of CNR IMM Headquarters and has been partially funded by the National Project MIUR-PON "Hyppocrates– Sviluppo di Micro e Nano-Tecnologie e Sistemi Avanzati per la Salute dell'uomo" (PON02 00355).

Part of the experiments were performed within the Biosensors and Bioelectronics laboratory of the Linköping Univestity in Sweden, under the supervision of Professors M.W.C. Mak and A.P.F. Turner.

Acknowledgements

This work would have not been possible without the support of all the people, which has been close to me and has supported me over these years, and for this reason, I want to thank them.

First, I want to thank my family that always accepted and supported my choices, always encouraging me to keep going. My family has always been close to me, especially in the months spent away from Italy to enrich this scientific research work. For all these reasons, I will never stop thanking and I dedicate this work to them.

I would like to express my deepest gratitude to my tutor Prof. Alessandro C. Busacca, mentor not only professional, but also human, who provided me not only educational concepts, but also the right determination and enthusiasm for the research work. I always thank him for conveying to me the passion for research and for believing in me always, from day one, providing me trust in myself and encouraged me to do even more.
In addition to the Prof. Busacca, I would like to thank all Laboratory of Optics and OptoelectroniX (LOOX) research team. In particular, my gratitude is directed to Doctors Salvatore Stivala, Riccardo Pernice e Gabriele Adamo, which with their friendship have always been close to me and helped me to overcome all the difficulties encountered in recent years.

Deep gratitude is also directed to my co-tutor Dr. Sebania Libertino, professional and personal mentor, friend, who with her patience, her availability and her skills has provided me the resources needed to carry out this work in the best way. She has always believed in me and has encouraged me to do even more making me grow both scientifically and personally. Moreover, she gave me the opportunity to carry out one of the best times of my career in one of the most important research centers involved in the research field of biosensors, i.e. the *"Biosensors and Bioelectronics Centre"*, at the Department of Physics, Chemistry and Biology (IFM) of Linköping University (Sweden). I will never forget what she did and she is still doing for me.
In addition to Dr Libertino, I would like to thank all people of CNR IMM headquarters who helped and supported me over these years. In particular, I enjoyed working with Emanuele L. Sciuto and I am grateful to him for his friendship and enjoyable technical discussions. I also thank Dr. Salvatore Lombardo, Dr. Roberto Pagano, Domenico Corso and Aldo Spada, for their availability and for having contributed with their skills and with their experience, to the realization of this work. My gratitude goes to all the CNR people, not only for their scientific support, but also for their friendship.

I would like to thank all people of STMicroelectronics' Catania site who helped me over these years. In particular, Dr. P.G. Fallica, team manager of R&D Sensor Device team, who provided me optical sensors used in this work. I enjoyed working with Sabrina Conoci, Maria Eloisa Castagna, Salvatore Abbisso and Salvatore Petralia and I am grateful to them for their friendship and for their help in this

work.

Deep gratitude is also directed to Prof. Anthony P.F. Turner of Linköping University for having given me the opportunity to carry out research in the center of which he is director. It was an honor for me to be part of the Biosensors and Bioelectronics Team even if for a short period. I would like to thank all team's staff, but in particular, Dr. Martin W.C. Mak, who has personally followed my research and that from the first day, left me feeling at home. Moreover, with his sympathy and willingness he has gladdened my stay in Linköping organizing party and small tourist tours.

Special thanks are addressed to Prof. Daniel Filippini of the Chemical and Optical Sensor Systems Team. I enjoyed working with him and I am grateful to him since he showed maximum availability towards me from the very first day, putting at my disposal his expertise and his equipment. Moreover, he helped me in the research activity carried out.

At last, I want thank my friends, who with their sympathy, their availability and their sensitivity were able to support me in difficult times and have rendered less difficult my path. A particular thank is directed to Oriana, Nadia and Filippa, more than friends, three real sisters, who in these years have been able to support me and help me when it was necessary, close despite the physical distance between us. Moreover, I cannot forget, Monica and Donatella, who were close to me and with their sympathy and their willingness have gladdened my days.

Since I probably have forgotten to thank someone, then I thanks to all people who I never felt alone and I enjoyed a lot these three years.

Ringraziamenti

La realizzazione di questo lavoro non sarebbe stata possibile senza il supporto di tutte quelle persone che in tutti questi anni mi sono state vicine e mi hanno aiutato, e per questa ragione le voglio ringraziare.

Innanzitutto voglio ringraziare la mia famiglia, che ha sempre accettato e supportato le mie scelte, incoraggiandomi sempre ad andare avanti. Mi è sempre stata vicina, soprattutto nei mesi trascorsi lontani dall'Italia con l'obiettivo di arricchire il mio bagaglio culturale e allo stesso tempo trasferire un valore aggiunto a questo lavoro di ricerca scientifica. Per tutte queste ragioni non smetterò mai di ringraziarli ed è a loro che tale lavoro è dedicato.

Voglio esprime la mia più profonda gratitudine al mio tutor, Prof. Alessandro C. Busacca, guida non soltanto professionale, ma anche umana, che mi ha trasferito non soltanto nozioni didattiche, ma anche la giusta determinazione e l'entusiasmo verso la ricerca. Lo voglio ringraziare per aver sempre creduto in me, sin dal primo giorno, fornendomi così fiducia in me stessa ed incoraggiandomi a fare sempre di più.

Oltre al Prof. Busacca, voglio anche ringraziare tutto il team del laboratorio di Ottica ed Optoelettronica (Laboratory of Optics and OptoelectroniX - LOOX). Voglio ringraziare in particolare il Dr. Salvatore Stivala, il Dr. Riccardo Pernice e il Dr. Gabriele Adamo, che con la loro amicizia mi sono stati sempre vicini e mi hanno aiutato a superare tutte le difficoltà incontrate in questi anni.

Profonda gratitudine è anche rivolta al mio co-tutor Dr. Sebania Libertino, guida professionale ed umana, amica, che con la sua pazienza, la sua disponibilità e le sue competenze mi ha fornito tutte le risorse necessarie per realizzare questo lavoro nel migliore dei modi. Ha sempre creduto in me incoraggiandomi a fare sempre di più, facendomi così crescere sia a livello professionale sia umano. Inoltre, mi ha dato l'opportunità di vivere uno dei più bei momenti della mia carriera professionale dandomi la possibilità di trascorrere un periodo come *visiting research* in uno dei più importanti centri di ricerca nel campo della biosensoristica, *Biosensors and Bioelectronics Centre* presso il Dipartimento di Fisica, Chimica e Biologia dell'Università di Linkoping (Svezia). Non dimenticherò mai tutto quello che ha fatto e che continua a fare per me, e per questo non la ringrazierò mai abbastanza.

Oltre alla Dr. Sebania Libertino, voglio ringraziare tutta la gente del CNR IMM sede di Catania che mi ha aiutata e supportata anche attraverso l'amicizia che ognuno di loro mi ha offerto in tutti questi anni. In particolare è stato un piacere per me lavorare con Emanuele L. Sciuto e gli sono grata per la sua amicizia e per il modo in cui abbiamo affrontato questo lavoro di ricerca in questi anni insieme. Voglio anche ringraziare il Dr. Salvatore Lombardo, il Dr. Roberto Pagano, Domenico Corso e Aldo Spada per la loro disponibilità e per aver contribuito con le loro competenze e la loro esperienza alla realizzazione di questo lavoro.

Voglio ringraziare anche tutta la gente del sito di Catania dell'STMicroelectronic che mi ha aiutata in questi anni. In particolare il Dr. P.G. Fallica, team manager del gruppo *Sensor Device* dell'R&D, che mi ha fornito i sensori usati in questo lavoro. E' stato un piacere lavorare con Sabrina Conoci, Maria Eloisa Castagna, Salvatore Abbisso e Salvatore Petralia e sono grata a tutti loro per la loro amicizia e per l'aiuto in questo lavoro.

Profonda gratitudine è anche rivolta al Prof. Anthony P.F. Turner dell'Università di Linköping per avermi dato la possibilità di condurre parte della mia attività di ricerca nel centro di cui lui è direttore. E' stato un onore per me far parte del suo staff, anche se solo per un breve periodo. Voglio ringraziare tutti i membri del suo staff, ma in particolare il Dr. Martin W.C. Mak che mi ha personalmente seguito la mia attività di ricerca e che, sin dal primo giorno, mi ha fatto sentire a casa.
Con la sua simpatia e la sua disponibilità ha allietato la mia permanenza a Linköping organizzando serate e piccoli tour turistici.
Un ringraziamento speciale è rivolto al Prof. Daniel Filippini del *Chemical and Optical Sensor Systems Team*, sempre dell'Università di Linköping. E' stato un piacere lavorare con lui e gli sono grata poiché sin dal primo giorno ha mostrato massima disponibilità nei miei confronti, mettendo a mia disposizione le sue competenze e le attrezzature presenti nel suo laboratorio. Inoltre, mi ha molto aiutato nell'attività di ricerca svolta lì e per questo ci tengo a ringraziarlo.

Infine voglio ringraziare i miei amici che, con la loro simpatia, la loro disponibilità e la loro sensibilità sono stati in grado di supportarmi nei periodi difficili rendendo meno duro il mio percorso. Un ringraziamento particolare è rivolto ad Oriana, Nadia e Filippa, più che amiche, tre vere e proprie sorelle, che in questi anni mi hanno aiutato e supportato quando necessario, vicine anche se fisicamente distanti. Inoltre non posso dimenticare Monica e Donatella, che con la loro amicizia, mi sono state vicine e con la loro simpatia hanno allietato i miei giorni.

Poiché sicuramente ho dimenticato di ringraziare qualcuno, voglio ringraziare tutti coloro che non mi hanno mai fatto sentire sola e mi hanno fatto divertire in questi tre anni.

Contents

List of Figures

List of Tables

Chapter 1

The Silicon Photomultiplier: principles and features

1.1   The origins

The photoelectric effect was discovered in 1887 by Hertz [1] by exposing a negative electrode to ultraviolet radiation. In the next year, 1888, the photoelectric effect was conclusively confirmed by Hallwachs [2]. In 1889, Elster and Geitel [3] reported the photoelectric effect, which was induced by visible light striking an alkali metal (sodium-potassium). Since then, many scientists have made a variety of experiments and discussions on photoemission. As a result, the concept proposed by Einstein (in the quantum theory in 1905) [4], "On a Heuristic Viewpoint Concerning the production and Transformation of Light", has been proven and accepted.

During this historic period of achievement, Elster and Geitel produced a photoelectric tube in 1913.

Photomultiplier tubes had a rapid progress since the development of photocathodes. More than 20 years passed until the first photomultiplier tube (PMT) was invented and became a commercial product in 1936 [5]. Single photons were detectable since then.

Light detection technology is a powerful tool that provides a deeper understanding of a variety of phenomena. Measurements using light offer unique advantages: non-destructive analysis of a substance, high-speed and extremely high detectability. Advanced fields such as scientific measurement, medical diagnosis and treatment, high-energy physics, spectroscopy and biotechnology require the development of photodetectors that exhibit the ultimate limit in various performance parameters. In many of these applications, the PMT has become the detector of choice. However, PMTs have different strong handicaps: they are very sensitive to magnetic fields, their bias voltages are high (hundreds of Volts), their price is high because of the complex mechanical structure inside the vacuum container is mostly handmade [6]. This forced research toward the finding of an alternative to PMT [7].

A promising candidate for low light detection was PIN photodiode, formed by three following regions: p-doped, intrinsic and n- doped silicon. However, the device has no internal gain; the noise is at the level of several hundred electrons and, consequently, the smallest detectable light flash needs to consist of even more photons [8].

Many of discussed problems are overcame by Avalanche Photodiodes (APDs). They show an internal gain which improves the signal-to-noise ratio with respect to PIN, but still around 20 photons are needed for a detectable light pulse. The excess noise factor, being connected to the fluctuation of the avalanche multiplication, limits the useful range of the gain [9].

The APD can also be biased at a voltage larger than the breakdown voltage resulting in an infinity gain operation. An external load of high value limits the maximum current to a safe mode. This working regime is named Geiger Mode and the devices operating in it are Single-Photon Avalanche Diodes (SPADs). This paved the way to the realization of the Silicon PhotoMultiplier (SiPM): a structure based on a planar pixel array of SPADs able to detect single photons like a PMT [9].

1.2 The SPAD

A SPAD is a solid-state photodetector in which a photo-generated carrier can trigger an avalanche current due to the impact ionization mechanism. This device is able to detect low intensity signals (down to the single photon) and to discern the arrival times of the photons with a jitter of a few tens of picoseconds. SPADs, like APDs, exploit the photon-triggered avalanche current of a reverse biased p-n junction to detect an incident radiation. The fundamental difference between SPADs and APDs is that SPADs are specifically designed to operate with a reverse-bias voltage well above the breakdown (BV, V_B). This kind of operation is also called Geiger mode in literature, in analogy with the Geiger counter [10]. SPADs are semiconductor devices based on a p-n junction reverse-biased at a voltage V_A that exceeds breakdown voltage, V_B, of the junction (Figure 1.1).
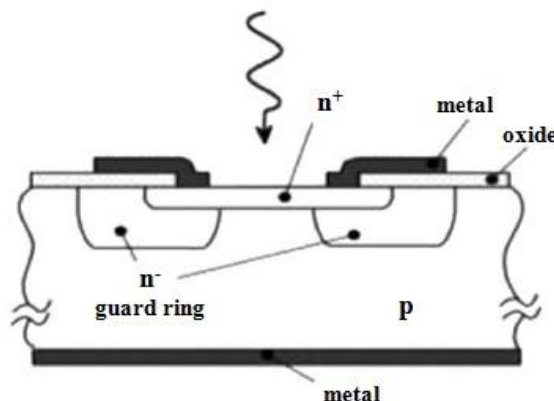
Figure 1.1: Planar n+-p junction operating in Geiger mode developed at the Shockley laboratory, by Haitz [9].

At this bias, the electric field is so high that a single charge carrier injected into the depletion layer can trigger a self-sustaining avalanche. Furthermore, this ensures that the internal gain of the device is high

(approximately 10^6). Consequently, the current rises swiftly (sub-nanosecond rise-time) to a macroscopic steady level in the milliampere range. These features make the SPAD preferable to APD in linear region.

In reverse biased photodiodes, the electric field increases with the applied voltage, causing the increase of both the drift velocity and the kinetic energy of charge carriers injected in the depletion region. An electron (or hole) with enough kinetic energy can break a bond when collides with lattice atoms thus creating an electron-hole pair. However, the carrier loses part of its energy in this process of impact ionization.

Both the original carrier and the secondary electron and hole will be accelerated by the electric field and possibly contribute to the generation of more electron-hole pairs, resulting in a positive feedback loop (avalanche) which gradually increases the overall number of carriers.

The magnitude of the avalanche phenomenon depends on two concurrent factors: the carrier ionization rates and the rate at which electrons and holes leave the high-field region and are collected at the device electrodes. Ionization rates strongly increase with the electric field [11].

Although silicon electrons have a higher ionization rate than holes, an electric field value of about 3×10^5 V /cm is required, on average, to create one electron-hole pair per 1 μm travelled.

For bias voltages beyond the breakdown voltage, ionization rates are very high and the carrier concentration and output current increase to very high values. This is the case of SPADs, whose gain reaches values above 10^6 [12; 13]. When a SPAD is biased beyond the breakdown voltage, the lower electric field is not able any more to accelerate the carriers to impact-ionize with lattice atoms. Therefore, the current ceases and the device will stay in an OFF state for a short time, until a carrier (electron or hole) will trigger an avalanche event bringing the device into its ON state.

In order to be able to detect another photon, the bias voltage must be raised again above breakdown. These operations require a suitable circuit, which has to:

- ✓ sense the leading edge of the avalanche current;
- ✓ generate a standard output pulse synchronous with the avalanche build-up;
- ✓ quench the avalanche by lowering the bias down to the breakdown voltage;
- ✓ restore the photodiode to the operative level.

This circuit is usually referred to as a quenching circuit.

In other words, the device operates in a binary mode and the need for quenching/recharging introduces a dead time between two consecutive events. The simplest way to quench the avalanche is by means of a high ohmic resistor in series with the SPAD, so that the voltage drop, caused by the avalanche current, lowers the SPAD bias down to the breakdown point.

1.3 The Silicon Photomultiplier

The Silicon Photomultiplier or SiPM was born from a patent of Z. Sadygov in 1996 [14] and it is currently under study and development to a growing demand for nuclear medicine, especially for positron emission tomography (PET) and diagnostic techniques used for the detection of tumours.

SiPM is a semiconductor photodetector operating in limited Geiger mode. Its structure is based on a pixel array of SPAD, which individually act as photon counters. A photon counting diode cannot distinguish between multiple photons incident on the detector at the same time [15]. The SiPM overcomes this limitation since each SPAD is connected to the power supply through an integrated large series-quenching resistor R_L. Being the outputs of the pixels connected together, the total device behaves like a proportional device for photon fluxes (analog behaviour), while each pixel, thanks to the individual integrated quenching resistors, works as an independent photon counter, i.e. as a binary device (digital behaviour) [16]. The analog behaviour and the electronic schematic of SiPM are reported in Figure 1.2.
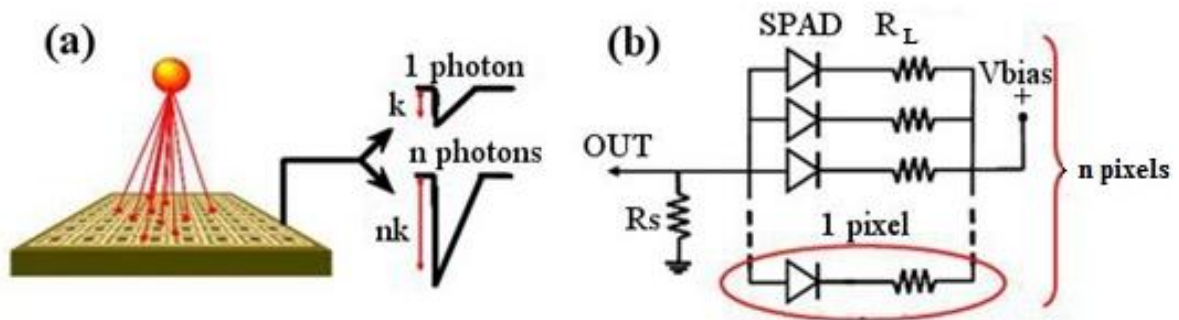
Figure 1.2: Operating principle (a) and equivalent electronic schematic (b) of SiPM.

The single pair generation, hence single photon detection, gives rise to an avalanche (high currents flowing in through the device) with an amplification factor around 10^6. The voltage drops across the resistor, leading the voltage across the junction of the device below the breakdown threshold. The current flowing in the photodiode at shutdown (latching current) is provided by a number of carriers so low that it is statistically unlike that they could trigger a new event of avalanche. The voltage across the junction returns to the overvoltage value imposed by external biasing circuit with a time constant of 50 ns (depending from the sensing resistor employed). The presence of a quenching resistor for each individual pixel of the array ensures a decoupling of the operation of each photodiode from all other devices of the matrix. In fact, each resistor switches off only the event of avalanche in the photodiode connected to it, while all other pixels continue to be biased to the overvoltage value imposed by the external bias circuit, as long as a couple of carriers photo generated or thermally generated will trigger an avalanche. The device output current is read on a resistor (R_s) common to all the pixels, whose value is between a few dozen and a few hundred of ohms, (see Figure 1.2). The voltage drop at this resistor terminal is proportional to the product between the number of pixels turned on and the current produced by each avalanche event (analog operation).

1.4 Main properties of SiPM

1.4.1 Photon Detection Efficiency(PDE)

The Photon Detection Efficiency (*PDE*) of a SiPM is the statistical probability that a photon impinging on the sensor surface is detected. It is a function of the wavelength and of the bias voltage and it is defined as the product of three components:

$$PDE\ (\lambda, V\ ) \ = \ QE\ (\lambda) \ \cdot \ P_t\ (V\ ) \ \cdot \ \varepsilon_{GEO} \tag{1.1}$$

where *QE* is the quantum efficiency of the photosensitive area; P_t is the triggering probability i.e. the probability that a photo-generated carrier has to trigger an avalanche breakdown; ε_{GEO} is the geometric fill factor of the device, i.e. the ratio of the photo-sensitive area to the total area of the sensor.

The quantum efficiency of the photosensitive area represents the probability for a photon, impinging on the active surface of the detector, to generate an electron-hole pair in the active thickness of the device that could trigger an avalanche breakdown. Some of the incident photons are not absorbed because of the probabilistic nature of the absorption process or because reflected at the surface of the detector. Furthermore, some electron-hole pairs produced near to the surface of the detector could quickly recombine due to the abundance of recombination centres close by and are, therefore, unable to trigger a breakdown. The quantum efficiency, can be expressed as:

$$QE\ = \ (1-\ R)\mathrm{e}^{-\alpha w}\ (1-\mathrm{e}^{-\alpha W}\ ) \tag{1.2}$$

where *R* is the optical power reflectance at the surface, α is the silicon absorption coefficient (cm^{-1}), *w* is the depth from the Si/SiO$_2$ interface of the depleted region (cm) and *W* is the width of the depleted region (cm). The first term of Equation 1.2, *(1-R)*, represents the effect of the reflection at the device surface; the second term, instead, $e^{-\alpha w}(1-e^{-\alpha W})$, represents the fraction of photon absorbed in the depleted region of the device.

The triggering probability is the probability that an electron-hole pair in the depletion region triggers a self-sustaining avalanche. It depends on the position where the primary electron-hole pair is generated and on the overvoltage. In a high-field region, the two carriers, an electron and a hole, travel in the opposite directions and contribute together to the overall triggering probability that can be calculated from the following relation [17]:

$$P_t = P_e + P_h - P_e \cdot P_h \tag{1.3}$$

where P_e and P_h are the electron and hole initiation probability, respectively.

Finally, the geometrical fill factor is the ratio of the active to the total area of the device. Since the silicon photomultiplier is a pixelated sensor, some space between the cells is required for the separation, for the individual quenching resistor, for metallization (it connects all the pixels to the same electrode) and to fabricate the optical trenches that provide the optical isolation between the

cells. The geometrical fill factor, ε_{GEO}, of a silicon photomultiplier is defined as the ratio of the photo-sensitive area (A_S) to the total area (A_{TOT}) of the device:

$$\varepsilon_{GEO} = \frac{A_S}{A_{TOT}} \tag{1.4}$$

However, SiPM with smaller pixel area has a smaller fill factor; therefore, the best filling (and obviously the best PDE) can be obtained with a small number of large cells. Unfortunately, a SiPM with few large cells has a reduced linear dynamic compared to a SiPM with the same total area but with a larger number of small cells. Moreover, a big cell has a greater dark noise than a smaller one, since the dark noise is proportional to the depleted volume of the cell.

The optimization of the fill factor, ε_{GEO}, of a SiPM is a compromise between the maximization of the PDE and the other performances required for the specific application.

1.4.2   Gain

The Gain of a SiPM is defined as the number of electron-hole pairs generated in the depletion layer of the device during an avalanche event. It is a function of the overvoltage (OV) applied to the device and of the temperature. The gain of the SiPM is defined as the ratio of the output charge Q_{TOT} produced by n_{ph} detected photons to the charge of an electron q:

$$G = \frac{Q_{TOT}}{n_{ph} \cdot q} \tag{1.5}$$

Considering the equivalent circuit of a single pixel reported in Figure 1.3 and assuming that one photon produces the avalanche of one pixel, the gain is (9):

$$G = \frac{Q_{pix}}{q} = \int \frac{I_L}{q} dt \approx C_D \cdot \frac{(V_{BIAS} - V_{BD})}{q} \tag{1.6}$$

where C_D is the diode capacitance and V_{BIAS}-V_{BD} is the applied overvoltage. Since C_D is typically in the range of 10÷100 fF and V_{BIAS}-V_{BD} is in the range of a few volts, a high gain, typically in the range of $10^5 \div 10^7$, is obtained.
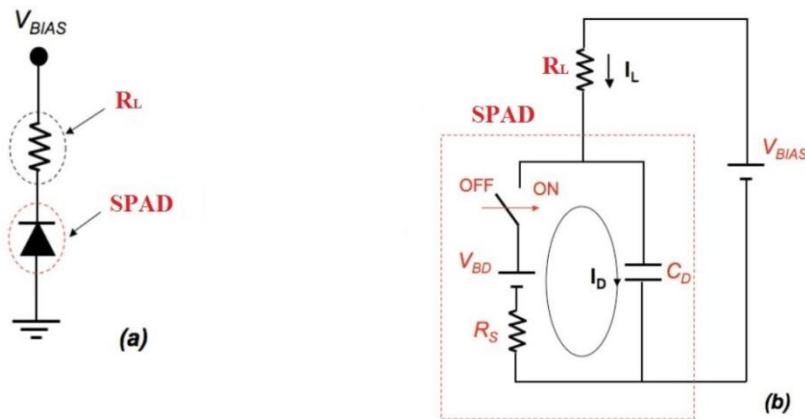
Figure 1.3: (a) Schematic representation of the SiPM single pixel. (b) Equivalent circuit of the SiPM single pixel.

1.4.3   Dark Count

One of the main factors limiting the performances and sizes of the silicon photomultiplier is the dark count (DC) of the signals with amplitude equivalent of single photon signal, initiated by the thermal electron-hole pair created in the device sensitive area. The thermally generated carriers in the depleted area could also initiate an avalanche breakdown and result in a current pulse that is indistinguishable from the one produced by the detection of a single photon.

Therefore, when a free carrier generated inside, or near, the depleted region, even in dark condition, triggers an avalanche breakdown in a SiPM, it produces a pulse that represents the intrinsic noise of the silicon photomultiplier. The frequency of such noise can be determined by counting the pulses occurring per second when the SiPM is in dark condition, and it is named Dark Counts (DC) of the SiPM. Dark count is mainly due to e-h pairs generated thermally and through generation–recombination (G–R) centres that are local levels at about mid-gap.

1.4.4   Afterpulsing

When the avalanche event takes place, a high quantity of charge crosses the region of space charge; energy traps can capture some carriers and release them after a certain time interval. If the electric field in the depletion region is high enough to trigger the avalanche, the released carrier can produce a delayed avalanche in the same pixel where breakdown occurred. This phenomenon is called afterpulsing and the probability of its occurrence depends on both the voltage and the temperature. Afterpulses can strongly enhance the total dark count rate of a SiPM. A simple strategy to reduce their contribution is to increase the recovery time of the pixels with a larger quenching resistance, in order to have enough time to depopulate the filled traps.

1.4.5   Cross-talk

The cross-talk is a noise common to all pixelated devices. The cross-talk noise has two different physical origins: optical and electrical. The optical one is due to the photons generation by radiative emission from the hot carriers produced during an avalanche discharge. In an avalanche breakdown there are in average 3 photons emitted per 10^5 carriers with a photon energy higher than 1.14 eV, the band gap of silicon [18]. When these photons travel to a neighbouring cell, they can trigger a breakdown there (Figure 1.6).
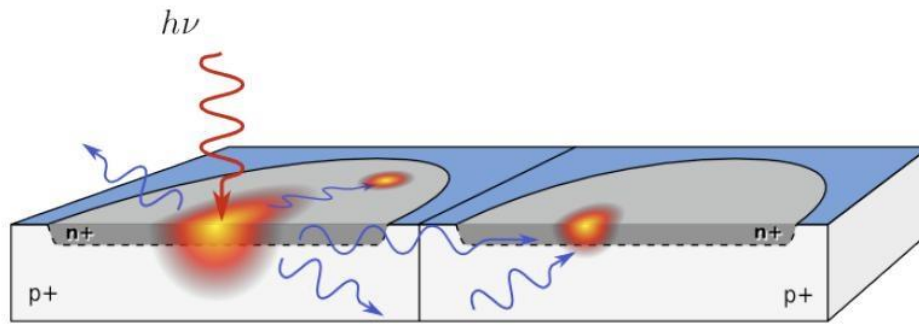
Figure 1.4: Schematic representation of the optical crosstalk between neighbouring pixels.

The corresponding output pulse current of the SiPM has, then, an amplitude peak proportional to the number of involved pixels in the single photo-detection and in the correlated cross-talk phenomena.

The electrical cross-talk can occur when carriers, generated during the avalanche breakdown in a cell, can cross the junction reaching a close pixel.

Travelling along the epitaxial layer, common to all pixels, these carriers can reach the neighbouring pixels and triggering there a new avalanche breakdown [19; 20]. There are two methods to reduce the optical and electrical cross-talk. The first is to increase the pitch, but it would decrease the fill factor; the second, is an excavation between a pixel and the neighbouring, called trenches, filled with oxide and / or metal so as to realize an optical-electrical isolation between the pixels.

1.4.6 Dynamic range

The dynamic range in a SiPM is defined as the maximum number of photons that can be detected simultaneously by the device. This characteristic is strongly limited by the finite number of pixels in a SiPM. In fact, as anticipated above, a pixel emits the same amount of charge even if it absorbs more than a photon at the same time. Furthermore, it should be observed that, during recharging (time during which, the voltage on the pixel gradually increases from the breakdown value to that of polarization), reveals photons with low efficiency, resulting in a lower charging signal compared to the standard. This worsens the resolution of the charge spectra. For these reasons, the SiPM works very well only when the number of incoming photons per pixel is unitary. If, however, this number is very high, the output signal from the device (i.e. the number of pixels turned on $N_{fired-pixel}$) saturates the pixel count of SiPM. The number of pixels simultaneously fired by the incoming photons depends on the total number of pixels of the detector according to the following expression [21]:

$$N_{fired-pixel} = n_{pix}\left(1 - e^{-\frac{n_{ph} \cdot PDE}{n_{pix}}}\right)$$

(1.7)

where $N_{fired-pixel}$ is the number of pixels that experience an avalanche breakdown, n_{pix} is the total number of pixels of the SiPM, *PDE* is the photon detection efficiency and n_{ph} is the number of

incoming photons. The SiPM response to a photons flux is linear for $n_{ph} \cdot PDE/ \, n_{pix} << 1$, i.e. if the average number of photon per one pixel is small enough.

1.4.7   *Recovery time*

The time of performance in silicon photomultipliers is defined by two parameters: the rising time of the avalanche breakdown signal and the recovery time, The last is defined by the time needed to the *pn*-junction to return to the initial state after the avalanche breakdown quenching and junction recharging through the quenching resistor processes. The recovery time is defined mainly by recharge process and could be estimated from values of RC, combination of the quenching resistor, diode capacitance and external circuit. Afterpulses can prolong the recovery time because the recharging starts anew. SiPMs need from one hundred of nanoseconds to hundreds of microseconds after a breakdown to achieve a second signal amplitude similar to the one of the first. Mostly the resistors used as quenching resistors are polysilicon made. They change their value with temperature; therefore, there is a strong dependence of the recovery time on the temperature [9].

1.5   SiPM, PiN, APD and PMT: a comparison

Low-light photon detectors constitute the enabling technology for a various and rapidly growing range of applications: nuclear medical imaging, radiation detection, fluorescence analysis, spectroscopy, quality control or meteorology. All these require detectors that serve to quantify and/or time stamp light signals with anywhere from one to ~1000 photons per event. The ideal detector provides a response proportional to the incident photon flux and incorporates an internal gain mechanism, yielding signals of sufficient magnitude to be easily processed. It should also offer sub nanosecond response times and broad spectral sensitivity, be robust, easy to operate and only generate manageable amounts of noise or dark count rates.

To date, the Photomultiplier tube (PMT) has been the detector of choice for such applications. A gain of 10^6 is achieved at the cost of a high bias voltage of 1-2kV, which requires the use of costly high-voltage power supplies and a bulky cooling system. PMTs are generally stable and low noise but are bulky and delicate due to their vacuum tube structure. They can also be adversely affected by magnetic fields which will limit their suitability for some applications.

Solid-state devices have many practical advantages over the PMT. As an example, the PIN diode is used in applications where PMTs were too bulky or delicate, or where high voltages were not possible. However, PIN diodes are severely limited by their complete lack of internal gain. The Avalanche Photodiode (APD) is a more recent technology, an extension of the simple PIN diode. The reverse bias is raised to a point where impact ionization allows for some internal multiplication, but is below the

breakdown bias where the Geiger mode would take over (see before). In this way, a gain of around a 100 is achieved for a bias of 100-200V.

Whilst the gain may be lower than that of a PMT, APDs have the advantage of a PDE, which can be > 65% and also a compact size, ruggedness and insensitivity to magnetic fields. Their main drawback is their excess noise (associated with the stochastic APD multiplication process).

The SiPM has high gain, very similar to the PMT, but has the physical benefits of compactness, ruggedness and magnetic insensitivity in common with the PIN and APD. In addition, the SiPM achieves its high gain (10^6) with very low bias voltages (~30V for SiPM produced by R&D of STMicroelectronics' Catania site) and the noise is almost entirely at the single photon level. The ability to measure a well resolved photoelectron spectrum is a feature which is generally not possible with PMTs due to the variability in the gain, or excess noise. Furthermore, solid-state technology owns the typical advantages of the planar integration process: SiPMs are manufactured at lower costs and with higher reproducibility with respect to PMTs [22]. In TABLE 1.1 the most relevant characteristics of the vacuum and semiconductor photodetectors already described are compared.

		PiN	APD	SiPM	PMT
PDE	**Blue**	60%	50%	30%	20%
	Green/yellow	80-90%	60-70%	50%	40%
	Red	90-100%	80%	40%	< 6%
Gain		1	100	10^6	10^6
Op. Bias		Low	High	Low	High
Temp. Sensitivity		Low	High	Low	Low
Shape characteristics		Robust, compact, mechanically rugged			Sensible, bulky
Readout / Electronics		Complex	Complex	Simple	Simple
Photon sensitivity		~100 ph.e	~10 ph.e	~1 ph.e	~1 ph.e
Sensitive to magnetic fields?		Yes	Yes	No	Yes
Noise		Low	Medium	High	Low
Rise Time		Medium	Slow	Fast	Fast

TABLE 1.1: Vacuum and semiconductor photodetector characteristics [23; 24].

Chapter 2

Experimental

2.1   Device structure

The SiPM under study in this work was developed by the R&D Sensor Team STMicroelectronics in Catania [16; 25]. The schematic cross-section of a SiPM is reported in Figure 2.1, where it is possible to identify the anode contacts (Anode metal back contact) and a cathode (Cathode pad) common to all the pixels of the device, which are placed, respectively, on the back and on the surface of the wafer. Each single pixel, formed by its p-n junction and its quenching resistor, is enclosed within a layer of epitaxial p⁻, previously grown on a p⁺ type substrate and having a crystallographic orientation <100>. The single pixel has a square shape with a 40×40 μm² active area.
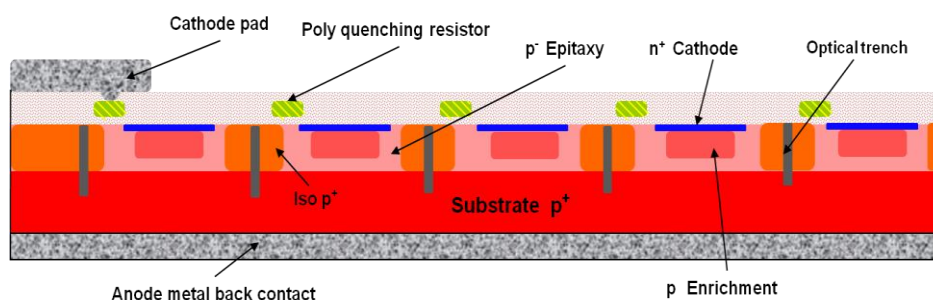
Figure 2.1: Schematic cross-section of the SiPM developed by ST Microelectronics.

Each cell is separated from the nearest by optical trenches and p⁺ isolation diffusions (Iso p⁺). The first of the wafer processing steps is the creation of p⁺ isolation regions through implants with high boron dose, in order to reduce the contact resistance of the anode and to provide, therefore, a low resistance path to the avalanche current. The fabrication proceeds with the realization of the active area. Subsequently, the enriched region p and n⁻ rings are made. An n⁺ polysilicon layer doped in-situ, provides the diode cathode. A second deposition of doped polysilicon, or equivalent material, provides the quenching resistor with the desired resistivity. The trenches around each single cell (Optical Trenches) have a width of about 1 μm and a depth of about $8 \div 10$ μm. The sidewalls of the trenches are covered with a thin layer of thermal oxide and a layer of Tetra Ethyl Ortho Silicate

(TEOS), having thickness in the range from 50 to 100 nm. The trenches fabrications is completed with the metal filling followed by a deposition of a thick layer of TEOS and one of spin-on glass (SOG) on the wafer, in order to electrically isolate them from the metal strips. The SOG material, often called organic silicate, is spin applied as a liquid across the underlying TEOS. After SOG deposition, the film is heated to convert the liquid based material to a silica film.

The active area of the device is covered by an anti-reflection coating, for example by using silicon nitride on oxide. It minimizes the surface optical reflection at a fixed wavelength. Finally, the anode and cathode terminals are fabricated through the oxide etching at the surface followed by the deposition of metal by sputtering. Figure 2.2 shows a detailed schematic cross-section of a single pixel developed by ST Microelectronics.
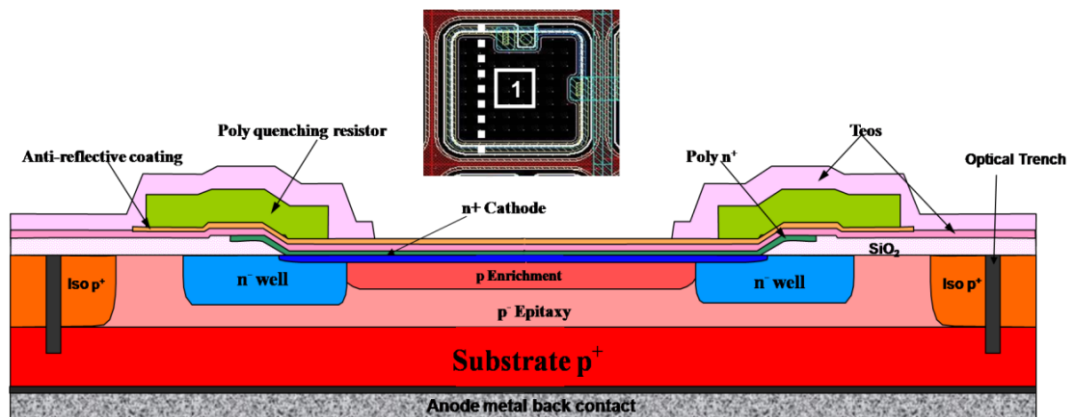
Figure 2.2: Schematic cross-section of the SiPM single pixel developed by ST Microelectronics.

2.2 Sensor details

The wafer has two main features: six stripes (in light gray in Figure 2.3) and 31 square regions (dark gray in Figure 2.3).
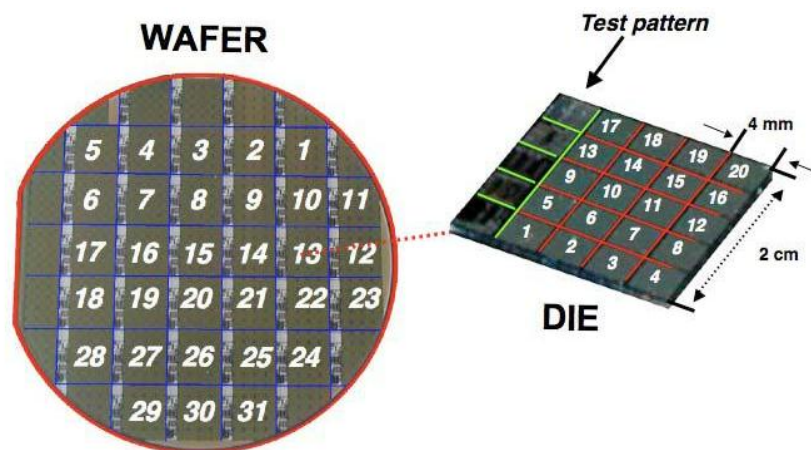
Figure 2.3: Picture of a wafer. The SiPMs are indicated with progressive numbers to facilitate the analysis.

The stripes contain all the test devices, where the single pixels and the small area SiPMs sit, while the square regions are the 64×64 pixels SiPMs.

The test pattern is formed by the single pixels (Figure 2.4 g), and a full set of small area SiPMs. In Figure 2.4 an enlarged picture of the test pattern, designed by STMicroelectronics, is shown. In particular, it is possible to identify the 5×5 pixels SiPM with (a) and without (d) optical trenches; 10×10 pixels SiPM with (b) and without (e) optical trenches; 20×20 pixels SiPM with (c) and without (f) optical trenches.
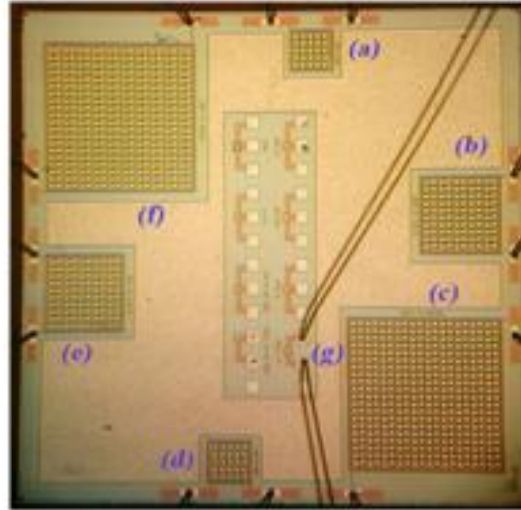
Figure 2.4: Layout of the test pattern produced by ST Microelectronics composed by: 5×5 pixels SiPM with (a) and without (d) optical trenches; 10×10 pixels SiPM with (b) and without (e) optical trenches; 20×20 pixels SiPM with (c) and without (f) optical trenches.

The sensor used in this work is formed by 25 pixels, insulated by optical trench (a), and each one has a square shape with a 40×40 μm^2 active area. Therefore, resulting physical size of the sensor is ~ 0.3×0.3 mm.

2.3   Electro-optical characterization

In order to identify the best sensor to be implemented in the experimental setup developed for the biosensing applications and described in the following sections, it was needed to characterize a set of sensors with different sizes (in terms of pixels number). Useful information on the device operation can be obtained from the reverse current voltage and DC characteristics in dark condition. All devices integrated in the test pattern are mounted in a 32 pin open package, through which it is possible to bias them and collect the output signals. The package, inserted in an appropriate socket welded on a board, is placed within a metallic box (miniDom) that allows their electrical and optical insulation [26]. The miniDom, equipped with a BNC input (to bias the device) and a BNC output (to collect the output signal), has a hole, with an area of ~ 3cm^2, which allows the sensor to be hit by the sample emitted fluorescence (Figure 2.5). Measurements of SiPM reverse current; breakdown voltage; and leakage

current were performed using a source/meter (Keithley 236) at room temperature and in dark conditions. To measure the DC, the SiPM input was connected to a Keithley 236 and its output to a digital oscilloscope (Tektronix DPO7104 with Bandwidth - 1GHz). Both instruments are connected to a PC trough GPIB. The measurement system is automated by a software opportunely developed in Labview®, that controls the bias voltage; the measurement conditions; and records the output signal automatically. The signal acquired is elaborated offline by a routine developed in Matlab®.
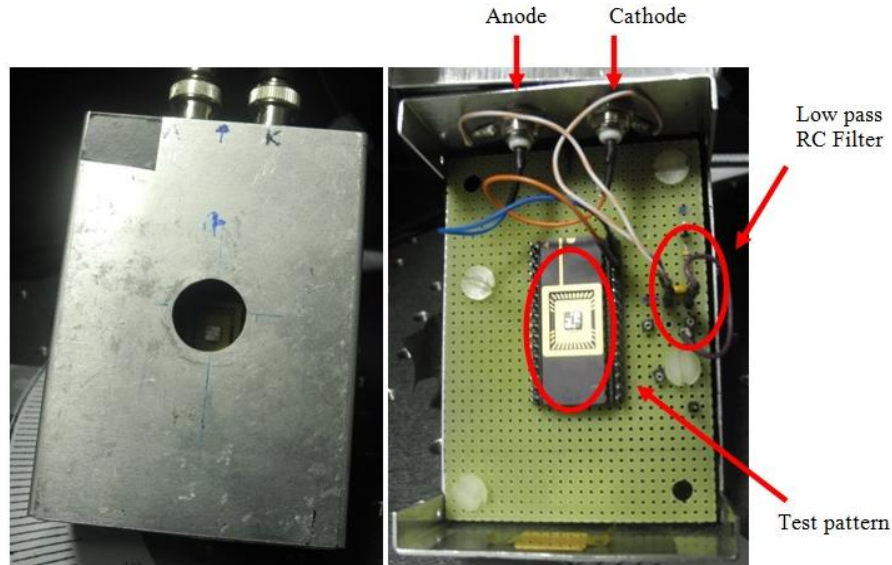
Figure 2.5: MiniDom.

To characterize electro-optically the devices, their current-voltage (I-V) characteristics and DC were measured. Figure 2.6 shows typical I-V characteristics in reverse voltage acquired at room temperature for arrays of 5×5 (green line), 10×10 (blue line), 20×20 (red line) pixels with trenches and 5×5 (cyan line) pixels without trenches.
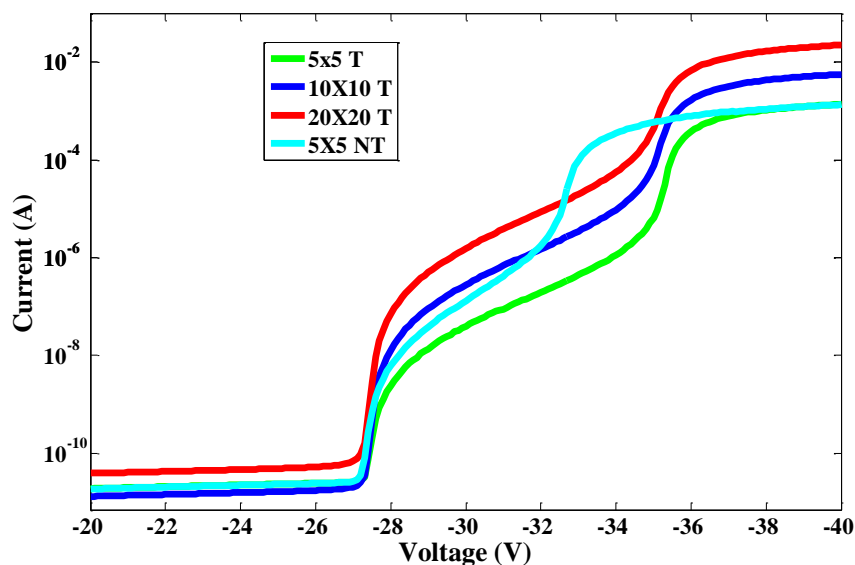
Figure 2.6: Reverse I-V characteristic of 25 (green line), 100 (blue line), 400 (red line) pixels SiPM with trenches and 25 (cyan line) pixels SiPM without trenches.

A great improvement in the device performances is observed when trenches are included in the device layout. The region between BV (occurring at 27.3 V) and -36 V is the range of interest for the Geiger mode operation (Over Voltage, OV, up to 8V). The direct comparison of the different arrays clearly shows two main features: BV is the same in all cases; increasing the number of pixels, the device noise (dark current and DC) increases linearly with the number of pixels as clearly observed in Figure 2.7 [27]. In fact, the device current for a bias voltage of -30 V is 39 nA in the 25 pixels SiPM, 281 nA and 1.56 µA in the 100 and 400 pixels devices measured, respectively (Figure 2.7).
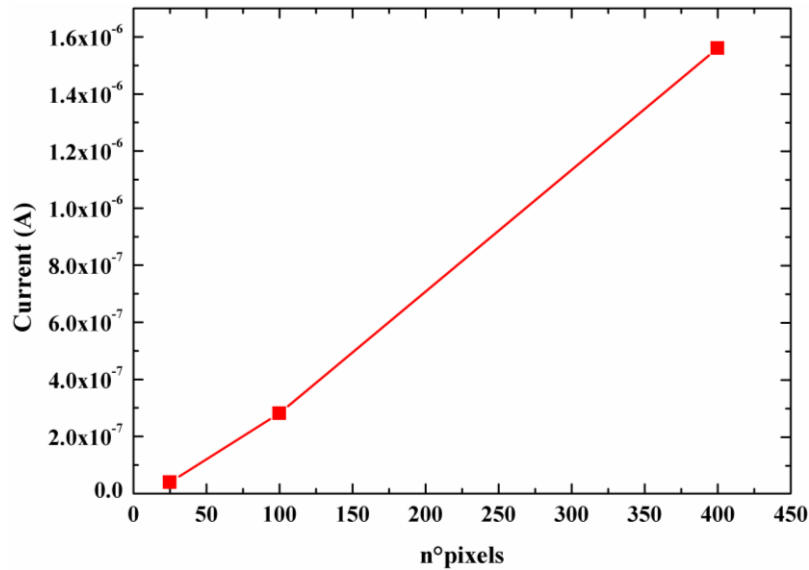
Figure 2.7: Current behaviour depending SiPM number of pixel for a bias voltage of -30V.

Once compared the different device dimensions, the importance to use an array with trenches is clear by the comparison of the performances of SiPM 5×5 pixels with and without trenches. The direct comparison clearly shows that the dark current of the device without trenches, in the operation region, is higher than the dark current of the device with trenches. The noise levels of the four devices can be easily evaluated from the inspection of Figure 2.8, reporting the DC rate in Hertz (average DC rate per pixel) as a function of the threshold, expressed in photon equivalent (p.e.) for the same devices. The three devices with trenches exhibit a very similar DC per pixel at 0.5 p.e. indicating the good quality and reproducibility of the technological processes (since all the pixels have similar characteristics). The small differences in the numbers arise from the cross-talk contribution to the single pixel DC. It becomes evident observing the devices response for two pixels breaking at the same time, the region around 1.5 p.e. The data provides the cross-talk probability (measured as the ratio of DC at 1.5 p.e. over the DC at 0.5 p.e.) and the direct comparison of the three devices, clearly shows that the 25 pixels SiPM is the device with the lowest cross-talk probability (0.03), hence, having the best signal to noise ratio (SNR). On the other hand, the DC for the device without trenches is about a factor of 3 higher than the DC of the corresponding device with trenches.
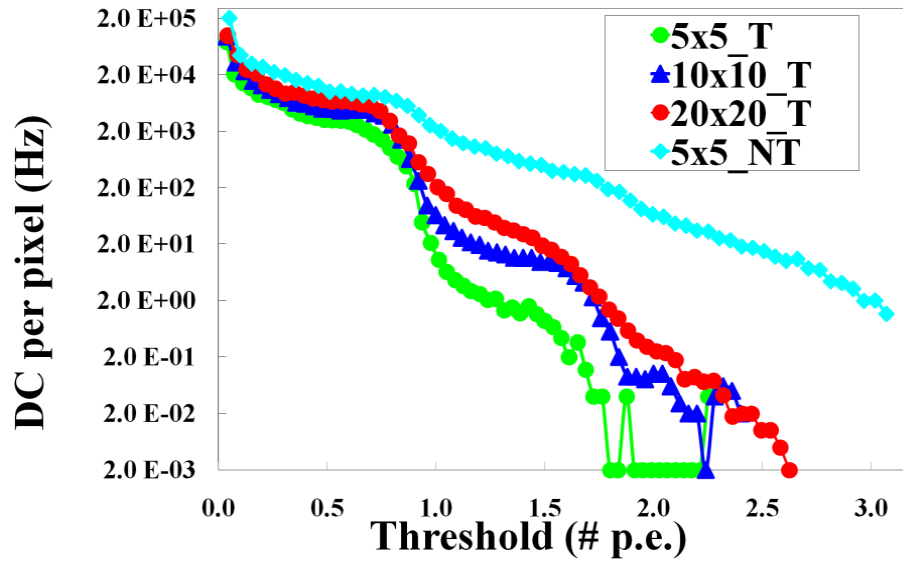
Figure 2.8: Dark Count of 25 (green line), 100 (blue line), 400 (red line) pixels SiPM with trenches and 25 (cyan line) pixels SiPM without trenches.

The difference is even more evident for the DC at 1.5, i.e. when two pixels are in avalanche at the same time, being <1 and ~ 344 for the device with and without trenches, respectively. It is the best way to define the cross-talk probability. The data indicate a cross-talk probability of ~ 3.4 for the device without tranches.

These results underline the trenches importance even in small devices: they allow the reduction of the interference between close pixels as well as the final measured DC. Moreover, the results allowed us to define the 25 pixels SiPM with trenches as the best device for our purposes, since it ensures the best signal to noise ratio, also considering that the signals to be detected are very weak, and exhibits the smallest size (0.3×0.3 mm) which is a great advantage for system integration.

The sensor figures of merit is shown in TABLE 2.1 [28].

Gain	Dark Count (Hz)	Sensitivity (nA)	Speed (ps)
$1.5 \cdot 10^6$	$7.9 \cdot 10^4$	76 ± 2	~150

TABLE 2.1: Figure of merit of the 25 pixels SiPM with trenches.

The choice of the sensor bias voltage is very important since increasing the bias voltage both the sensor gain and its noise increase. In order to measure low fluorescence levels, a trade-off between gain and noise must be found [29]. For this reason we characterized electro-optically the sensor, measuring its current versus bias voltage (reverse I-V characteristic), as reported in Figure 2.9.
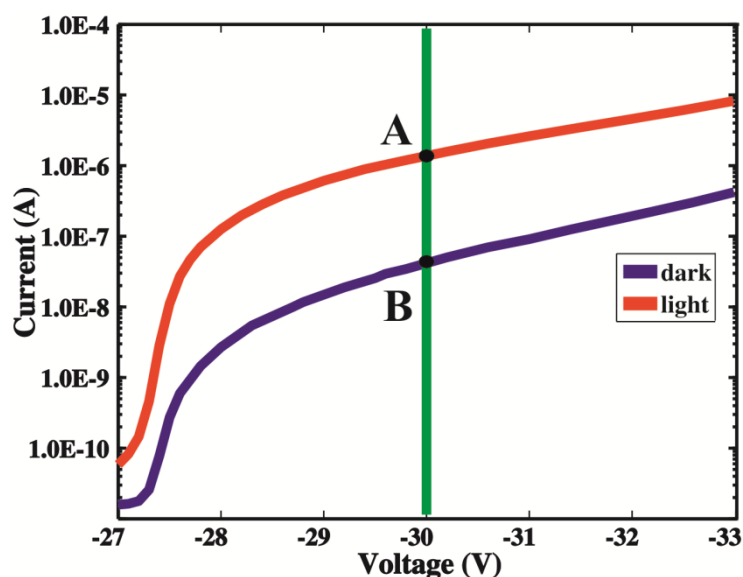
Figure 2.9: Reverse current collected from a sample with CY5 (red line) and a sample without CY5 (dark condition, blue line) using a 25 pixels SiPM.

The sensor reverse current during fluorophore emission (I_A, red line) and when no fluorophore is on the sample (dark condition, I_B, blue line) were measured. The bias voltage of -30V was chosen since it ensures the best signal-to-noise ratio. Once fixed the bias voltage at -30V (green vertical line), we measured the net fluorescent current value as:

$$\Delta I = I_A - I_B \qquad\qquad 2.1$$

The current value reported in all the following figures (ΔI) is the net current measured as the difference between the current due to the fluorophore and the reference (laser radiation diffused by the surface) using a device bias voltage of -30V .

2.4 Lifetime measurements

The fluorescence lifetime (FLT) has been widely used for the characterization of fluorescence species and in biophysical studies of proteins, e.g. to define the distances between particular amino-acid residues by Förster Resonance Energy-Transfer (FRET). FLT is a parameter that is mostly unaffected by inner filter effects, static quenching and variations in the fluorophore concentration. For this reason, FLT is one of the most robust fluorescence parameters. Therefore, it is advantageous in clinical and high throughput screening (HTS) applications, where it is necessary to discriminate against the high background fluorescence in biological samples. The ability to discriminate between two fluorophores with similar spectra but different lifetimes is another way to increase the number of parameters to measure.

There are two complementary techniques of lifetime measurement: the time domain and the frequency domain. In the time domain, a short pulse of light excites the sample, and the subsequent fluorescence

emission is recorded as a function of time [30]. This usually occurs in the nanosecond timescale. In the frequency domain, the sample is excited by a modulated source of light. The fluorescence emitted by the sample has a similar waveform, but is modulated and phase-shifted from the excitation curve. Both modulation (M) and phase-shift (φ) are determined by the lifetime of the sample emission; lifetime is calculated from the observed modulation and phase-shift. Both of these domains yield equivalent data and take advantage of the fluorescence decay law, which is based on first-order kinetics. The decay law postulates that if a population of molecules is instantaneously excited when photons are absorbed, then the excited population (and hence the fluorescence intensity as a function of time, I(t)) gradually decays to the ground state. Decay kinetics are described by

$$I(t) = I_0 \cdot e^{-\frac{t}{\tau}}$$ 2.2

where I_0 is the intensity at time t = 0, t is the time after the absorption, and τ is the lifetime, that is, when the fraction of the population of molecules in the excited state (and the fluorescence intensity) has decreased by a factor of 1/e, or ~37%. This fluorescence decay law implies that all excited molecules exist in a homogenous environment, as it is true for many single-exponential fluorescence lifetime standards in solution [31; 32]. Apart from such standards, however, single-exponential decays are usually a real-life exception, since most populations of excited molecules do not exist in homogeneous environments, and are influenced by various factors, including the presence of quenchers, energy-transfer processes among members of the population, and different rates of molecular rotation. Hence, in most instances, multi-exponential or non-exponential forms of the decay-law equation apply.

In this work, the time domain approach was used; the sample is illuminated with a short pulse of light and the intensity of the emission versus time is recorded. If the decay is a single exponential and the lifetime is long compared to the exciting light, then the lifetime can be determined directly from the slope of the curve. If the lifetime and the excitation pulse width are comparable, some type of deconvolution method must be used to extract the lifetime.

Two different fluorophores, with more different behaviour, were characterized: CY5 and $Ru(bpy)_3^{2+}$. The first is widely used in DNA labelling and recognition; the second is a promising candidate to be used for the same purposes. Therefore, two different experimental setups were implemented.

2.4.1 CY5 characterization

Cyanines have been used for many years as dyes, for example in photographic emulsions. Cyanine dyes began to be used widely as labels for nucleic acids in the early 1990s, when CY3, CY5 and CY7 were made commercially available as succinimidyl esters (by Molecular Probes, Inc., now part of Life Technologies). These CY dyes were different from previous cyanine dyes in that they contain sulfonate groups, which makes the CY dyes soluble in water (and reduce fluorescence-quenching due

to dye–dye interactions). Since their introduction, CY dyes have found widespread use in DNA and RNA labelling. In this work, CY5 was characterized. It exhibits absorption and emission peaks at 650 nm and 670 nm, respectively (Figure 2.10).
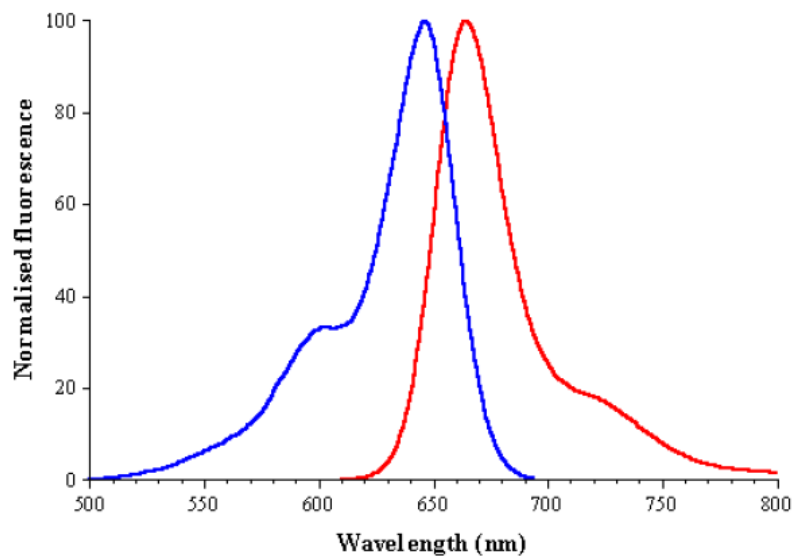
Figure 2.10: Absorption (blue lines) and emission (red lines) spectra of CY5 [33].

In order to characterize CY5 behaviour and the biosensor performances, many sets of measurements were performed: emission in various solutions; for variable dye concentration; excitation laser power (Figure 2.11) (34).
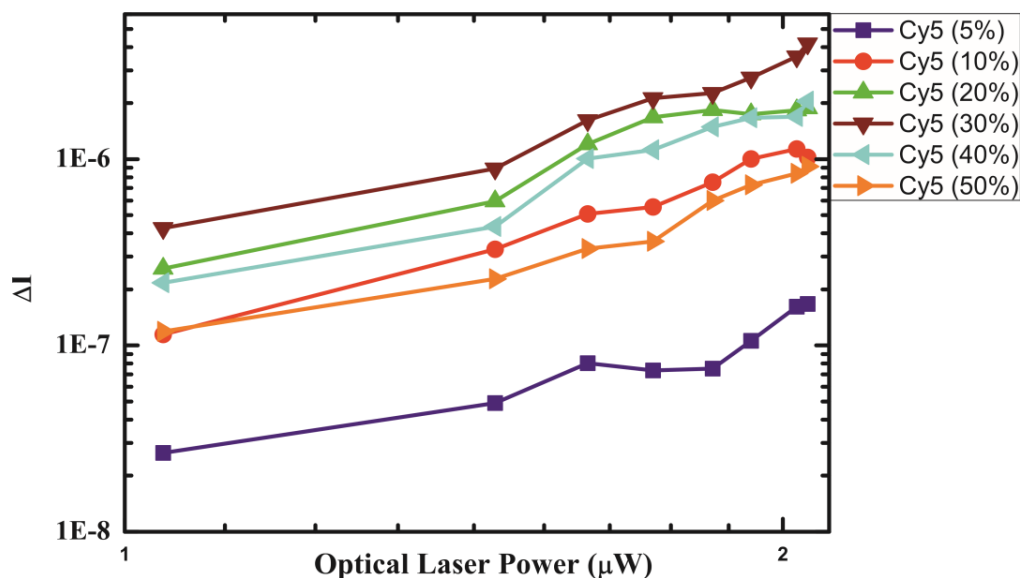
Figure 2.11: CY5 Fluorescence behaviour as a function of optical laser power at CY5 concentration of: 5% (blue lines), 10% (red lines), 20% (green lines), 30% (brown lines), 40% (cyan lines), 50% (orange lines).

Some interesting results emerged from these analyses: the increase in CY5 concentration causes an increase in the fluorescence signal measured up to a concentration of 30%, where a maximum in the emitted signal is measured. For concentrations above 30%, self-absorption phenomena become evident [34] and a reduction in the fluorescence signal is measured. This phenomenon is likely to occur due to

the small stokes' shift between the CY5 absorption and emission peaks, ~20 nm. The photon emitted by one deposited layer (at 670 nm) is absorbed to excite a CY5 molecule in the layers above or below with an efficiency of 70% with respect to the maximum absorption peak [35]. It should be noted that the laser photons (at 633 nm) excite the fluorophore molecules with a lower efficiency (~60%). As a result, only the photons emitted by the upper layer are detected. Moreover, the emitted fluorescence increases linearly with the optical laser power and the saturation value is not reached even at the highest fluorescence signal provided.

After identifying the optimal operating conditions (in terms of analyte concentrations and excitation power), lifetime was measured using the experimental setup whose schematic is shown in Figure 2.12.
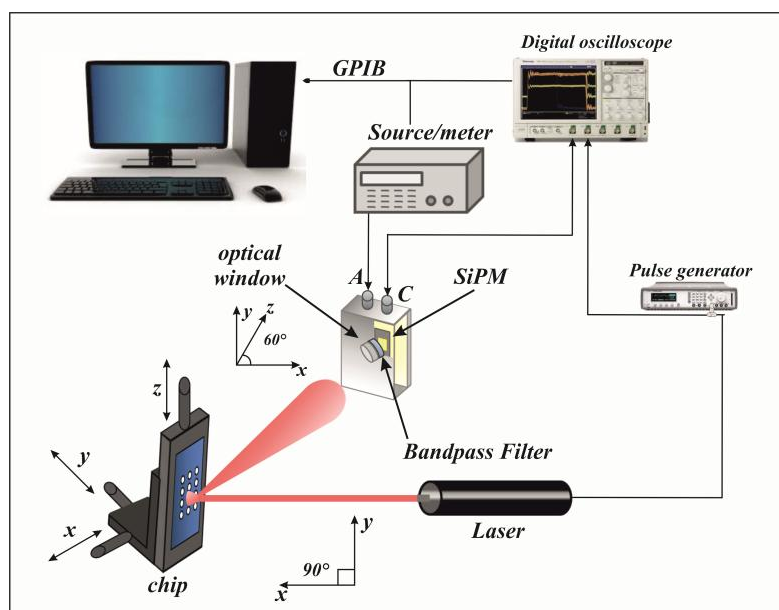
Figure 2.12: Schematic of the experimental setup used for lifetime measurements.

CY5 samples were excited by the light emitted by a laser diode (Coherent laser Cube operating at 660 nm) and controlled by PC. The samples were mounted on a xyz stage to allow their movement thereby intercepting the laser beam within the small spot to be measured. The miniDom, containing the sensor, was placed on a goniometer to allow the operator to monitor the emitted fluorescence as a function of the detection angle. Between the miniDom's hole and the sensor is interposed a bandpass filter, centred at 670nm (FWHM 10±2nm). The filter allows suppressing the laser radiation reflected by the sample surface, thus reducing the background noise.

CY5 lifetime was measured using pulsed laser waveforms (period 10ms and length 3 ns), obtained driving the laser diode through a pulse generator Agilent 81110A. The laser hit normally the sample, placed on the same optical axis and its fluorescence was detected by a SiPM lying in the same plane, at 60° with respect to the laser optical axis. The chosen angle ensured the lowest optical noise (laser light reflected by the slide) detected. The signal was recorded by an oscilloscope (Tektronix DP07104) and then, through a Labview® software developed for this purpose, was acquired by PC and post elaborated with Matlab®.

Figure 2.13 reports the operating principle on which are based lifetime measurements performed in this work. The laser pulse and SiPM response are shown in red and in blue respectively. The output signal is triggered on the falling edge of laser pulse and the delay between this last and SiPM signal is measured (Δt). However, a distribution of measured delays is performed and it represents the lifetime trend of the analysed fluorophore. Through the mathematical fit of the distribution, the fluorophore lifetime value is calculated.
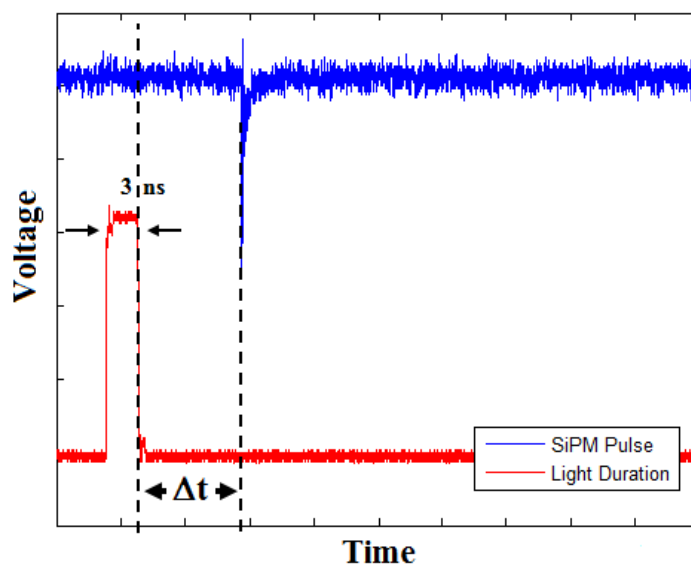
Figure 2.13: Operating principle of lifetime measurement.

The lifetime of CY5 sample at 30% diluted in H_2O milliQ and spotted on a coverslip was measured and reported in Figure 2.14.
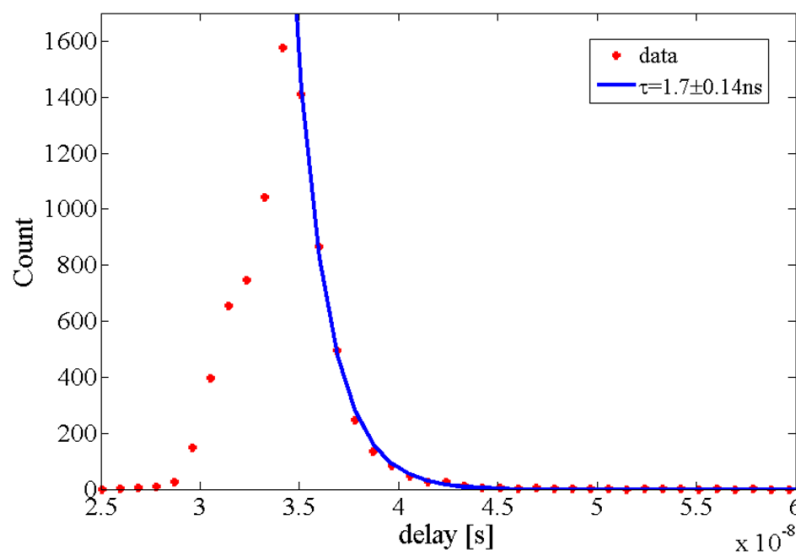
Figure 2.14: Data acquired (red dots); mathematical fit (blue lines) of lifetime measurement.

Figure 2.14 shows as a very fast lifetime was measured with the experimental setup based on SiPM technology. In this case, the measured CY5 lifetime was ~ 1.7 ns. However, this is a very critical analysis because the time value measured are very close to the system physical limits, mainly given by

the laser. With the available equipment, described above, it is not possible to measure very short lifetime values. Therefore, it was needed to identify a fluorophore with a lifetime slower then CY5, thus allowing the use of a simpler system of management and control of the signals, for a possible system integration. A suitable fluorophore that exhibits optimal characteristics with respect to the measurement system, in term of emission spectrum and lifetime value, is tris(2,2′-bipyridyl)ruthenium(II), $Ru(bpy)_3^{2+}$. Its properties and characterization are described in the following section.

2.4.2 $Ru(bpy)_3^{2+}$ *characterization*

The tris(2,2′-bipyridyl)ruthenium(II), $Ru(bpy)_3^{2+}$, is an octahedral metal transition complex composed by the transition metal ruthenium bounded to three heteroaromatic bypiridine units. Its optical properties would allow overpassing some issues, related to the use of CY5, and already highlighted. The fluorophore has two absorption peaks at 290 nm and 450 nm, ligand-centre (LC) and metal–ligand (MLCT) electronic transitions respectively, and a quantum yield of 0.042 ± 0.002 (compared to 0.2 of CY5) (Figure 2.15 a). The absorption peaks are far away from the emission peak at 630 nm [36; 37], 100 nm to the closest, thus avoiding the fluorescence self-absorption (Figure 2.15 b). Moreover, $Ru(bpy)_3^{2+}$ fluorescence exhibits a very long lifetime ($\tau \sim 350$ ns) [38], allowing one the use of pulsed LED for excitation.
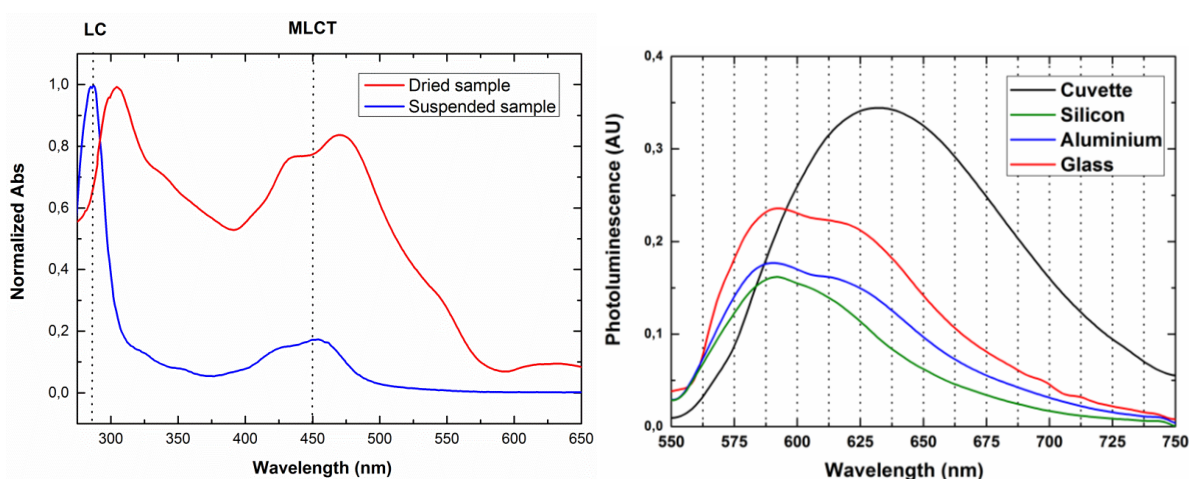
Figure 2.15: (a) Absorption spectra of suspended (blue solid line) and dried (red dashed line) form of $Ru(bpy)_3^{2+}$. The ligand-centre (LC) and metal–ligand (MLCT) electronic transitions are highlighted with vertical dashed lines; (b) $Ru(bpy)_3^{2+}$ emission spectra dissolved in water (black line) or deposited on: silicon (green dot-dashed line), glass (red dashed line), aluminum (blue dotted line) [39].

The data obtained from the dissolved form (blue line) perfectly reproduce literature results [36; 37]. The fluorophore exhibits two characteristic absorption peaks at 290 nm and 450 nm (highlighted in figure with dashed vertical lines). Samples dried over glass slides showed a red shift of about 20 nm, with electronic transition peaks at 310 nm and 470 nm, as shown in Figure 2.15(a) (red line). The absorption "red shift" is probably due either to the intensification of inter-molecular interactions or to

a slight distortion of the intramolecular bonds. Data, reported in Figure 2.15(a), clearly show a difference in the ratio between LC and MLCT transitions. The MLCT–LC ratio goes from ∼0.2 of the dissolved form to more than 0.8 of the dried form, suggesting a strong increase of the absorption efficiency, more than a factor four, of the MLCT electronic transitions with respect to the LC ones [39]. The emission spectrum of the 0.7 mg/ml sample in cuvette is shown in Figure 2.15(b) (black line). The curve, in according to literature emission spectra, exhibits a peak at about 630 nm [36]. Some differences in the case of the fluorophore dried form appear. The emission spectra are, for such form, quite different from literature data [37]. The curve morphology changed and a new and dominant peak around 590 nm appeared (red line in Figure 2.15(b)). In order to exclude any contribution given by the solid surface used for deposition, $Ru(bpy)_3^{2+}$ was spotted on different surfaces. An insulator (glass), a semiconductor (Si, to be sure that the surface was Si, a sample dip in HF was performed just before fluorophore deposition), and a metal (Al) were used as deposition surfaces. The goal was to determine if the surface electronic properties could modify the fluorophore emission properties. All samples were diluted in Milli-Q water before being spotted on the different surfaces. The emission data are also shown in Figure 2.15(b) (red, green and blue line, respectively): they exhibit the same morphological alteration of the curve (the new dominant peak at 590 nm) already observed for the dried sample on glass slide, only the relative height are different, but no conclusion can be drawn from the PL intensity at room temperature. The data clearly show that the surface role is not the dominant effect ruling the $Ru(bpy)_3^{2+}$ emission properties, at the deposition conditions used.

The last optical characterization was the $Ru(bpy)_3^{2+}$ lifetime measurement using the experimental setup reported in Figure 2.16.
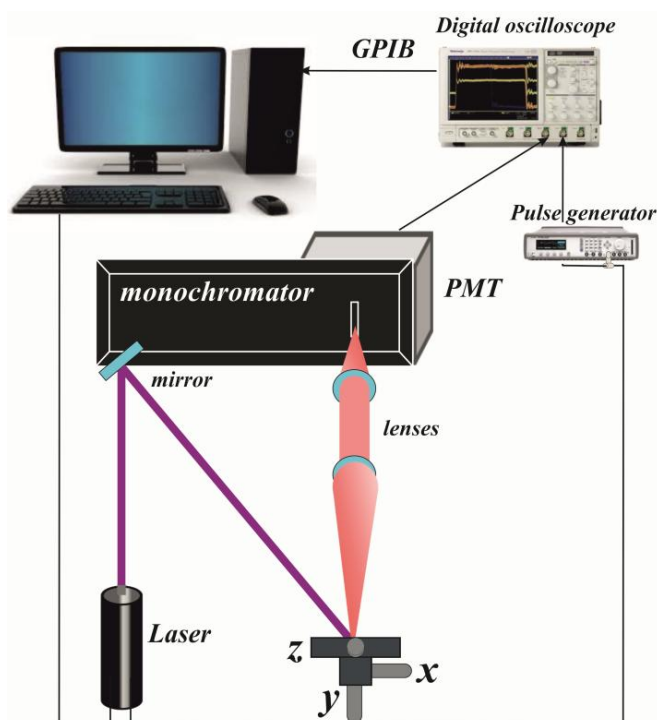
Figure 2.16: Schematic of experimental setup for lifetime measurements using a PMT as photodetector.

The light emitted by a laser diode (Coherent laser Cube operating at 405 nm) and controlled by PC, excited Ru(bpy)$_3^{2+}$ samples. The laser light, pulsed by the Agilent 81110A pulse generator (period 10ms and length 100 ns), hits a mirror and reaches the sample. The sample was mounted on a xyz stage to allow its movements thereby intercepting the laser beam within the small spot to be measured. The fluorescence emitted was collected by two lenses and focused on the input slit of a monochromator (Digikrom DK480) and detected by a Photomultiplier Tube (PMT, Hamamatzu R943-02) placed on the monochromator's output slit. The monochromator is set to let only the light at 630 nm to pass (wavelength of Ru(bpy)$_3^{2+}$ emission peak). The signal detected by the PMT was recorded by an oscilloscope (Tektronix DP07104), triggered on the pulse generator signal, and then, through a Labview® software developed for this purpose, was acquired by PC and off-line elaborated with Matlab®.

An example of Ru(bpy)$_3^{2+}$ lifetime measurements performed in this work is reported in Figure 2.17. The laser pulse and PMT response are shown in red and in blue, respectively. The output signal is triggered on the falling edge of laser pulse and is averaged over 10000 sampling before being acquired.
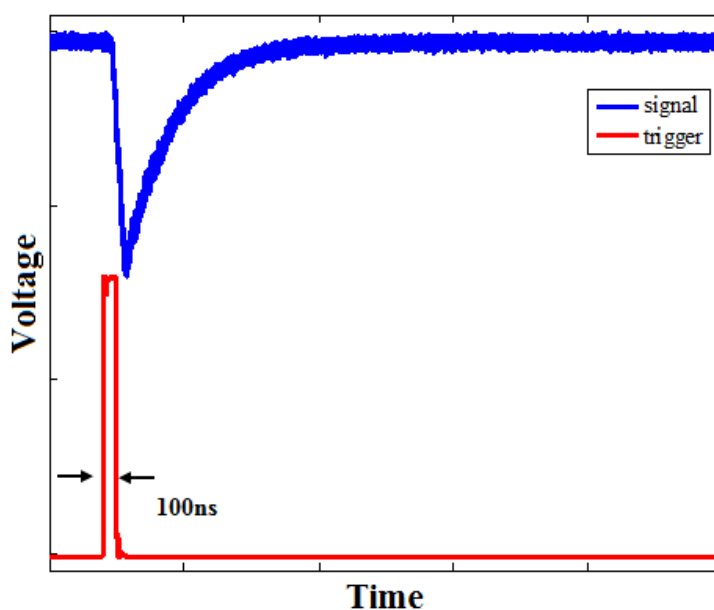
Figure 2.17: Example of lifetime measurement using PMT as photodetector.

As already observed for the emission, also the lifetime value changed depending on the fluorophore physical state (suspended or dried), as shown in Figure 2.18. The experimental data were fitted to obtain the lifetime (τ) values, using a multi-exponential as indicated by the following equation:

$$F(t) = \sum_{i=1}^{n} A_i \cdot e^{-\frac{t}{\tau_i}} \qquad 2.3$$

where A is the intensity at time t = 0, t is the time after the absorption, and τ is the lifetime. The lifetime measured in solution (0.7 mg/ml of fluorophore in MilliQ water) was 358 ± 0.9 ns (see Figure 2.18 black line and TABLE 2.2), the same value reported in literature [40], within the experimental errors.

For Ru(bpy)$_3^{2+}$ dried samples, the lifetime was given by two components. These data confirmed that the fluorophore inter and/or intra molecular interactions modified the fluorescent properties. In fact, we observed a second emission peak with a shorter lifetime. The lifetime was measured for all the surfaces used to deposit the fluorophore: glass, Si and Al. The data, shown in Figure 2.18, are also summarized in TABLE 2.2. The three lifetime values are reported in the table to allow an easier comparison. In fact, all the samples exhibit the τ_2 component, typical of the suspended form. A strong difference is observed in Ru(bpy)$_3^{2+}$ deposited on the three different surfaces with respect to the suspended form. In fact, dried Ru(bpy)$_3^{2+}$ samples exhibit a shorter lifetime component.

Sample	τ_1 [ns]	τ_2 [ns]
Ru(bpy)$_3^{2+}$ dissolved	-	358 ± 0.9
Ru(bpy)$_3^{2+}$ dried on glass	118 ± 1	358
Ru(bpy)$_3^{2+}$ dried on silicon	130 ± 3	372 ± 49
Ru(bpy)$_3^{2+}$ dried on aluminum	130 ± 3	370 ± 3

TABLE 2.2: Ru(bpy)$_3^{2+}$ lifetime values measured using the experimental setup reported in Figure 2.16.
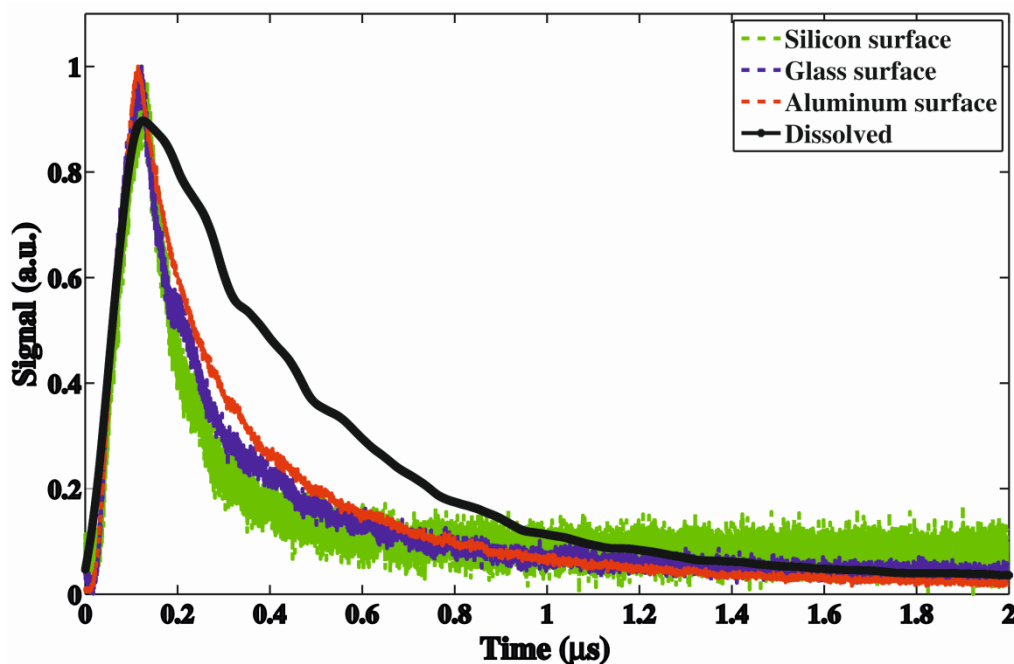
Figure 2.18: Lifetime of suspended (black line) and Ru(bpy)$_3^{2+}$ dried form spotted on Silicon (green lines), glass (blue lines) and aluminum (red lines) surface.

In particular, the lifetime of Ru(bpy)$_3^{2+}$ deposited on glass is a bit faster than other samples. It is probably due to the insulating nature of the surface that interferes less with the homo-lumo transitions. In all measurements, the lifetime is always over 100 ns, a promising feature for easy, compact and portable applications.

2.5   Photon counting measurements

The SiPM can be used in many applications where extremely weak light signals, at the level of few photons (photon counting regime), must be detected. It provides all the performances needed in photon counting, such as high gain at low bias voltage, high photon detection efficiency, good time resolution, high count rate, and large spectral response. SiPMs performances in photon counting regime have been deeply investigated in literature, using picosecond pulsed lasers. They can be used in positron emission tomography [7], magnetic resonance imaging, nuclear physics instrumentation [7], high energy physics [41], time-resolved fluorescence spectroscopy [42; 43].

In biomedical instruments, fluorescence detection can be accomplished with simple photodiodes, photomultiplier tubes (PMT's), Charged Couple Devices (CCD's) and, now, photon counting devices. New technologies based on Single Molecule Detection use confocal microscope and photon counting technology to excite and detect single photons fluorescing from single molecules. Thanks to the small sample sizes, speed of counting and sensitivity of the overall system, this technology allows for collecting multiple parameters such as: fluorescence intensity, molecule diffusion times, fluorescence lifetime and fluorescence polarization information [44].

In this work, an experimental setup for photon counting measurements was developed and it is reported in Figure 2.12.

SiPM, in photon counting operation mode, was used to measure the number of photon emitted by a sample of CY5 at 30% diluted in H_2O milliQ and spotted on a coverslip. This measure was performed in two steps: SiPM was biased to -30V to analyze a reference sample (sample without CY5 deposited on top) and the CY5 sample, and the signal collected through the oscilloscope operating in continuous mode. In the first case, the collected signal on the oscilloscope was due to SiPM intrinsic noise and to the residual noise due to the laser radiation reflected by the coverslip. Then, we placed the CY5 deposited sample on the same optical axis of the laser and, on the oscilloscope screen; it was possible to see signals at different amplitudes due to up five fired pixels, on average, by photons. The elaboration of the acquired data is shown in Figure 2.19. In particular, the blue solid line indicates the emitted photons distribution, while the red line indicates the noise acquired from the reference sample.
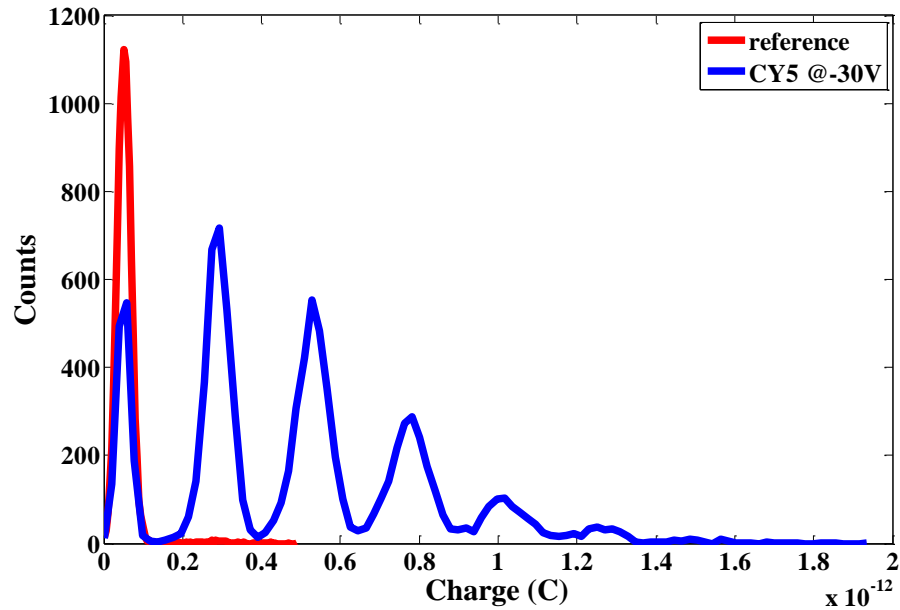
Figure 2.19: Photon counting distribution of CY5 fluorescence (blue lines) and noise (red lines) from reference sample.

The peaks separation in the photoelectron spectrum measured was about $2.34 \cdot 10^{-13}$ C corresponding to a gain value of $1.5 \cdot 10^6$, assuming $n_{ph}=1$ and $V_{BD} = $ -28V (Eq. 1.6). However, increasing the SiPM bias voltage an increase of both the gain and the measured noise is recorded, hence, a compromise that will ensure a good signal to noise ratio must be found [45; 46]. Since the CY5 absorption and emission peaks are very close (650 nm and 670 nm, respectively), the integrated detection set-up would be very difficult to implement. In addition, its short lifetime (1÷3ns) would force to design and fabricate a complex control and management circuitry.

2.6   Conclusion

The SiPM produced by the R&D of STMicroelectronics in Catania was used to detect low fluorescence signals, allowing the design and fabrication of easy-to-use optical system for biomedical applications.

Multichip characterization allowed defining the 5x5 pixels with trenches SiPM as the most suitable for biosensing applications, since it had the lowest DC and cross-talk probability. Pulsed measurements showed as SiPM can be used as photon counter also for biosensing applications.

Two different experimental setups for lifetime measurements (fast and slow fluorophores) have been developed.

Photochemical properties of CY5 and $Ru(bpy)_3^{2+}$, for optical sensing application, have been studied. The analysis showed that this last molecule is a viable alternative to the conventional fluorophore CY5 for target gene labelling in optical DNA-chip application. In fact, $Ru(bpy)_3^{2+}$ reduces the risk of fluorescence self-absorption, thanks to the large distance between the absorption/emission peaks, and allows using a simple electronics for the fluorescence analysis, thanks to the long lifetime.

The measurements showed a cooperative effect of the molecules by increasing their density after drying of sample. This caused the red shift of the absorption peaks at 310 nm and 470 nm and the appearance of a dominant emission peak at 590 nm in dried samples. These samples exhibit an additional faster component in the lifetime of ~100ns, in addition to the 350 ns lifetime value of dissolved samples.

The properties of SiPM and $Ru(bpy)_3^{2+}$ would allow miniaturization of the measurement systems, opening up the possibility of lab-on-chip fabrication using the optical transduction ("traditional") for detection.

Chapter 3

DNA microarray

3.1 Introduction

Lots of DNA microarrays and DNA chip devices have been developed and are commercialized. These devices allow DNA and/or RNA hybridization analysis of large numbers of samples simultaneously to be carried out in microminiaturized highly parallel formats. DNA microarray applications are usually used for gene expression analysis or screening samples for single nucleotide polymorphisms (SNPs) [47]. In addition to molecular biological analyses and genomic research applications, microarray systems are also being used for pharmacogenomics research, infectious and genetic disease, cancer diagnostics, forensic and genetic identification purposes [48]. Microarray technology continues to improve in sensitivity and selectivity and is becoming a more economical research tool. The use of DNA microarrays already had revolutionized genetic analysis and many important diagnostic areas.

They are generally fabricated on glass, silicon, or plastic substrates. The microarrays may contain from a hundred to many thousands of test sites that can range in size from 10 to 500 microns. DNA probes are selectively spotted or addressed to individual test sites by several techniques. Probes can include synthetic oligonucleotides or larger DNA/RNA fragments. The DNA probes are attached either covalently or physically to a support material. Depending on the array format, probes can be the target DNA or RNA sequences to which other "reporter probes" would subsequently be hybridized. The fabrication of microarrays involves the immobilization or in situ synthesis of DNA probes onto the specific test sites of the solid support material. High-density DNA arrays are fabricated using physical delivery techniques (e.g., inkjet or microjet deposition technology) that allow the dispensing and spotting of nano/picoliter volumes onto the specific test site locations on the microarray. In some cases, the probes or oligonucleotides on the microarrays are synthesized in situ using a photolithographic process. Microarray devices with a low density of test sites have been developed, and provide direct electronic detection of the hybridization reactions. Active electronic microarray devices with electronic addressing or spotting of probes as well as rapid high-performance hybridization analysis are now also available for research and diagnostic applications [49]. The

successful implementation of microarray technologies has required the development of many methods and techniques to fabricate the microarrays and spot the probes, to carry out and detect the hybridization reactions, and informatics to analyse the data. DNA hybridization analysis on microarrays usually involves detecting the signal generated by the binding of a reporter probe (fluorescent, chemiluminescent, colorimetric, and radioactive, etc.) to the target DNA sequence. The microarray is scanned or imaged to obtain the complete hybridization pattern. Fluorescence scanning/imaging or mass spectroscopy are two of the most common methods used to read the microarrays. For high-density type microarrays, a variety of bioinformatics tools has been used to reduce the complex data into useful information. The automation of DNA microarray systems greatly facilitates their use and ease of operation and helps to eliminate many of the human errors that would be involved in manually carrying out the multiplex hybridization analyses. The development of microarray technology, as well as all other innovations in the biosensor field, is the result of the integration of many different disciplines such as molecular biology, genetics, advanced microfabrication and micromachining technologies, nucleic acid chemistry, surface chemistry, analytical chemistry, software, and robotics and automation. In fact, microarray technology represents a truly successful synergy of these many different scientific and engineering fields.

In the following sections an experimental setup, based on SiPM technology, for DNA microarray analysis is described. It exhibits higher sensitivity than traditional commercial systems and also provides a quantitative output signal. For these reasons, SiPM is a promising candidate to replace traditional optical scanner used, until now, for this kind of analysis. Moreover, a composite of recent general reviews and comments on microarray technologies and their applications (in research and diagnostics) are discussed.

3.2 DNA microarray Technology

In the past several years, many different microarray technologies, devices, and instrument systems are commercially available to fabricate DNA microarrays. They are used for gene expression, genotyping, and other applications [50]. Many microarray spotting technologies and techniques now exist. Two of the most important spotting techniques used are the pin-based fluid transfer systems [51-53] and the piezo-based inkjet dispenser systems [54-56]. Other methods to fabricate DNA arrays include the use of photolithography for the in situ synthesis of high-density DNA microarrays, developed by Affymetrix, as well as the electronic-based addressing of microarrays developed by Nanogen.

3.2.1   *Affymetrix Technology*

High-density DNA arrays fabricated by Affymetrix provide a massively parallel approach to DNA hybridization analysis that is having a significant impact on genomic research and diagnostics. In the early 1990s, Steve Fodor and colleagues at Affymetrix began to develop photolithographic techniques to carry out the parallel synthesis of large numbers of oligonucleotides on solid surfaces [57; 58]. This light-directed synthesis has enabled the large-scale manufacture of arrays containing hundreds of thousands of oligonucleotide probe sequences on glass slides, or "chips", less than 2 cm^2 in size [59]. This method is used now by Affymetrix to produce the high-density GeneChip® probe arrays, used for the detection and analysis of point mutations and SNPs and for gene expression studies (Figure 3.1).
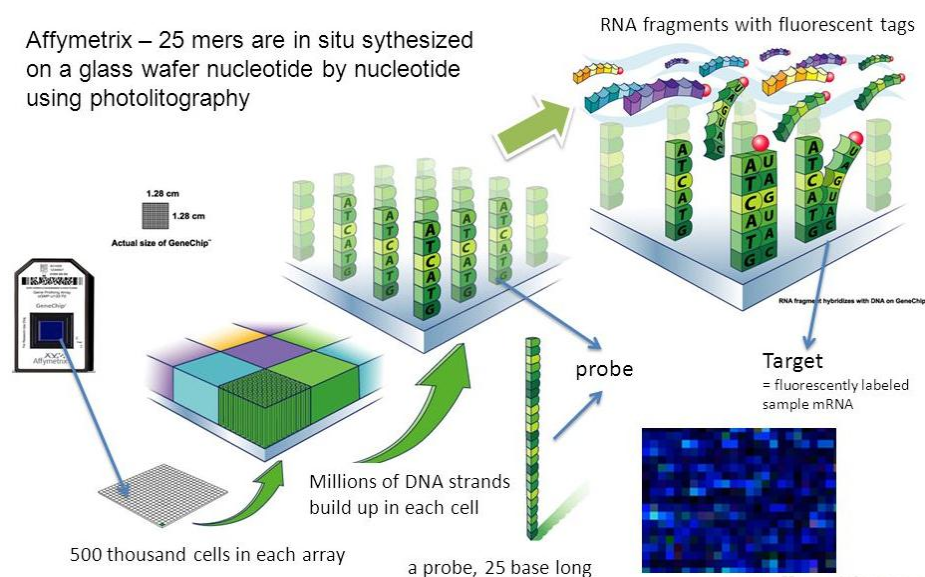
Figure 3.1: Operating principle of Affymetrix Microarrays.

The Affymetrix in situ process combines DNA synthesis chemistry with photolithographic techniques. In this process, 5'-terminal protecting groups are removed selectively from growing oligonucleotide chains in predefined regions of a glass substrate by controlled exposure of light through photolithographic masks. The glass substrate, or chip, is covalently modified with a silane reagent to provide hydroxyalkyl groups, which are needed for the initial synthesis sites. Then, these sites are extended with linker groups protected with special photolabile protecting groups. When specific regions of the surface are exposed to light (through masks), the groups are selectively removed, allowing the sites to now be coupled with the next appropriate nucleoside phosphoramidite monomer. The monomers, which are also protected at their 5' position with a photolabile group, are coupled to the substrate using standard phosphoramidite DNA synthesis protocols [48].

Many of the semi-automated manufacturing techniques and lithography tools used in the GeneChip® array production process were adapted from the microelectronics industry. The Affymetrix method for highly parallel synthesis of oligonucleotide (probe) sequences provides an excellent process to

fabricate high-density microarrays. With this process, a complete set, or subset, of all probe sequences of length n requires 4n synthesis steps. Currently, arrays made using photolithographic synthesis have individual probe features 24×24 microns on a 1.6-cm^2 size chip. The technology will ultimately allow arrays to be fabricated with densities $>10^6$ sequences/cm^2, which corresponds to a feature size of less than 10^2 microns. Typical arrays comprise customized sets of probes that may range from 14 to 25 bases in length [48].

3.2.2   Nanogen Technology

Microelectronic chip/array devices developed by Nanogen combine many aspects of technology from the microelectronics industry to improve uniquely molecular biology techniques such as DNA hybridization. Microelectronic arrays provide high-performance hybridization that overcomes many of the problems of passive array hybridization techniques. These active microelectronic arrays have the ability to produce reconfigurable electric fields (more specifically electrophoretic fields) on the microarray surface that allow rapid and controlled transport of charged DNA/RNA molecules to any test site [49; 60; 61]. Nanogen, Inc. has developed an electronic microarray based technology (NanoChip® Electronic Microarray) for manipulation, concentration and hybridization of biomolecules on the chip array (Figure 3.2) [62]. Nanochip® microarray technology uses electronic addressing of charged biomolecules on the electrode array to separate and concentrate analyte targets. Negatively charged DNA targets and molecular probes (Figure 3.2 top) are moved to a particular site by energizing the electrodes at a reverse potential (Figure 3.2 bottom). Targeted molecules concentrate at the array site where they can be bound chemically or hybridized to a DNA probe. Fluorescent signal is obtained from the reporter probes hybridized to the target DNA and signal proportional to the concentration of analyte DNA is measured. This approach extends the power of microarrays using electronics by connecting each test site on the NanoChip® array to an electrode.
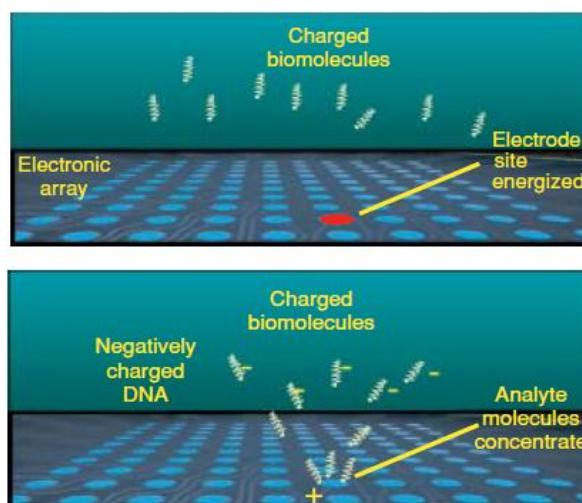
Figure 3.2: Operating principle of Nanochip® microarray technology.

Most biological molecules have a natural positive or negative charge. When biological molecules are exposed to an electric field (Figure 3.2), those with a positive charge move to electrodes with a negative potential, and molecules with a negative charge move to electrodes with a positive potential. Current and voltages are applied to the test sites via individual electrode activation to facilitate the rapid and controlled transport of charged molecules to any test sites. Additional advantages of electrically facilitated transport include: (*i*) the ability to produce reconfigurable electric fields on the microarray surface. It allows the rapid and controlled transport of charged molecules to any test sites [48; 63-65]. *ii*) The ability to carry out site selective DNA or oligonucleotide addressing and hybridization [66]. (*iii*) The ability to significantly increase DNA hybridization rate by concentration of target at the test sites; (*iv*) The ability to use electronic stringency to improve hybridization specificity. In Figure 3.3 Nanogen's system is reported.

Figure 3.3: Photograph of the Nanochip® cartridge containing the electronic microarray (left), and Nanogen's Workstation which allows fully automated processing of 4 cartridges simultaneously in the loader and fluorescent detection in the reader (right) [62].

NanoChip® Cartridge is composed by 100-site array, assembled into a complete cartridge (Figure 3.3 on the left) by ultrasonically welding two molded polymethyl methacrylate (PMMA) cartridge bodies that contain fluidic channels and inlet and outlet ports. The cartridge eliminates sample evaporation, prevents sample contamination and provides a fluidic interface to the Workstation. The NanoChip® electronic microarrays are operated through a fully integrated and automated workstation (Figure 3.3 on the right). The system consists of three major subsystems: (1) the loader for loading patient samples on one to four cartridges, (2) the reader, a highly sensitive, laser-based fluorescence scanner for detection of assay results and (3) computer hardware and software, which automates import, analysis and export of sample information making data analysis simple.

3.2.3   STMicroelectronics Technology

A novel biochip platform for rapid analysis/identification of nucleic acids, including DNA and microRNAs, with very high specificity was developed by STMicroelectronics [67-69]. Their In-Check platform is based on a miniaturized silicon Lab-on-Chip (LoC) that integrates a PCR reactor - formed

by buried microchannels 1µl in volume – together with a customable microarray. Temperature Control System (TCS) and Optical Reader (OR), driven by a bioinformatic system, complete the platform (Figure 3.4). These features allow achieving both DNA amplification and DNA detection in an integrated cost effective and convenient format silicon chip.

Figure 3.4: In-Check™ lab-on-chip Platform developed by STMicroelectronics [70].

Two silicon microreactors fluidically connected to a microarray chamber compose the LoC. Each silicon microreactor (maximum volume of 12 µl) contains resistors and sensors at different positions to activate and control the thermal process. Such reactors are connected fluidically to a microarray area of 3.5×9 mm where, after PCR, DNA hybridization takes place. The microarray chamber contains a microarray of 126 spots consisting of 25 bp oligo-probes, spotted onto the surface through a piezo-array system. In order to guarantee the microreactor sealing during the sample preparation, PCR amplification and hybridization reactions, Polydimethylsiloxane (PDMS) clamps were designed. The clamps are made of a mixture of PDMS silicone and a curing agent [68].

LoC was chemically treated to make a biocompatible the surface for the PCR amplification and the DNA microarray hybridization. After silicon standard cleaning, the surface is first modified using 3-glycidoxypropriltrimethoxysilane (GOPS) to obtain an epoxy derivative coating suitable for the microarray fabrication. Next, a 5' amino-modified oligo solution in phosphate buffer is printed on LoC hybridization area through the piezo microarray system. An anchoring process performed in a climatic chamber at 30 °C with 30% relative humidity guarantees the covalent bonding of the amino-modified-oligo to the epoxy surface. A coating with protein is performed to guarantee the biocompatibility with both the silicon microreactor and the hybridization area [68].

The chip contains integrated sensors and heaters and it is thermally driven by an external Temperature Control System (TCS). It is an electronic device to perform the enzymatic thermal cycling and hybridization reactions and allows very accurate and fast thermal managing of the chip. A microcontroller that reads the embedded temperature sensors drives the system and triggers embedded

heaters. A cooling rate of about 10 °C/s is achieved with a ventilator fan. The temperature cycle is controlled with high accuracy (±0.1 °C). Fast heat ramping (40 °C/s) improves the PCR performances and reduces the amplification time [68].

The DNA detection in the microarray is based on fluorescent labels and it is performed by means of ST's Optical Reader (OR). It is an optical device to acquire images of LoC. The camera offers up to 1392×1040 pixels and operates in 8-bits mode. It has two programmable outputs that are used for turning on an excitation system based on two identical illuminators placed symmetrically to the sides of the camera and tilted at 45°. Each illuminator is composed by a 5 mm white LED, a red LED, two aspherical lenses and an excitation filter for Cy5. A dedicated software drives the optical reader. A multi-shot acquisition procedure allows increasing the dynamic linear range and the camera blooming effect [68].

With its compact bench-top "footprint" requiring only a single technician to operate, the biochip system promises to transform and expand routine clinical diagnostic testing and screening for genetic diseases, cancers, drug toxicology and heart disease, as well as employment in the emerging companion diagnostics market.

3.3   Novel promising technology based on SiPM

Nowadays, commercial available system for DNA microarray analysis are very expensive benchtop system, which means that measurements "in vivo" and "in situ" are very difficult. Moreover, they provide an image as a result, which means that an image off-line analysis is needed to obtain a quantitative output signal.

The challenge of reducing the system physical size, the cost of analysis and increasing the low detection limit of analyte concentration led us to implement a new platform for DNA microarray analysis, based on SiPM technology. This platform, as described in the following sections, implements a very low cost and small sensor, which means: miniaturisable system; opportunity of doing measurements "in vivo" and "in situ"; cheap DNA analysis. Moreover, the system based on SiPM provides as output a quantitative signal, which simplifies the analysis of the results.

3.3.1   *Experimental setup*

In this section an optical system, based on SiPM technology, able to detect the fluorescence emitted by ss-DNA amino-terminated labelled with CY5, immobilized on Al-TEOS surfaces using GOPS protocol is described [28; 29]. Aim of this work is to demonstrate that SiPMs are able to detected low-levels of fluorescence signals emitted by CY5 and that they are a promising substitute for traditional optical scanners. The schematic of the experimental setup developed for DNA microarray application is reported in Figure 3.5.
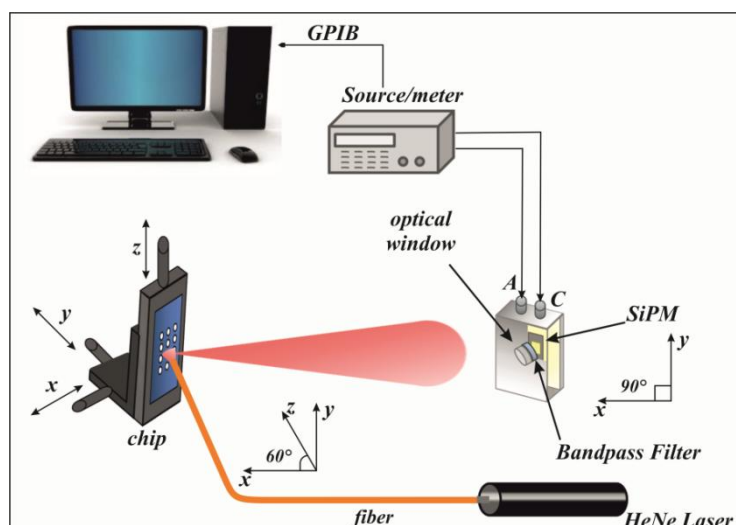
Figure 3.5: Schematic of experimental setup, based on SiPM Technology, for DNA microarray application.

The optical system implemented for DNA microarray is based on a fiber-coupled laser that hits at 60° with respect to the normal axis to the sample. CY5 is the marker to detect DNA hybridization and a HeNe laser at 633 nm was used to excite it. The sample was mounted on a xyz stage to allow its movement thereby intercepting the laser beam within the small spot to be measured. The miniDom, containing the sensor, is placed on a goniometer to allow the operator to monitor the emitted fluorescence as a function of the detection angle. Between the miniDom's hole and the sensor is interposed a bandpass filter, centred at 670 nm (FWHM for both 10 ± 2 nm). The filter allows suppressing the laser radiation reflected by the sample surface, thus reducing the background noise. The sensor is biased through a 236 Keithley Source Meter, that measures also the sensor output signal. The measurement system is based on a software opportunely developed in Labview®, that allows to control the bias voltage, the measurement conditions (angle of analysis and other key parameters), and to acquire the output signal automatically. The signal acquired is elaborated offline by a routine developed in Matlab®.

3.3.2   *Experimental results and data analysis*

To evaluate the optical sensor performances in DNA microarray applications, the fluorescence signal emitted by 25 bp oligonucleotides CY5 labelled was analysed.

30.7 nmol of GAPDHCy5 (/5Cy5/TGCCAACGTGTCAGTGGTGGACCTG/3AmMO/) lyophilized powder (from MWG Biotech) in 300 μl of water (DNase–RNase–Protease free) were suspended; then, sample were centrifuged at 5500 rpm for 30 minutes, after agitation in vortex, obtaining a 100 μM solution. A Sodium Phosphate Dibasic buffer (150 mM at pH 9.2) was used to dilute solution from 100 μM to 1 μM; 0.5 μM; 0.1 μM; 0.01 μM; and 0.001 μM, for optical measurements. After dilution, samples were dropped on 865 nm thickness aluminium-TEOS slides, following a specific layout (5 ×

10 array) reported in Figure 3.6; ten drops of 0.1 µl for each concentration were spotted, in order to study SiPM sensitivity, stability and reproducibility of the measurement. Samples dried at room temperature for 10 minutes.
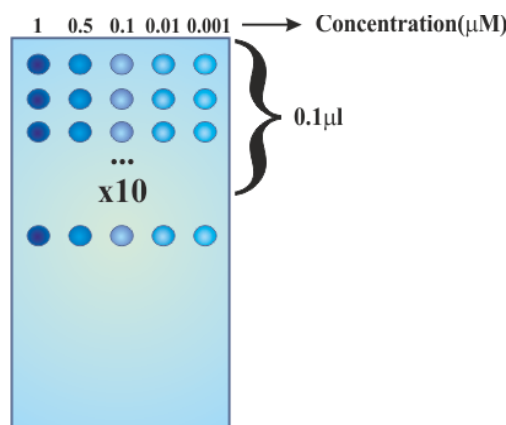
Figure 3.6: Schematic of spotting layout.

In order to define the SiPM experimental detection limit, the fluorescence emitted in different operating conditions in terms of analyte concentration and angle of analysis were measured (Figure 3.7). In particular, five different concentrations of ss-DNA labelled with CY5 were analysed: 1 µM (black dashed line), 0.5 µM (red dashed line), 0.1 µM (blue dashed line), 0.01 µM (green dashed line), 0.001 µM (orange dashed line).
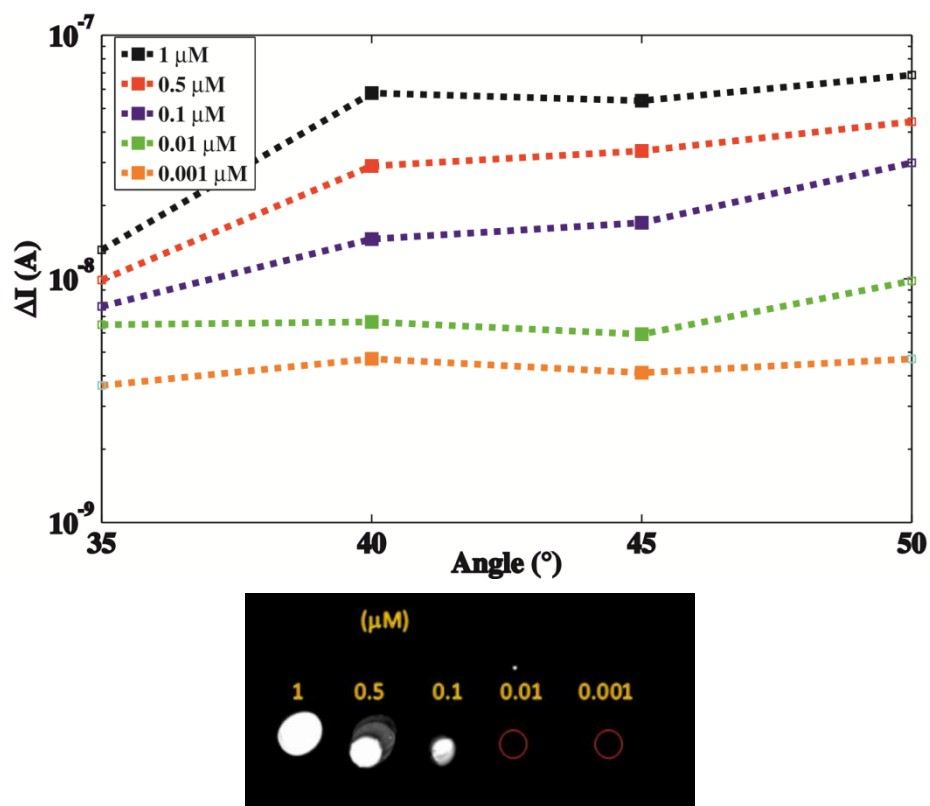
Figure 3.7: (top) Fluorescence behaviour of the ss-DNA labeled with CY5 as a function of the angle of analysis at a concentration of: 1µM (black dashed line), 0.5 µM (red dashed line), 0.1 µM (blue dashed line), 0.01 µM (green dashed line), and 0.001 µM (orange dashed line); (bottom) acquired image acquired by STMicroelectronics' OR.

Four angles of analysis were chosen to study the fluorescence behaviour: 35°, 40°, 45° and 50° with respect to the normal axis to the sample. Figure 3.7 shows that as the sample concentration increases, the emitted fluorescence increases as well. The current signal value at each concentration is roughly constant in the measurement angular range chosen, confirming the isotropic emission of fluorescence [34; 45; 46]. In existing measurement systems, an image is acquired and elaborated offline, after acquisition, to obtain a quantitative signal (Figure 3.7). The system based on SiPM technology, instead, provides directly a quantitative signal as output, in real time. This simplifies the software of analysis used to elaborate the data acquired. The system is easy to use, automated and more sensitive than commercial systems. In fact, it allows to measure also the small signal difference between two concentration values very close, that are indistinguishable with a commercial optical reader (section 3.2.3) (i.e. 1 µM and 0.1 µM). To define the measurement stability and the reproducibility, a 5×10 matrix, with drops of 0.1 µl for each concentration, was tested. The average value and the corresponding error for each concentration, for a fixed angle of analysis (40° with respect to the normal axis to the sample), are reported in Figure 3.8 and in TABLE 3.1.
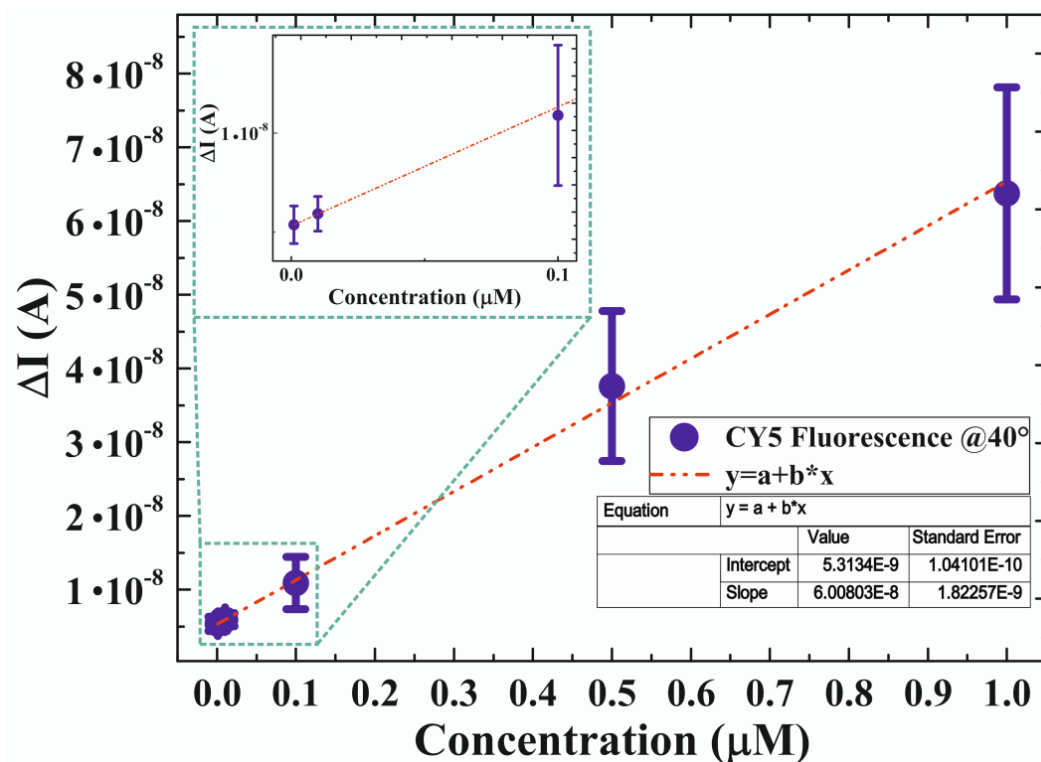
Figure 3.8: Fluorescence behavior of the ss-DNA labeled with CY5 varying the analyte concentration in the sample with the sensor placed at 40° with respect to the normal axis to the sample. The dashed line is the linear fit.

Concentrations (μM)	Average values (A)	Standard deviations	Errors %
1	$6.38 \cdot 10^{-8}$	$1.44 \cdot 10^{-8}$	22.588
0.5	$3.76 \cdot 10^{-8}$	$1.02 \cdot 10^{-8}$	27.000
0.1	$1.09 \cdot 10^{-8}$	$3.54 \cdot 10^{-9}$	32.511
0.01	$5.93 \cdot 10^{-9}$	$8.76 \cdot 10^{-10}$	14.768
0.001	$5.37 \cdot 10^{-9}$	$9.51 \cdot 10^{-10}$	17.695

TABLE 3.1: Average values and corresponding errors for ss-DNA CY5 labeled.

Figure 3.8 shows that the fluorescence current measured increases proportionally to the analyte concentration in the sample and the signal is linear in the range 1 nM–1 μM.

The data clearly show that the errors decrease with decreasing the analyte concentration in the sample. As mentioned before, it is because by reducing the fluorophore concentration the interaction between molecules reduces. At high dye concentrations, the interaction probability increases, hence a higher variability in the final fluorescence signal is measured. The measurement variability, due to cooperation phenomena, is not a dominant factor at low concentration. The measurements shown directly provide quantitative signal unlike traditional commercial systems [67; 68; 71].

Other interesting results are obtained by comparing the results of Figure 3.8 and 3.9 where the same samples have been measured with SiPM and a commercial reader, respectively. The data in Figure 3.9 were elaborated using two different image software: open-source software J-image [72] and the H-Mat software developed by STMicroelectronics [67].
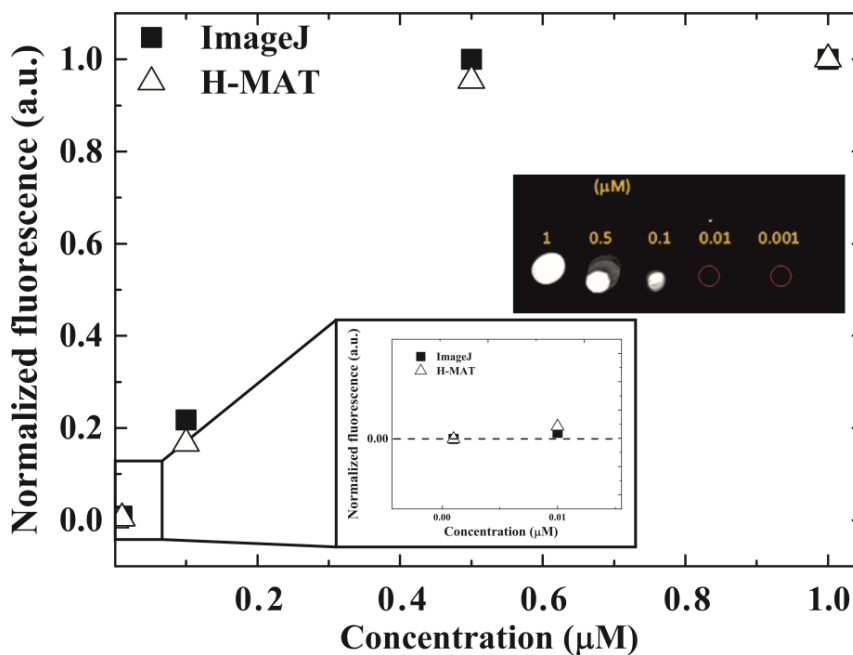
Figure 3.9: Fluorescence of CY5 spotted samples on Al/TEOS slides, as a function of the dye concentration, as acquired by using a commercial optical reader.

For high analyte concentrations (1 μM), the SiPM does not saturate; it is able to measure the small signal differences between the two highest concentrations, indistinguishable with a commercial optical reader. For low analyte concentrations (1 nM) the high SiPM sensitivity allowed to detect very low emitted fluorescence signals, not visible with a commercial reader. In fact, the enlargement of the two first points in Figure 3.9 clearly show that the signal is not detectable (the horizontal dashed line is the zero).

3.4   Conclusion

In this chapter the ability of SiPM, developed by R&D Sensor Team STMicroelectronics in Catania, to replace traditional detection system for DNA microarray applications was demonstrated.

Some interesting results were carried out from this work. First, the system based on SiPM technology provides a quantitative output signal. This feature simplifies considerably the output signal analysis with respect to traditional systems. In fact, optical readers, provide an image as output so an offline analysis allows the understanding of the results.

Moreover, from the analysis performed on five different concentrations of DNA labelled with CY5, GAPDHCy5, emerged that as the sample concentration increases, the emitted fluorescence increases as well. The current signal value at each concentration is roughly constant in the measurement angular range chosen, confirming the isotropic emission of fluorescence and the signal linearity in the range 1 nM–1 μM.

The direct comparison between traditional optical reader and SiPM showed that, thanks to its high sensitivity, SiPM is able to measure also the small signal difference between two concentration values very close, that are indistinguishable with a commercial optical reader. Finally, the high SiPM sensitivity allows to detect very low emitted fluorescence signals (1 nM), not visible with commercial reader.

Definitely, the system based on SiPM technology is easy to use, automated and more sensitive than commercial systems. These results open the possibility to fabricate and commercialize SiPM based detection systems for DNA hybridization.

Chapter 4

Real Time PCR

4.1 Introduction

The polymerase chain reaction (PCR) is one of the most powerful technologies in molecular biology. The PCR has been invented in 1983 by Kary Mullis (Nobel Prise in 1993) [73]. Three years after its invention, there was an incredible expansion of its use thanks to the commercialization of the Taq polymerase, a polymerase able to resist at high temperatures. In 1992, the technique was improved by the use of Ethidium Bromide (EtBr), which emits fluorescence when it binds to duplex DNA [74]. The kinetics of fluorescence accumulation during thermocycling was directly related to the starting number of DNA copies. This was the starting point of quantitative PCR (qPCR). Today, 33 years after Mullis's discovery, both PCR and qPCR are widely used technologies. The principle, and aim, of the PCR technology is to increase specifically a target from an undetectable amount of starting material. In end-point PCR, at the end of the amplification, the product can be run on a gel for detection of this specific product. In Real-Time PCR, this step is avoided, since the DNA amplification and the immediate detection of the products occur in the same tube. Thus, it reduces the significant contamination risk caused by opening tubes for post-PCR manipulation. Moreover, less time than gel-based analysis is needed and it provides quantitative result [75].

PCR amplifies DNA exponentially, doubling the number of target molecules with each amplification cycle. When it was developed, scientists reasoned that the number of cycles and the amount of PCR end-product could be used to calculate the initial quantity of DNA copies by comparison with a known standard. In order to obtain a robust quantification, the technique of real time quantitative PCR was developed and end-point PCR is used mostly to amplify specific DNA for sequencing, cloning, and use in other molecular biology techniques. In real time PCR, the amount of DNA is measured at the end of each cycle via fluorescent dyes that emit increasing fluorescent signal proportional to the number of PCR product molecules (amplicons) generated. Data are collected in the exponential phase of the reaction and provide quantitative information on the starting quantity of the amplification target. Fluorescent reporters used in real time PCR include double-stranded DNA (ds-DNA)-binding dyes, or

41

dye molecules attached to PCR primers or probes that hybridize with PCR product during amplification. An instrument that is able to realize thermal cycling and a scan measures the fluorescence over the course of the reaction. By plotting fluorescence versus the cycle number, the real time PCR instrument provides an amplification plot that represents the accumulation of product over the duration of the entire PCR reaction [76]. The advantages of real-time PCR include:

- ability to monitor the progress of the PCR reaction as it occurs in real time;
- ability to precisely measure the amount of amplicon at each cycle, which allows highly accurate quantification of the amount of starting material in samples;
- an increased dynamic range of detection;
- amplification and detection occur in a single tube, eliminating post-PCR manipulations.

Over the past several years, real time PCR has become the leading tool for the detection and quantification of DNA or RNA. Using sequence-specific primers, the number of copies of a particular DNA or RNA sequence can be determined. By measuring the amount of amplified product at each stage during the PCR cycle, quantification is possible. If a particular sequence (DNA or RNA) is abundant in the sample, amplification is observed in earlier cycles; if the sequence is low, amplification is observed in later cycles. Quantification of amplified product is obtained using fluorescent probes or fluorescent DNA-binding dyes and real time PCR instruments that measure fluorescence while performing the thermal cycling needed for the PCR reaction. The method relies on a DNA-based probe with a fluorescent reporter at one end and a quencher of fluorescence at the opposite end of the probe. The probe arranges in a circle. The close proximity of the reporter to the quencher inhibits the fluorescence. The probe breakdown operated by the 5' to 3' exonuclease activity of the Taq polymerase [77] breaks the reporter-quencher proximity, thus, allowing unquenched emission of fluorescence, which is detected after light excitation. An increase in the product targeted by the reporter probe at each PCR cycle, therefore, causes a proportional increase in fluorescence.

Three major steps make up each cycle in a real time PCR reaction.

1. *Denaturation:* High temperature incubation is used to "melt" double-stranded DNA into single strands and loosen secondary structure in single-stranded DNA. The highest temperature that the DNA polymerase can withstand is typically used (usually 95°C).

2. *Annealing:* During annealing, complementary sequences have an opportunity to hybridize, so an appropriate temperature is used that is based on the calculated melting temperature (T_m) of the primers (5°C below the Tm of the primer).

3. *Extension:* At 70-72°C, the activity of the DNA polymerase is optimal, and primer extension occurs at rates of up to 100 bases per second. When an amplicon in real time PCR is small, this step is often combined with an annealing step at 60°C.

Reactions generally run for 40 cycles.

PCR can be divided into four major phases (Figure 4.1): the linear ground phase, early exponential phase, log-linear (also known as exponential) phase, and plateau phase [78].
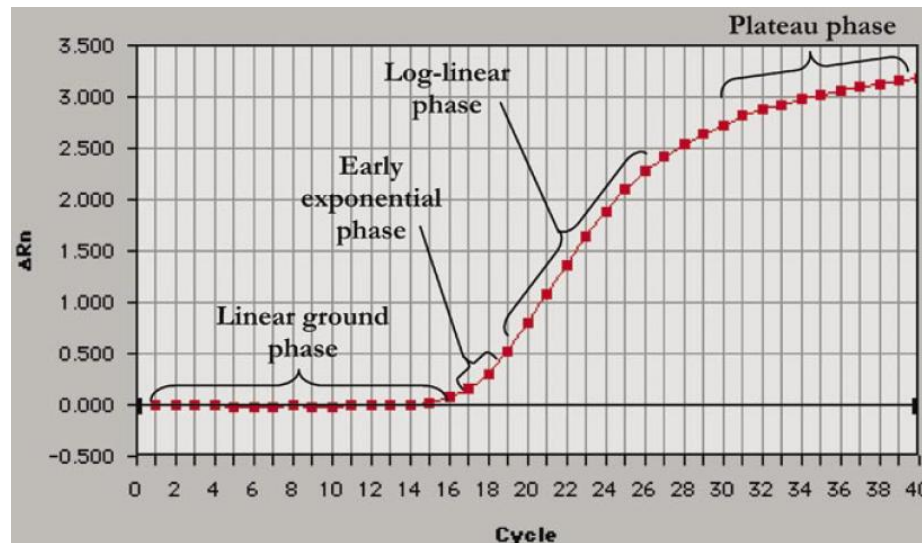
Figure 4.1: Phases of the PCR amplification curve.

During the linear ground phase (usually the first 10-15 cycles), PCR is just beginning, and fluorescence emission at each cycle has not yet risen above background. Baseline fluorescence is calculated at this time. At the beginning of exponential phase, the amount of fluorescence has reached a threshold where it is significantly higher (usually 10 times the standard deviation of the baseline) than background levels. The cycle at which this occurs is known as C_T in ABI Prism® literature (Applied Biosystems, Foster City, CA, USA) or crossing point (C_P) in LightCycler® literature (Roche Applied Science, Indianapolis, IN, USA) [77; 79]. This value is representative of the starting copy number in the original template and is used to calculate experimental results [77]. During the log-linear phase, PCR gets its optimal amplification period with the PCR product doubling after every cycle in ideal reaction conditions. Finally, the plateau stage is reached when reaction components become limited and the fluorescence intensity is no longer useful for data calculation [80]. Reactions generally run for 40 cycles because many DNA copies are needed to be detected by traditional optical detection systems. The implementation of a optical sensor more sensitive than traditional detectors could reduce the C_T value, and translate on the left the output curve, reducing the time of analysis, since less cycles of reactions are needed.

4.2   Real Time PCR Technology

4.2.1   Bio-rad Technology

The Real time PCR detection systems developed by Bio-rad consist of:

- *Reaction module* - samples are heated and cooled to precise temperatures to obtain nucleotide denaturation, annealing, and then polymerase-mediated extension for each round of DNA amplification;

- *Optical detection system* - in the presence of a fluorescent reporter, such as a DNA-binding dye or labelled probe, measurement of the fluorescence intensity of each PCR reaction allows the determination of the target of interest presence within an experimental sample;

- *Instrument software* - real time PCR detection systems are typically controlled by a computer running specialized software that initiates and monitor runs and then facilitate the interpretation of the results.

The reaction module is based on a Peltier cell. Most thermal cyclers in use employ this approach. It uses a solid-state active heat pump that transfers heat from one side to the other versus a temperature gradient with the consumption of electrical energy. One very useful feature of Peltier blocks is that a thermal gradient (Figure 4.2) can be established, allowing optimization of an assay annealing step in a single run [81]. This type of instrument uses a chamber in which tubes are suspended and air at a defined temperature is circulated for specified periods as required for PCR.
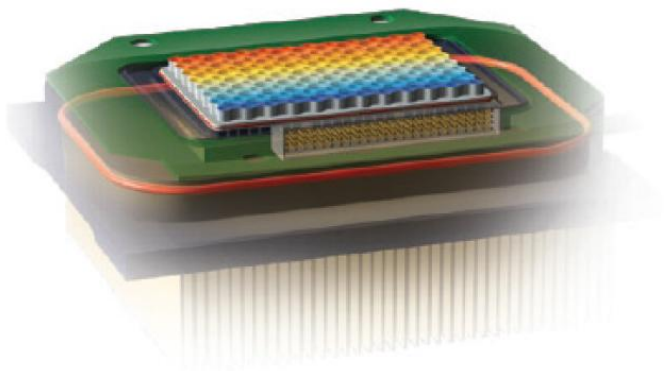
Figure 4.2: Reaction module of Real Time PCR Platform developed by Bio-rad [81].

Reaction blocks come in multiple formats with the most common being a 96 wells block (Figure 4.3) with reaction volumes ranging from 1 μl to 125 μl. Blocks with more than 384 wells typically use microfluidics with volumes from the pico to the nanoliter range.
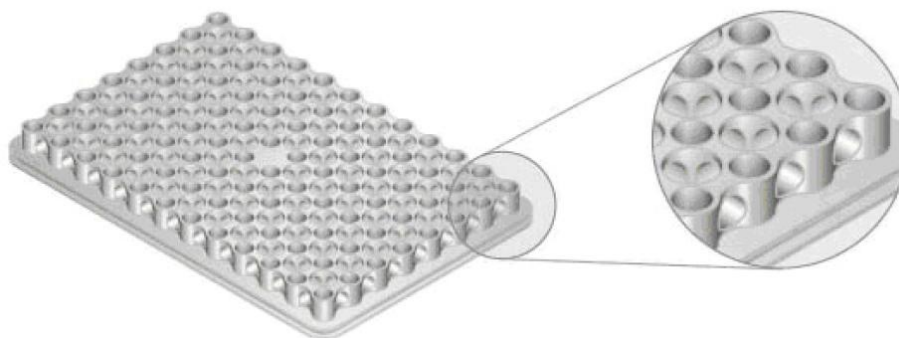
Figure 4.3: Reaction block of RT PCR Platform [81].

To measure the amount of fluorescence in real time PCR reactions there is a wide variety of optical systems using a combination of light sources, filters, and detectors. In figure 4.4 are reported three different optical systems used in three RT-PCR platforms developed by Bio-rad (CFX96, MiniOpticon™, iQ™5).
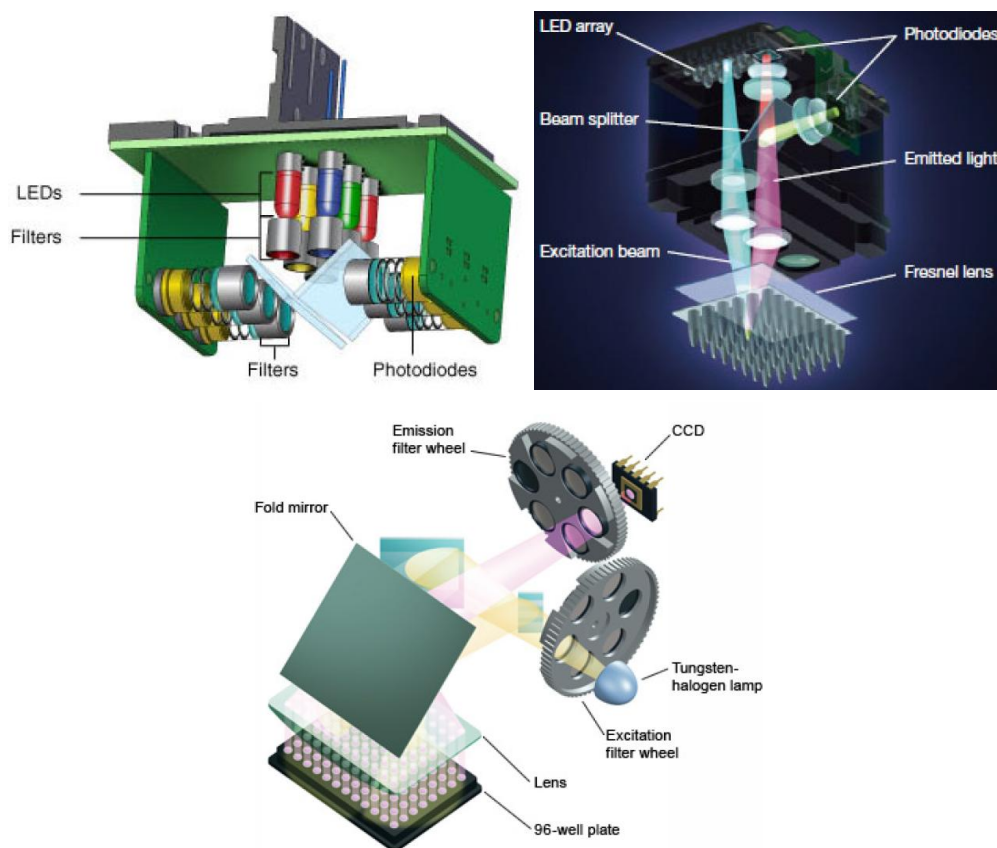
Figure 4.4: RT PCR detection system optics of CFX96(top left), MiniOpticon™(top right) and iQ™5(bottom) [81].

In CFX96 Six filtered LEDs and six filtered photodiodes are used for excitation and detection. Light is filtered in a narrow bandwidth, ensuring that only data from the desired fluorophores are collected. In this case, a movable device detects the light emitted by excited fluorophores.

In MiniOpticon™ forty-eight LEDs fire in rapid succession, illuminating a single sample at a time, while a Fresnel lens focuses each beam directly down into the centre of the corresponding well, minimizing light loss. Emitted fluorescence is split into two beams that pass through separate filters to two sensitive photodiodes. In this case, a stationary device detects the light emitted from excited fluorophores.

In iQ™5 all 96 wells are excited by a combination of narrow bandpass filters and a tungsten-halogen lamp. Filtered light from the lamp is reflected off mirrors, passes through a condensing lens, and is focused into the centre of each well. Fluorescent light emitted from the wells reflects off the main fold mirror, passes through an emission filter, and is detected by a 12-bit charge-coupled device (CCD).

There are several types of detectors used in real time PCR instruments.

- Photodiode (CFX96 and MiniOpticon™) has a wide spectral range, is rugged, with low failure rates, and can be quite compact in size.
- CCD (iQ™5) converts the light that it captures into digital data. The quality of the image captured is determined by the resolution (measured in megapixels). CCDs capture an image of the reaction plate, whose content is interpreted offline by a software.

4.2.2 *STMicroelectronics Technology*

The miniaturization of a real time PCR amplification system is one of the most important features needed for genetic point-of-care (PoC) diagnostics to offer *sample-in answer-out* analysis. Miniaturization typically allows shorter analysis times, reduces reagent consumption, the risk of sample contamination, and often enhances assay performances. This section describes the genetic real time PCR PoC system based on a silicon microchip able to address the quantitative and qualitative identification of multiple analytes of specific nucleic acids (DNA, RNA) sequences developed by STMicroeletronics [82]. This platform exhibits an improvement of sensitivity with respect to other commercial tools thanks to the combination of integrated silicon temperature sensors and heaters, specific chip design architecture and smart detection software. Figure 4.5 shows the miniaturized Bio2Bit Q3 Real time PCR platform able to perform quantitative and qualitative identification of multiple analytes of specific nucleic acids (DNA, RNA) sequences in a PoC format. The platform is based on a silicon microchip, which integrates in the same device both real time PCR micro reactors (6-15 µl in volume), silicon temperature sensors and integrated heaters. Thanks to the integrated sensors and heaters, the chip allows a temperature control accuracy of ±0.2°C, heating rate of 15°C/s and cooling rate of 8°C/s. Moreover, the specific chip design architecture [83] enhances the optical fluorescent signal and, in combination with a smart detection software, provides an improvement of sensitivity with respect to the commercial tools. A miniaturized instrument, specifically developed, drives the chip thermally and optically.

Figure 4.5: qRT PCR platform developed by STMicroelectronics [82].

The real time PCR System is composed by the following components: (a) disposable chip equipped by reaction chambers for the real time PCR process; (b) portable and customized thermocycler instrument (Q3 reader) which thermally and optically drives the chip during the real time PCR process; (c) software package, which manages the PCR, process and carries out the data analysis. Figure 4.6 reportes the Q3 instrument reader developed by STMicroelectronics.
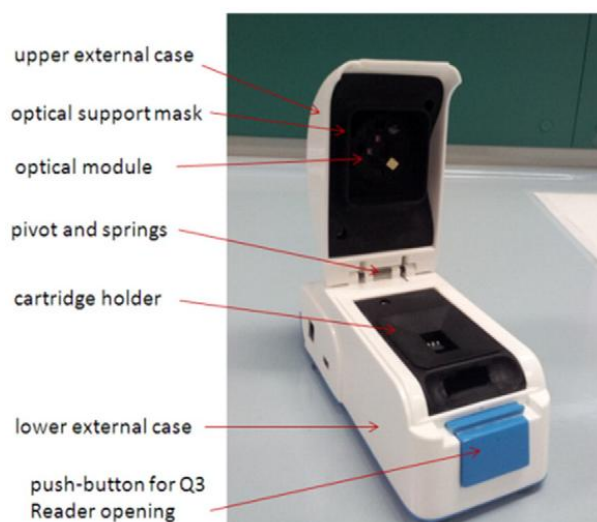
Figure 4.6: Q3 reader of Real Time PCR Platform [84].

The Q3 thermally and optically drives the chip during the real time PCR process. It has a size of 14 L × 7.1 W × 8.7 H (cm) (weight: 322 g). Up to two independent optical channels equip the optical module, for multiple fluorescent reporters (FAM, VIC®). The LED light sources are centered at 470 and 530 nm. A CMOS camera that contains a high-pass filter at 520 nm and a 20 nm wide band-pass filter centered at 556 detects the emission. Finally, the thermal Module drives the temperature sensor and heater of the chip to reach the pre-set temperatures. The smart-software developed for the image analysis is based on three main core modules. A fully automatic image quantification, a set of algorithms for the digital image analysis process, a numerical computation module containing a set of algorithms for the numerical analysis of raw data coming from real time PCR. A graphical user interface to show the fluorescence curves for the PCR. The core of the platform is a silicon-plastic hybrid microchip (Figure 4.7) composed by:

a. A bottom part made in silicon by VLSI (Very-large-scale integration) technology on a six-inch silicon wafer. It contains the temperature sensors and heaters integrated. (Figure 4.7a). They consist in AlCu metal strips (size 4.0 ± 0.1, spaced 5.0 ± 0.1 μm for the temperature sensor, size 115.0 ± 0.1 μm spaced 30.0 ± 0.1 μm for the heater). The device perform thermal cycling in combination with the driving instrument (Q3-reader below described) with the following performances: temperature sensor maximum power consumption 55 mW, heater maximum power consumption 10 mW, temperature control accuracy of ± 0.2°C, heating rate of 15°C/s, cooling of rate: 8°C/s and temperature resolution: 0.1°C (82).

b. A top part (ring) made in polycarbonate. The ring was manufactured by molding technology and combines an architecture containing six reaction chambers with cylindrical shape featured by a volume of 25 μl (Figure 4.7b). A silicone glue glues the ring onto the silicon part.

c. A plastic holder to facilitate the chip handling (Figure 4.7c).
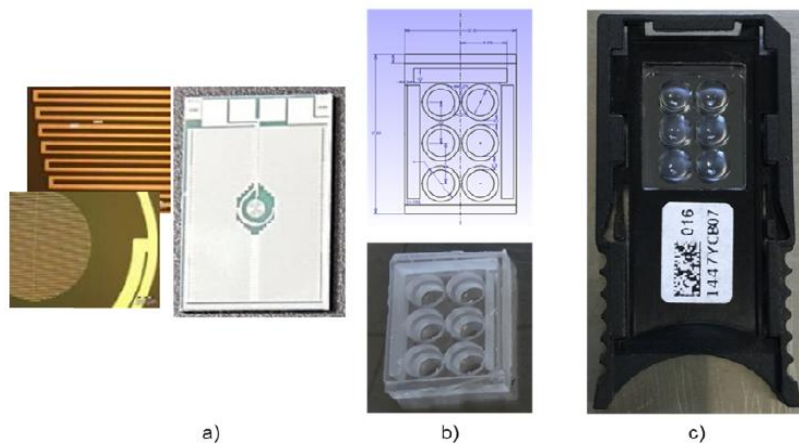
Figure 4.7: qRT PCR platform developed by STMicroelectronics: a) silicon part; b) polycarbonate ring and c) disposable microchip.

4.3   Novel promising technology based on SiPM

The challenge of reducing the system physical size and increasing the low detection limit of analyte concentration in the sample led us to implement a new platform, based on SiPM technology, for Real Time PCR [28].

4.3.1   Experimental setup

The platform implemented for the measurements suitable in real time PCR applications, is similar to the setup previously described for DNA microarray application (section 3.3). The main difference lies in the sample positioning, since the measurement is performed on liquid. The dies used are hybrid polycarbonate-silicon chips equipped with six or 12 wells (volume of each well 20 μl) developed by STMicroelectronics similar to those already developed for the Q3 platform (see previous section). They are inserted in an "x, y mount" parallel to the optical table. The sensor, placed on an "articulating base" that provides free spherical motion over a complete hemisphere, is blocked at 45° with respect to the normal axis to the optical table; laser hits normally to the sample (see Figure 4.8). A "fibre optic cannula" is used since a small and compact optical probe is needed (insert of Figure 4.8). This improvement allows exciting the single well and collecting the fluorescence signal it emits. This work reports only measurements performed at room temperature. Measurements by performing the thermal short cycle involve a Peltier cell (programmed by PC) placed under the "x, y mount", very close to the sample. Setup arrangement and measurements are still in progress.

In this optical systems, the sensor is biased through a 236 Keithley Source Meter, that measures also the sensor output signal. The measurement system is automated by a software opportunely developed in Labview®, that controls the bias voltage, the measurement conditions (angle of analysis and other key parameters), and records the output signal automatically. The signal acquired is elaborated offline

by a routine developed in Matlab®. Depending on the analyzed fluorophore, both the band-pass filter and the excitation source were changed. HeNe laser at 633 nm or Ar laser, at 488 nm, and bandpass filters either centred at 670 nm or at 520 nm (FWHM for both 10 ± 2 nm) were used to excite CY5 and FAM (see after) and collect their emitted signals, respectively. The measurement system is very versatile and lends itself to many applications that can space from biomedical, to environmental fields [71; 85].
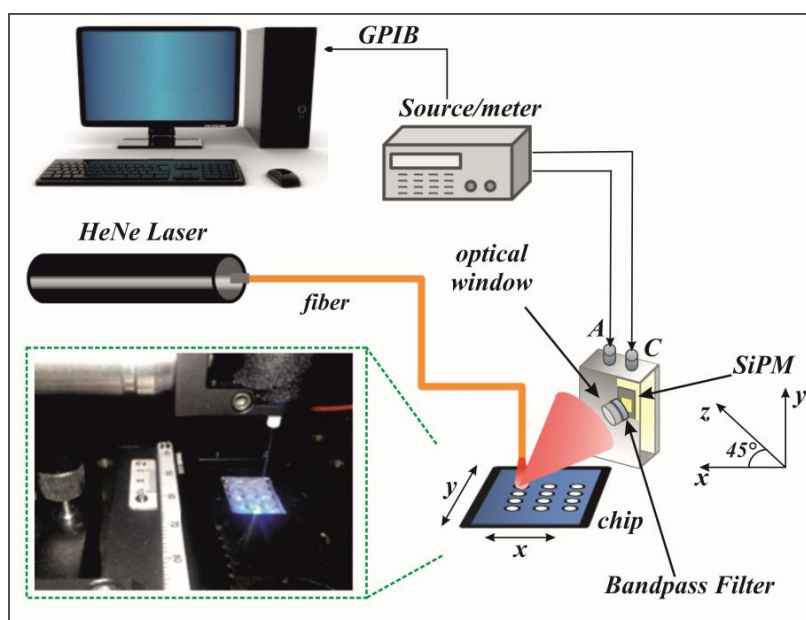
Figure 4.8: Experimental setup for liquid samples characterization.

4.4 Experimental results and data analysis

The optical sensor performance evaluation for real time PCR applications was carried out measuring the fluorescence signal emitted by two different fluorophores commonly used in PCR, CY5 and Fluorescein amidite (FAM), and by changing their concentration in the sample. The reference, needed to subtract the background noise to the fluorophores measurements, was prepared by filling a well with 10 μl of milliQ water and 2 μl of oil. The current detected when the laser light was scattered and/or diffused by the reference well was the reference current. The fluorescent signals from the remaining wells were calculated subtracting this reference. The characterization performed for both fluorophores is described in the following sections.

4.4.1   *FAM characterization*

FAM powders (from Sigma-Aldrich) was suspended in water, to obtain a 1 μM solution and diluted to a concentration of: 5 nM, 500 pM, 50 pM, 5 pM, 500 fM. 10 μl of solution and 2 μl of a mineral oil,

used to prevent liquid samples evaporation, were dropped in three identical chips equipped by six wells following the spotting layout reported in Figure 4.9. The wells are 3 mm in diameter and 2 mm in heights. All the water used was DNase-RNase-Protease free water (from Sigma Aldrich). In each chip, a reference well filled by water and oil is present. The laser light diffused by this well provides the reference and is subtracted to the signal collected by the other wells in order to obtain the real value of fluorescence emitted by samples.
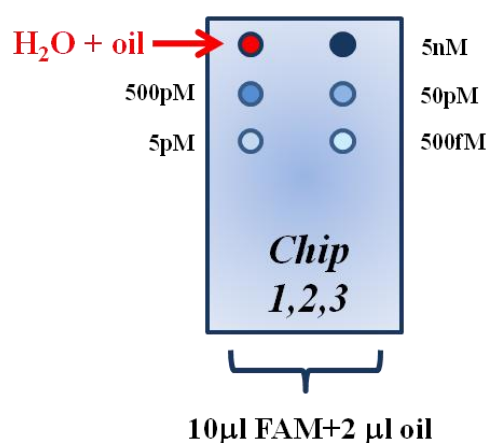
Figure 4.9: Schematic of FAM spotting layout.

FAM characterization consisted in the measurement of the five different concentrations above indicated. The average values and the corresponding errors for each concentration were calculated and are reported in Figure 4.10.
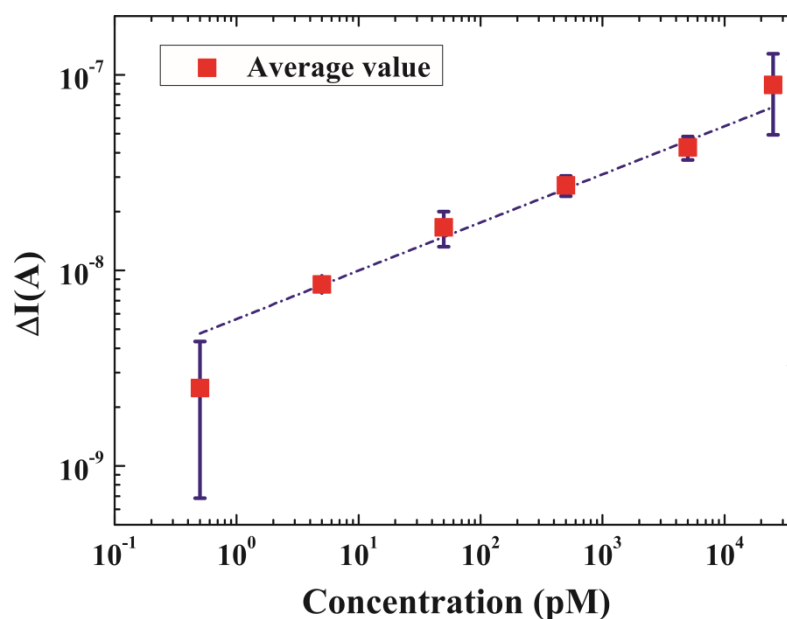
Figure 4.10: Fluorescence of the FAM solutions varying the concentrations of fluorophore in the sample with the sensor placed at 45° with respect to the normal axis to the sample.

The measured fluorescence current increases proportionally to the analyte concentration in the sample in the range 500 fM–5 nM, over four orders of magnitudes.

4.4.2   CY5 characterization

CY5 powders (from Lumiprobe) was suspended in water, in order to obtain a 1 μM solution and diluted to a concentration of: 100 nM, 10 nM, 1 nM, 100 pM, 10 pM, 1 pM, 100 fM. 10 μl of solution and 2 μl of a mineral oil, used to prevent liquid samples evaporation, were dropped in two identical chips equipped by 12 wells, following the spotting layout reported in Figure 4.11. Also in this case, the wells are 3 mm in diameter and 2 mm in heights. Each chip is equipped by a reference well filled by water and oil. The laser light diffused by this well provides the reference signal and is subtracted to signal collected by the other wells in order to obtain the real value of fluorescence emitted by samples.
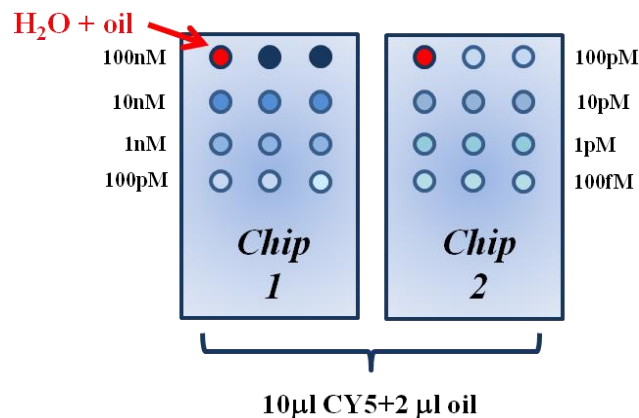
Figure 4.11: Schematic of CY5 spotting layout.

CY5 characterization consisted in the measurement of the seven different concentrations just mentioned. The average values and the corresponding errors for each concentration were calculated and are reported in Figure 4.12.
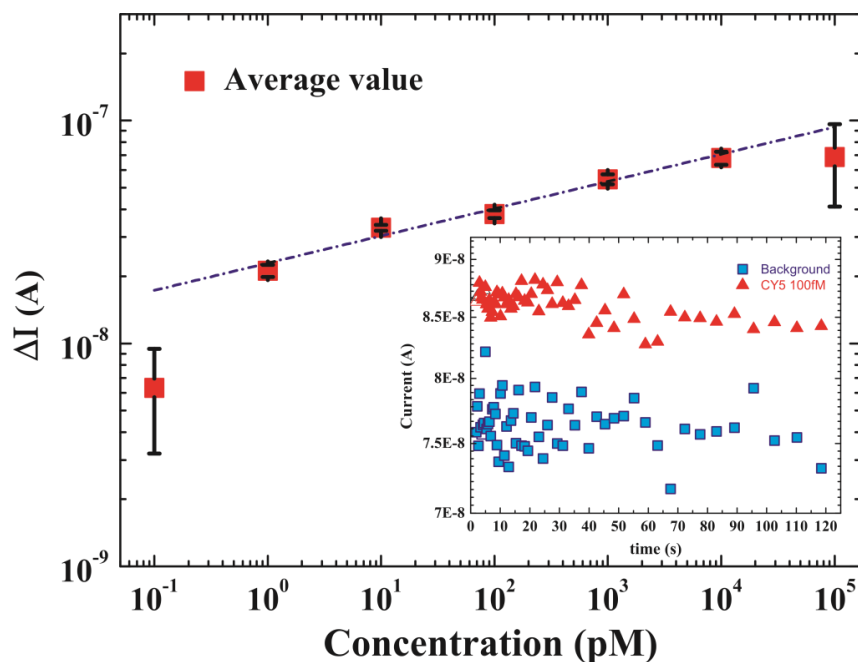
Figure 4.12: Fluorescence of the solutions of CY5 varying the concentrations of fluorophore in the sample with the sensor placed at 45° with respect to the normal axis to the sample.

The measured fluorescence current increases proportionally to the analyte concentration in the sample in the range 100 fM–100 nM, over six orders of magnitudes. The fluorescence current as a function of time for the lowest concentration of CY5 measured, is also shown as insert in Figure 4.12, with the noise current plotted for comparison. The data show a signal well above the noise. Moreover, the current is roughly constant over time. It should be mentioned that the laser light was shining the entire well and only one.

4.5   Conclusion

In this chapter, the potentialities of SiPM, developed by R&D Sensor Team STMicroelectronics in Catania, to replace traditional detection system for Real Time PCR applications were demonstrated. Some interesting results were carried out from this work. The system based on SiPM technology provides a quantitative output signal. This result simplifies considerably the output signal analysis with respect to traditional systems. In fact, traditional systems, provide as output an image and an offline analysis is needed to quantify the results.

The analysis performed on FAM and CY5, indicate that the system, based on SiPM technology, is able to detect very low fluorophore concentrations (500 fM for FAM and 100 fM for CY5). Moreover, when the sample concentration increases, the emitted fluorescence increases as well. In particular, both fluorophores exhibit a nonlinear increase of the luminescence signal with dye concentration. It is because when the dye concentration in the sample increases, the probability of interaction between molecules increases accordingly. It is known that CY5 aggregation causes a decrease of the emitted fluorescence for a fixed concentration, since, probably, non-radiative de-excitation paths form [86; 87]. Therefore, an increase of the concentration will produce an increase in the luminescence signal only as long as no interaction occur. The aggregates do not emit any fluorescence; hence, the florescence characteristics in terms of lifetime and emission spectrum does not change. In our samples, the aggregate presence can be inferred by the non-linearity of the signal as a function of the concentration. The results reported underline the SiPM extreme sensitivity and open up new possibilities to all those applications in which very small amounts of analyte must be detected.

Chapter 5

ATP bioluminescence sensor

5.1 Introduction

Optical transduction is certainly the most used detection method in biomedical field and, usually, it is employed in detecting the fluorescence emitted by markers used to label DNA fragments in DNA microarray and Real Time PCR applications. However, this method is used also to detect the bioluminescence emitted by living organisms. Bioluminescence is a process in which living organisms convert biochemical response into light. Such light is generated as a by-product of the excitation and subsequent de-excitation of electrons after a biochemical reaction. The main advantage with respect to fluorescence is that it does not require external sources of light excitation. An example is the adenosine tri-phosphate (ATP), the biological energy source, which reacts with luciferin with the aid of the enzyme luciferase to yield an intermediate complex. This complex combines with oxygen to produce a highly chemiluminescent compound. Luciferase systems are widely used in biomedical research, to label cells to make them visible under the microscope. Common applications of bioluminescence detection include in vivo studies of infection (with bioluminescent pathogens) [88], cancer progression (using a bioluminescent cancer cell line), and reconstitution kinetics (using bioluminescent stem cells) [89]. The luciferin - luciferase bioluminescence assay has successfully evidenced the effects of antibiotics on bacterial populations [90] and allowed scientists to distinguish cytostatic versus cytocidal potential of anticancer drugs on malignant cell growth [91].

This methodology allows the researchers to improve cancer investigation in several systems such as blood, brain, breast, fibrosarcoma, melanoma, pancreatic, prostate, and colorectal cancers.

For example, the monitoring of bioluminescence emitted by cancer cells could enable physicians in the evaluation of the individual response to cancer surgery and to the following treatments. Nowadays, the treatments used may include some combination of surgery, radiation therapy, chemotherapy and targeted therapy. Sometimes, cancers that are confined and may be curable with surgery while cancers that spread widely are usually not curable, with the treatments focusing on improving quality of life and reduce symptoms.

In cancer cells, the use of living cells as sensing systems is proved as valuable for prediction of the physiological response to radiotherapy and chemotherapy. Using bioluminescent assays, the toxic effects and specific biological activities of both radiotherapy and chemotherapy can be evaluated in an easy and straightforward manner. This methodology gives the researchers unparalleled sensitivity, wide dynamic range, versatility, no endogenous interferes from host cells and ease of use. For example, several studies present biomarkers in colorectal cancer that can predict a subpopulation of patients who are likely to respond to a given therapy [92-94]. The technology development on bioluminescent assays will provide a rapid and convenient mean for achieving better control over the biological significance of reporter data about these biomarkers by differentiating genetic responses of interest from irrelevant influences in cancer research. The technology may even be an application for identifying the biomarkers, which could be used for determining the therapy response of cancer patients in the future. Current technology for detecting bioluminescence, such as ATP assays or luciferase assays for studying promoter activity and signal transduction, is based mainly on performing tube-based reaction followed by detection of bioluminescent signal. This approach needs expensive laboratory equipment such as bioluminescent readers and bioluminescent imaging systems. These techniques do not allow kinetic measurements. Information on kinetics is obtained by sampling at discrete time points, which requires intensive and time consuming procedures. In addition, the detection is based on far-field optics, which limits the technology sensitivity.

This section describes the use of SiPM to detect luciferase bioluminescence. In particular, a SiPM-based detection system was design and applied to a real case, the ATP detection by using luciferase. The system proof of concept was performed using standard ATP bioluminescence assays.

5.2   ATP bioluminescence reaction

In order to fully understand the biological system that was chosen as testing case the Adenosine Triphosphate (ATP) structure and functionalities must be briefly addressed. ATP consists of adenosine, composed by an adenine ring and a ribose sugar, and three phosphate groups (Figure 5.1).
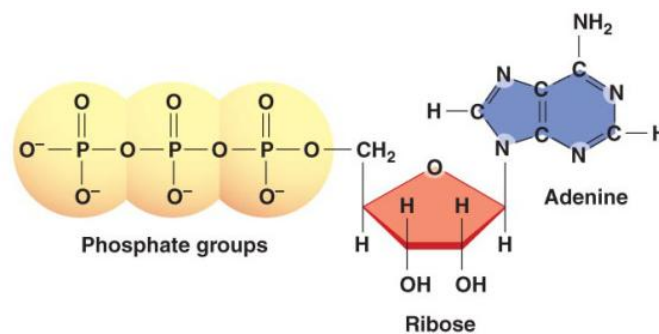

Figure 5.1: Adenosine Triphosphate (ATP) chemical structure [95].

ATP transports chemical energy within cells for metabolism and is involved by enzymes and structural proteins in many cellular processes, including biosynthetic reactions, motility, and cell division [96].

Since ATP is present in all living cells and decreases once the cells die, its presence is used also as an indication of the cell's viability and of the presence of cellular injuries. Besides of human health monitoring, ATP allows determining microbial activity in soil materials, freshness of fish, and is used as quality control of the functionality of blood prior to transfusion. Recent works indicate that ATP plays a key role in signal transduction [97-99] and in one type of neurotransmitters that is related to the sense of taste [100; 101].

ATP bioluminescence assays used in this work are obtained from Molecular Probes' ATP Determination Kit (A22066), which offers a convenient bioluminescence assay for quantitative determination of ATP with recombinant firefly luciferase and its substrate D-luciferin [102]. The assay is based on luciferase's requirement for ATP in producing light (emission maximum ~560 nm at pH 7.8) from the reaction:

$$luciferin + ATP + O_2 \xrightarrow[luciferase]{Mg^{2+}} oxyluciferin + AMP + CO_2 + pyrophosphate + hv \quad (5.1)$$
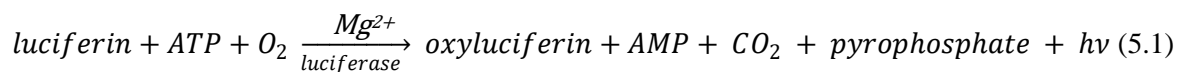
The assay typically involves the light-emitting pigment luciferin and the enzyme luciferase to catalyze the luciferin oxidation. This type of luciferin requires cofactors such as magnesium ions (Mg^{2+}) and the energy-carrying molecule adenosine triphosphate (ATP). Moreover, the amount of light emitted by luciferase is directly associated with the amount of ATP. Carbon dioxide (CO_2), adenosine monophosphate (AMP) and pyrophosphate (PP) are released as waste products.

5.3   Experimental

Nowadays, biomedical platforms to perform biological testing such as gene expression analysis, DNA sequencing, DNA amplification and quantification are expensive, bulky, characterized by large power consumption and require large amounts of reagents. Therefore, the growing need of point-of-care systems to perform biological analysis is driving the scientific community to develop miniaturized and low cost platforms, which allow cheap and in situ measurements. The challenge of reducing the system physical size, cost, power consumption and increasing the low detection limit of analyte concentration in the sample led us to implement a new platform, based on SiPM technology, for ATP bioluminescence detection.

Three different arrangements of the optical system were developed, in which three different sample holders are involved, respectively: glass tubes, PDMS chambers, and fluidic chip fabricated by a 3D printer. To test the systems designed and fabricated for this purpose, ATP solutions were prepared. The stock ATP solution was provided by Molecular Probes' ATP Determination Kit, with a concentration of 5 mM. We prepared seven different concentrations through successive dilutions: 1 µM; 500 nM; 250 nM; 125 nM; 62.5 nM; 31.25 nM; 15.625 nM. Moreover, the "Standard Reaction Solution (SRS)" was prepared. It is composed by: dH_2O (deionized water), 20X Reaction Buffer, dithiothreitol (DTT) with a concentration of 0.1 M, D-luciferin with a concentration of 10 mM and

firefly luciferase 5 mg/ml. Mixing between the SRS and ATP produces the biolominescence at 560 nm. Several concentration of ATP, ranging from 15.625 nM to 1 µM, were tested in this work and different arrangements of the experimental setup, optical systems, were developed, as described in the following sections.

5.3.1 *Optical system using glass tubes*

The optical sensor performances evaluation for ATP bioluminescence detection was carried out measuring different concentrations of ATP ranging from 15.625 nM to 1 µM (see before).

To demonstrate the power of the system based on SiPM technology, same samples were analyzed using both systems: a traditional commercial bioluminescence reader (PerkinElmer Victor 2030 with a detection limit able to measure a total flux from sample of 10^5 photons/s [103]) and the innovative system based on SiPM whose schematic is reported in Figure 5.2 (right).
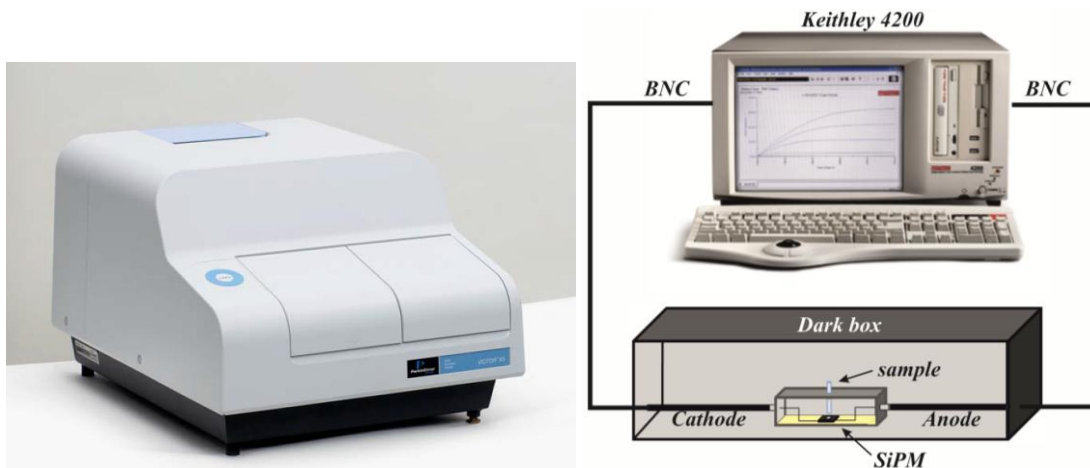
Figure 5.2: PerkinElmer Victor 2030 bioluminescent reader (left); Schematic of experimental setup for glass tube support based on SiPM technology (right).

The sensor, placed inside the MiniDom [26], was biased through a 4200 Keithley Source Meter, that measured and acquired the sensor output signal. The MiniDom was equipped by a glass tube (d=~5mm) containing the sample to be analyzed inserted in an opportunely fabricated hole (d=~6mm) in the MiniDom upper shield. The bottom surface of the glass tube was very close to the active area of the sensor (approximately 2 mm). All the described parts were placed inside a dark box to reduce the background noise. The measurement system is based on a specific setting of Keithley 4200, which allows to control the bias voltage (fixed at -30V), the measurement conditions (time of measurement), and to acquire the output signal automatically. The signal acquired was elaborated offline by a routine developed in Matlab®. For both measurements (using the commercial or the innovative optical system), a set of 24 samples having a volume of 100 µl (10 µl of ATP and 90 µl of SRS) were analyzed (three for each concentration and three of water, used as a reference). It should be pointed out that two different supports were used in the commercial reader and in the innovative system: Vision Plate™ 96 Well [104] and small glass tube with a 5 mm of diameter, respectively.

5.3.2   *Optical system using PDMS chambers*

The growing need to design miniaturized systems for biological analysis led us to fabricate several types of transparent PDMS chambers, with a thickness of 6 mm and different diameters: 2, 3, 4, and 6 mm (Figure 5.3). To fabricate flexible PDMS layers on Polyethylene Terephthalate (PET) films were involved two agents: the "Silicone Elastomer Base" and the "Silicone Elastomer Curing". The materials were mixed for few minutes and then deposited on a PET film having an aluminum foil as a flexible and low cost holder. The mixture of curing agent and PDMS base were prepared by a weight ratio of 1:10. To achieve a thickness of 6 mm different layers of PDMS are needed. In particular, each day a new layer of PDMS (with a ratio 4:40 between curing agent and PDMS base) was deposited, for a total time of 5 days. Then, using biopsy punches with different diameters, we realized holes inside the PDMS structure. After washing with water and ethanol, coverslips and PDMS wells underwent a plasma etching step and, then, wells were fixed on coverslips and put in the oven (at ~80°C) for few minutes.
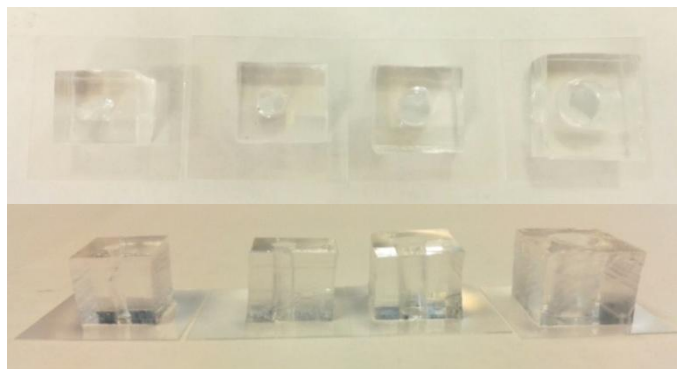
Figure 5.3: PDMS chambers of 6 mm thickness and having different diameters: (from left to right) 2, 3, 4, and 6 mm.

The experimental optical system used to measure the bioluminescence signal emitted by PDMS chambers filled by ATP solutions is very similar to the one reported in Figure 5.2. The main difference lies in the sample positioning, since PDMS chambers are placed on the top of sensor package, very close to the sensor active area (less than 2mm, Figure 5.4).
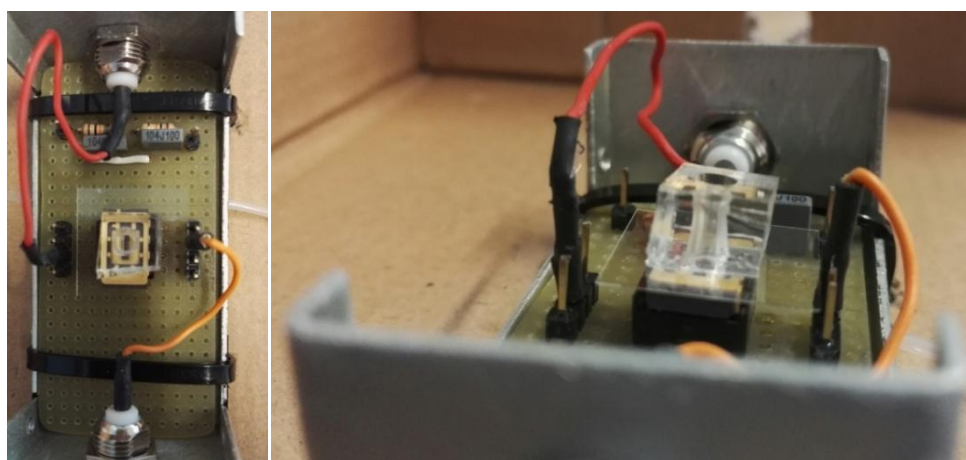
Figure 5.4: Experimental setup used to test ATP presence using PDMS chambers.

In this case the MiniDom was completely closed to reduce the optical background noise. In order to define the best PDMS chamber size and sample volume, different set of measurements were carried out following the scheme reported in TABLE 5.1. Several parameters are involved in these measurements: ATP concentration, solution volume, chamber diameter.

ATP initial Concentration	Chamber diameter [μl]	ATP volume [μl]	SRS volume [μl]	Total volume [μl]	ATP final concentration
2μM, 250nM, 31.25nM	2	2.5	2.5	5	1μM, 125nM, 15.625nM
		5	5	10	
		7.5	7.5	15	
	3	7.5	7.5	15	
		15	15	30	
		20	20	40	
	4	7.5	7.5	15	
		15	15	30	
		20	20	40	
		30	30	60	
	6	7.5	7.5	15	
		15	15	30	
		20	20	40	
		30	30	60	
		50	50	100	

TABLE 5.1: Scheme of measurement set.

Several volumes of three different concentrations (1μM, 125nM, 15.625nM) spotted in PDMS chambers with 2, 3, 4, and 6 mm of diameter were analyzed. As an example, Figure 5.5 reports the bioluminescent behaviours of four different volumes, in a chamber having a diameter of 4 mm, for three ATP concentrations.
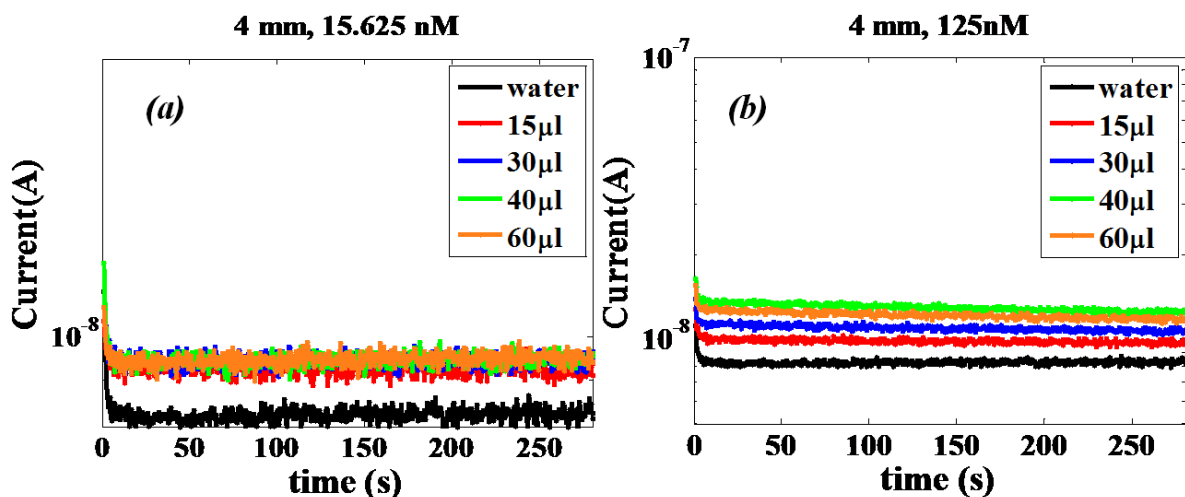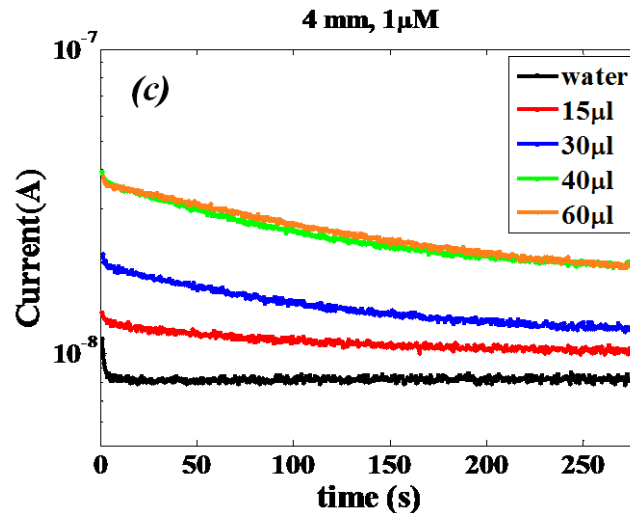
Figure 5.5: Bioluminescence signal acquired by SiPM for water (black lines), 15µl (red lines), 30µl (blue lines), 40µl (green lines), 60µl (orange lines) of three ATP concentrations: (a) 15.625nM; (b) 125nM; (c) 1uM, in a chamber having a diameter of 4 mm.

Figure 5.5 shows three different regimes:

- At low ATP concentrations, ~ 15 nM, the emitted bioluminescence signal is the same regardless of the solution volumes analysed. In fact, in this regime, by increasing the solution volume also the number of molecules increases but the reaction probability remains the same.

- Increasing the ATP concentration and the solution volume, 125 nM, the bioluminescence signal increases, but only up to a maximum volume value (40 µl). Further increasing the solution volume, the signal remains almost constant.

- At high ATP concentration, 1 µM, by increasing the solution volume both the number of molecules and the bioluminescence signal increase up to a limit, reached when the number of molecules is so high that the saturation level is approached (40 µl).

Figure 5.6 reports the comparison of the water (reference sample, black lines) signal and the bioluminescence signals emitted by 15µl of solution at 1µM (a), 125nM (b) and 15.625nM (c) of ATP inserted in PDMS chambers with four different diameters: 6mm (red lines), 4mm (blue lines), 3mm (green lines), and 2mm (dark green lines). Due to the small solution volume and different size of the PDMS chambers' diameter, the distribution of the solution is different for each structure. In fact, for chambers with 2 or 3 mm of diameter, the solution covers totally the surface and reaches different heights (thicknesses). In structures having 4 or 6 mm of diameter, the solution covers only partially the surface forming a drop. Hence, for medium and low levels of ATP concentrations (125nM and 15.625nM), the best diameter size is 6 mm because in this structure the solution is very close to the active area of the sensor and the bioluminescence produced is fully detected. On the other hand, for chambers having 2 or 3 mm of diameter, the bioluminescence produced is partially adsorbed by the solution along the path (thickness). At high ATP concentration (1µM), in chambers having 4 and 6 mm of diameter, either intermolecular effects prevail over adsorption phenomena or the other reagents are not in a suitable quantity to allow all the ATP to react. Hence, at high ATP concentration,

chambers with 2 or 3 mm of diameter ensure a detected bioluminescence signal higher than for chambers having larger diameters.
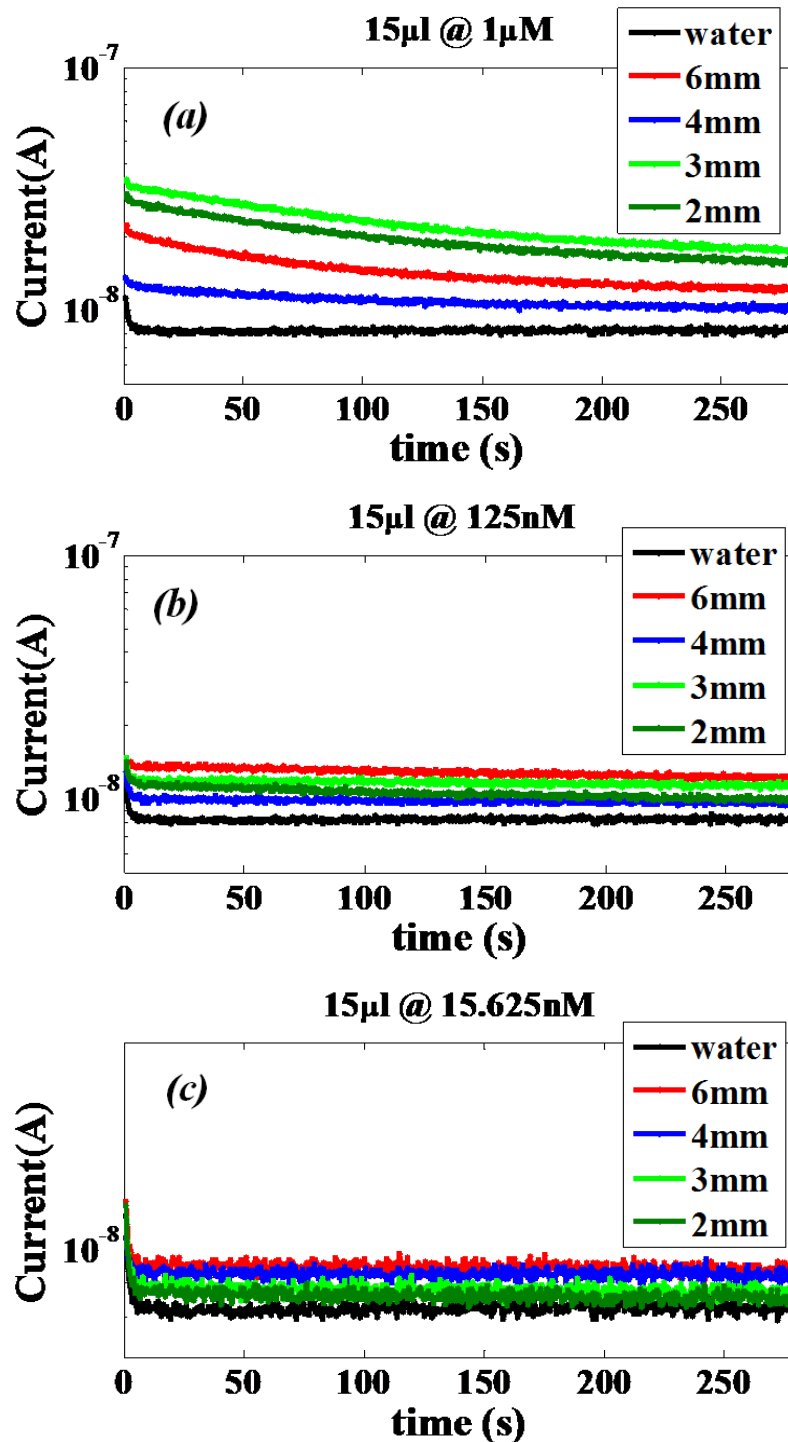
Figure 5.6: Bioluminescence signal of water (black lines) and 15μl of solution poured in PDMS chambers having a diameter of 6 mm (red lines), 4 mm (blue lines), 3 mm (green lines), 2 mm (dark green lines) at three ATP concentrations: (a) 1uM; (b) 125nM; (c) 15.625nM.

The reported experiments allowed defining the best operating conditions: 100μl of sample solution and 6 mm of chamber diameter size. These data were very useful for the design of the 3D printed microfluidic chips.

5.3.3   *Optical system using 3D printed microfluidic chips*

Fluidic chips commonly used for biological assays in most laboratories are fabricated using traditional methods suited for fast prototyping. Nowadays, efforts have been made for quick and easy fabrication of fluidically sealed devices with the development of three-dimensional (3D) printers. 3D printers build a chip layer by layer based on 3D computer software, such as Computer Aided Design (CAD). The fluidic chip developed and discussed in the following sections was designed using a CAD software (Autodesk® Inventor® Fusion 360, Autodesk Inc.), with a reaction chamber and open channels, providing easy access for functionalization, and the sub-micro-metric surface finishing enable to seal it with regular adhesive tape [105; 106]. Form 1+ 3D printer [107], reported in Figure 5.7, was used to fabricate the microfluidic chip, and a proprietary resin [105], with different proportions of modified acrylate and acrylate oligomer, epoxy monomer, acrylate monomer, photo initiator and additives as principal components was used.

Figure 5.7: 3D printer FormLabs (Form1+).

Less than 30 minutes are needed to print the chip and the prototype cost is less than 1 US$. The advantage is clear if one compares the fabrication time with the 5 days needed to fabricate the PDMS chambers. The microfluidic chip is composed by two different inlet ports with a diameter of 500 µm, through which ATP and standard reaction solution are separately injected; a mixing area formed by a single channel with a diameter of 500 µm in which the two different reagents react, thanks to the gravity; a reaction chamber, very close to the active area of the optical sensor, with a diameter of 6 mm and a volume of 100 µl; an outlet channel with a diameter of 1mm and an outlet port 500 µm large (Figure 5.8).
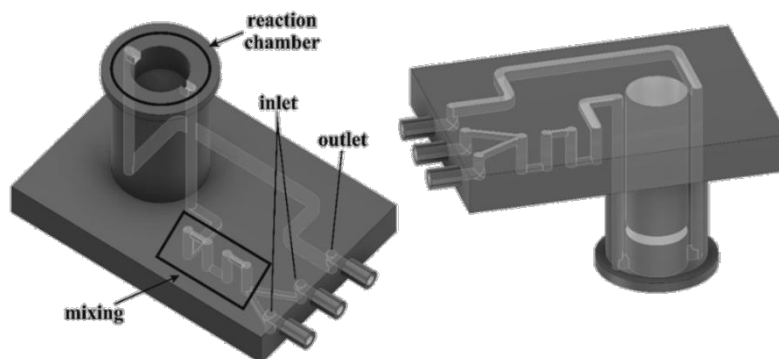
Figure 5.8: 3D printed microfluidic chip designed for a SiPM detection system.

The otpical setup used to measure the bioluminescence signal emitted in the reaction chamber filled by ATP solutions is very similar to the one reported in Figure 5.2. The main difference lies in the sample positioning, since the reaction chamber is inserted in the miniDom hole and it is very close to the sensor active area.

5.4   Results

The optical sensor performance evaluation for bioluminescence detection was performed measuring different ATP concentrations ranging from 15.625 nM to 1 µM and comparing two different optical systems setup. They are those having the glass tube and 3D printed microfluidic chip as sample holders. To demonstrate the sensitivity and the improved performances of the system based on SiPM technology, the same samples were analyzed also by using a commercial bioluminescence reader (PerkinElmer Victor 2030). The experimental data provided by the commercial reader were elaborated and the average values and the corresponding errors for each concentration calculated and reported in Figure 5.9 as luminescence counts in linear scale, and in Figure 5.10 after reference subtraction and in logarithmic scale.
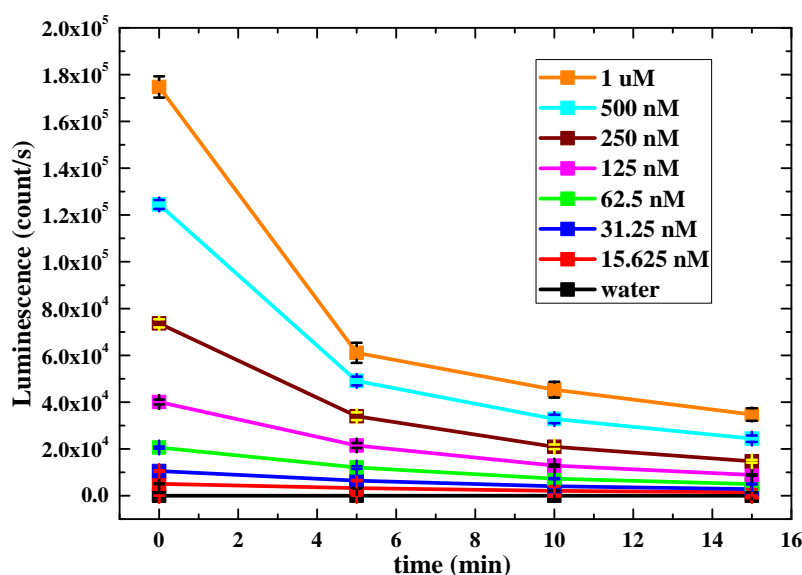
Figure 5.9: ATP bioluminescence signal at four time points (0, 5, 10, 15 minutes) for water (black lines) and seven ATP concentrations: 1uM (orange lines); 500nM (cyan lines); 250nM (brown lines); 125nM (magenta lines); 62.5nM (green lines); 31.25nM (blue lines); 15.6125nM (red lines).

Figure 5.9 shows the behaviour of seven ATP concentrations: 1uM (orange lines); 500nM (cyan lines); 250nM (brown lines); 125nM (magenta lines); 62.5nM (green lines); 31.25nM (blue lines); 15.625nM (red lines). The water signal (black lines) is also reported as reference. Data were acquired at four different time points: as inserted in the reader (indicated as zero), after 5 min, 10 min, and 15 min. Data show clearly that after 5 minutes the bioluminescence emitted is reduced by almost 60% of the maximum value. To remove the background signal, the water signal was subtracted to each signal, and the net bioluminescence value is reported in Figure 5.10.
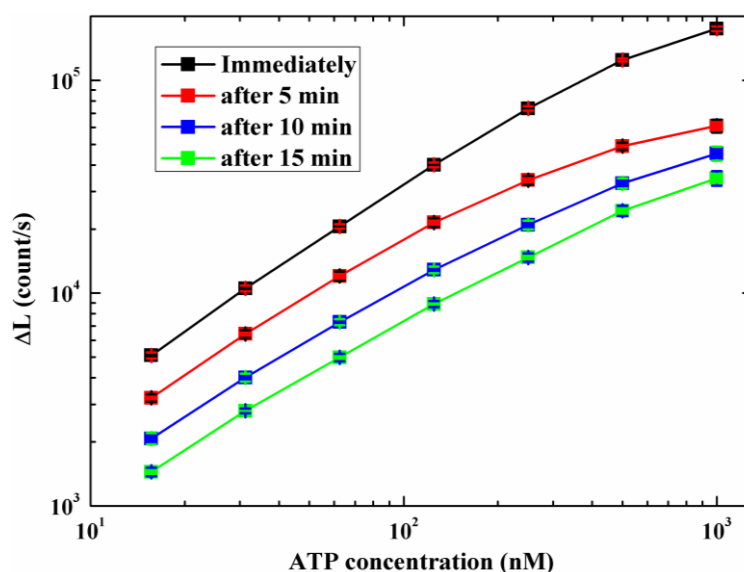
Figure 5.10: ATP bioluminescence signal as a function of the ATP concentration at four time points: 0 (black lines), 5 (red lines), 10 (blue lines), 15 (green lines) minutes.

Figure 5.10 shows as the signal reduction after the first five minutes mainly involves high concentrations. In fact, at low concentrations, the bioluminescence reduction is less pronounced. Moreover, the signals are not linear with ATP concentrations. Using the PerkinElmer Victor 2030 bioluminescent reader it was not possible to acquire the signal as a function of time from the reaction start, hence only four time points were selected. This limit was overcome by the innovative system based on SiPM technology we developed, which allows monitoring the bioluminescence signal as a function of the time from the reaction start instant. Three replicas for water and for each ATP concentration were analysed, for both systems. The average values for each concentration were calculated and are reported in Figure 5.11.
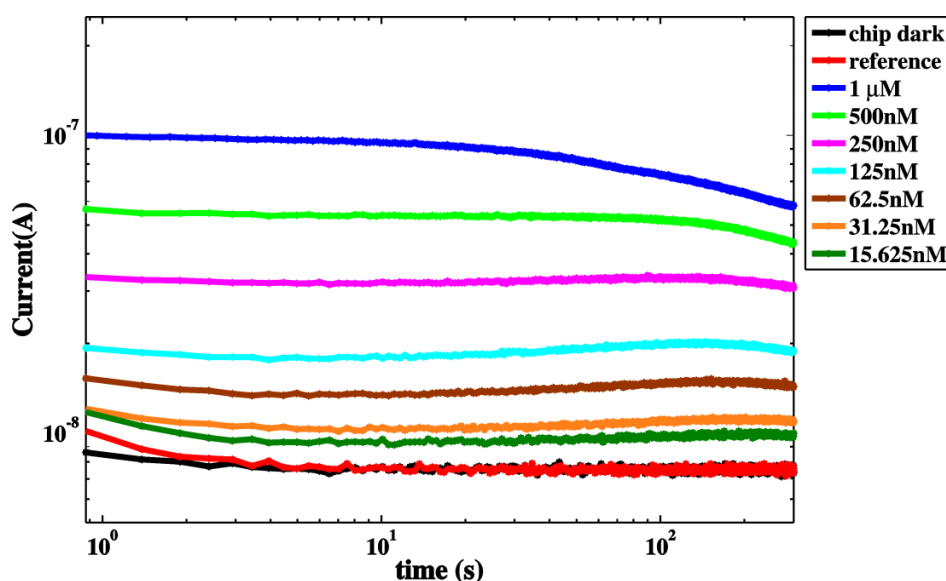
Figure 5.11: ATP bioluminescence signal versus time for seven different ATP concentrations: 1uM (blue lines); 500nM (green lines); 250nM (magenta lines); 125nM (cyan lines); 62.5nM (brown lines); 31.25nM (orange lines); 15.625nM (dark green lines); water (red lines) and dark (black lines) signals are also reported for comparison.

Figure 5.11 shows the good performances of SiPM in real time monitoring of the ATP bioluminescence. Moreover, it is able to detect the weak signals emitted by very low ATP concentration (15.625 nM). The possibility to make real time monitoring allows studying the bioluminescence reaction kinetics. Some interesting information can be carried out from the inspection of Figure 5.11: increasing the ATP concentration, the bioluminescence signal increases and, at high ATP concentration (1µM), a different behaviour with respect to the other concentrations can be observed. In fact, after 30 s a fast quenching occurs (please note the horizontal scale is logarithmic). It is probably due to the reaction components: when the ATP concentration is high, a lot of product forms in short times, hence the other reaction components (included in the SRS) are quickly consumed and the reaction tends to stop. It is confirmed by the fact that reducing the ATP concentration, the quenching occurs after longer reaction times. As an example, for ATP concentration of 500nM the quenching occurs after more than 100 s.

Analysing the reaction kinetics in Figure 5.11 it is possible to distinguish three different phases:

- a stabilization phase due to the technical time needed to the instrument for the auto setting (about 2s);
- an intermediate phase in which the signals are roughly constant;
- a final phase in which the signals slowly decrease due to the SRS consumption.

The bioluminescence signals recorded at 1µM, 125nM and 15.625nM of ATP concentration and reported in Figure 5.11 confirm the results already observed in Figure 5.5. The main difference between the two set of results is the signal intensity. In fact, at the same ATP concentration and solution volume the signal measured by using the glass tubes is higher than the signal measured by using the PDMS chambers.

The direct comparison between traditional and innovative systems showed that, thanks to its high sensitivity, SiPM is able to detect very low emitted bioluminescence signals (15.625 nM), as well as very expensive instrument commonly used, and it also allows monitoring the reaction kinetics in real time. Moreover, a disposable 3D printed microfluidic chip for continuous flow monitoring of ATP bioluminescence was developed during this Ph.D. experience and has been here described.

In order to demonstrate the power of the 3D microfluidic chips, three different ATP concentrations and the SRS are separately and manually injected, through two different inlet ports, using two syringes. Figure 5.12 reports the ATP bioluminescence signal as a function of time for three concentrations of ATP: 1uM (red lines); 125nM (blue lines); 15.625nM (green lines) and water (black lines).
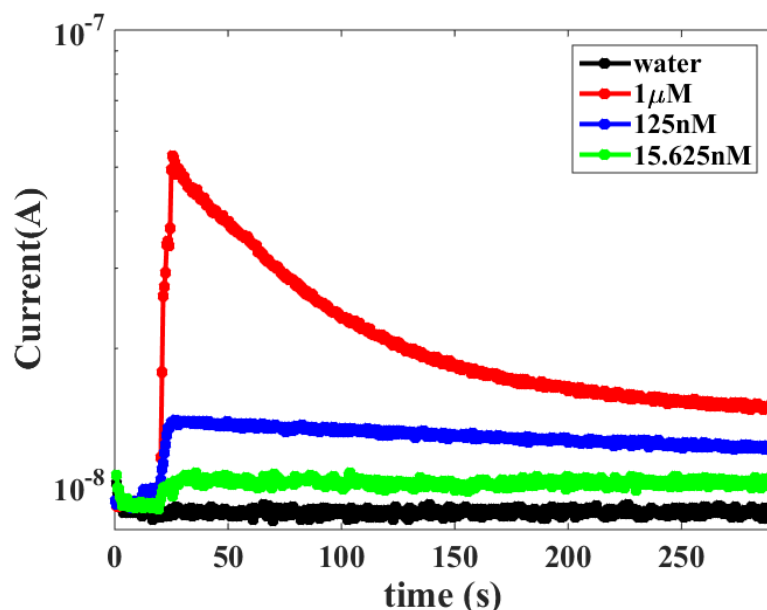
Figure 5.12: ATP bioluminescence signal versus time for three different concentrations of ATP: 1uM (red lines); 125nM (blue lines); 15.625nM (green lines) and water (black lines).

The signals at 1µM (in red), 125nM (blue) and 15.625nM (green) of ATP reported in Figure 5.12 confirm the results already discussed in Figure 5.5 and Figure 5.11. The direct comparison between the net bioluminescence signals acquired with all the instruments discussed (commercial reader, SiPM with glass tube and SiPM with a 3D chip) is reported in Figure 5.13.
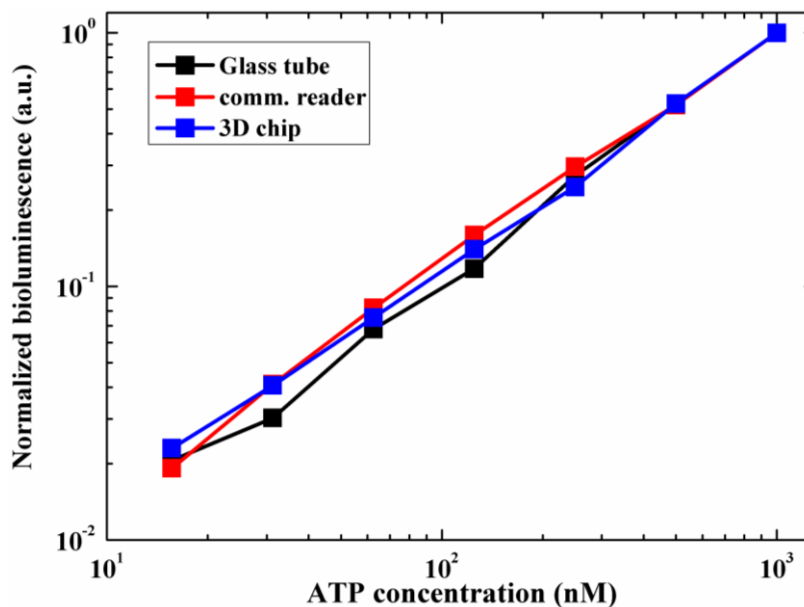
Figure 5.13: Comparison between data acquired by commercial reader (red lines), system for glass tube (black lines) and system based on 3D chip (blue lines).

Figure 5.13 shows as all the system compared exhibit the same sensitivity within the experimental errors in the analysed range of ATP concentrations.

By taking advantage from the SiPM high sensitivity and low noise, low levels of ATP concentrations were measured, showing good stability and reproducibility.

Finally, two NE-1010 Higher Pressure Programmable Single Syringe Pumps [108] were used to inject automatically the ATP solutions and SRS in the disposable 3D printed microfluidic chip in order to perform the continuous flow monitoring of the ATP bioluminescence signal. The same ATP concentrations already tested were analysed in continuous flow mode, using the same flow rate for both ATP and standard reaction solution (1 ml/min). In this case, the SRS was used also as buffer solution to clean the channels between two following repetitions. Figure 5.14 shows as the signal for low, medium and high ATP concentrations (15.625nM, 125nM, and 500nM, respectively) is stable and reproducible over time. Signals reported in Figure 5.14 were mathematically filtered through adjacent-averaging method, using 15 points for window, in order to eliminate the mechanical noise introduced by automatic pumps.
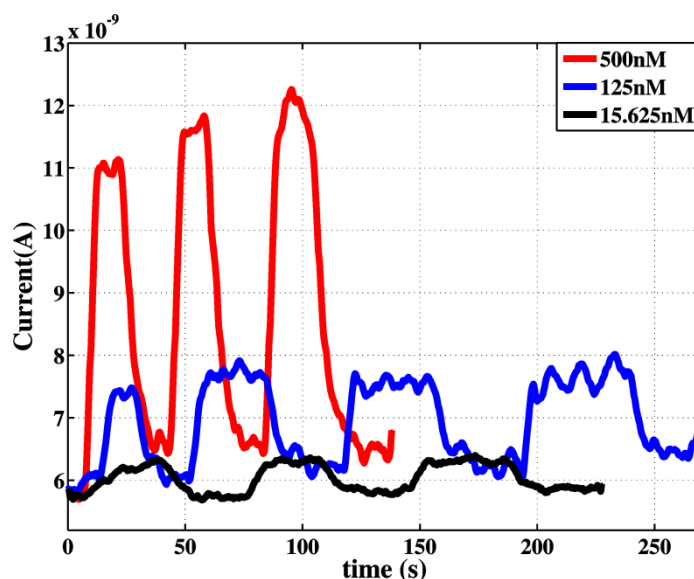
Figure 5.14: Bioluminescence signal acquired during a continuous flow monitoring for two different ATP concentrations: 15.625nM (red line); 125nM (blue line).

Several ATP concentrations were tested in continuous flow mode by simply changing the flow rate ratio of ATP and SRS as reported in TABLE 5.2. The flow rate of SRS was fixed at 19.2 ml/h, while the flow rate of ATP solution with a concentration of 1μM ranged from 0.6 to 19.2 ml/h, in order to obtain a final ATP concentration in the range 15.625 – 500nM (Figure 5.15).

SRS Flow rate (ml/h)	ATP Flow rate (ml/h)	Final ATP concentration (nM)
	0.6	15.625
	1.2	31.25
19.2	2.4	62.5
	4.8	125
	9.6	250
	19.2	500

TABLE 5.2: Flow rates of ATP and SRS used for the continuous flow monitoring of bioluminescence signal.
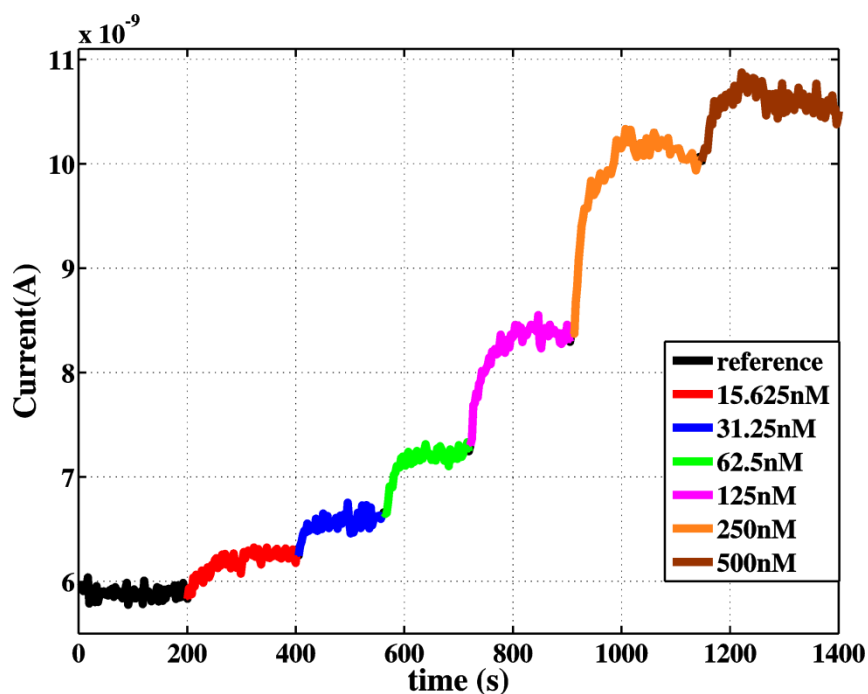
Figure 5.15: Continuous flow monitoring of ATP bioluminescence.

Figure 5.15 shows as the SiPM and 3D printed microfluidic chip coupled system is very sensitive to flow rate changes and, consequently, ATP concentration changes.

Analysing the graph it is possible to observe as increasing the ATP concentration also the bioluminescence current detected increases.

These results open the possibility to fabricate and commercialize SiPM based detection systems for bioluminescence detection. The combination of SiPM with 3D printed microfluidic chips provides a means of creating compact, sensitive and potentially low-cost bioluminescence devices detection with wide-ranging applications in chemical and biological analysis and clinical diagnostics.

5.5 Conclusion

In this chapter, the potentialities of SiPM, developed by R&D Sensor Team STMicroelectronics in Catania, to replace traditional detection system for bioluminescence measurements were demonstrated. It was shown that the optical system based on SiPM technology provides a quantitative output signal. This result simplifies considerably the signal analysis with respect to traditional systems, which provide as output an image and an offline analysis is needed to quantify the results.

The analysis performed on ATP solutions indicate that increasing the ATP concentration, the bioluminescence signal increases and, at high ATP concentration levels (1μM), a different behaviour during measured time can be observed. A fast partial quenching is present in the first phase, but then the signal decreases exponentially. In fact, due to the reaction nature, when the ATP concentration is high, a lot of product is available and it is released immediately in the form of light. Moreover, due to

the large amount of ATP with respect to the other reagent molecules (SRS), the other reagents consumes before all the ATP is reacted, hence a quenching is observed. It is more evident as the concentration increases.

The direct comparison between traditional and innovative systems using glass tubes showed that, thanks to its high sensitivity, SiPM is able to detect very low emitted bioluminescence signals (15.625 nM), as well as the very expensive instrument commonly used. In addition, SiPM based systems allow monitoring the reaction kinetics in real time. In fact, with the PerkinElmer Victor 2030 bioluminescent reader it was not possible to acquire in continuous mode the signal during time, hence only four time points were chosen. This limit was overcome by the innovative system based on SiPM technology we developed, which allows monitoring the bioluminescence current in a continuous mode.

In order to design the best structure for the 3D printed microfluidic chip, that will allow a continuous flow monitoring of bioluminescence signals, PDMS chambers having different sizes, hence containing different volume of solution, were tested. The analysis performed showed that the best operating conditions are: 100μl of sample solution and 6 mm of chamber diameter size.

However, to demonstrate the potentialities of the 3D microfluidic chips the ATP bioluminescence as a function of the reaction time for three different concentrations of ATP: 1uM, 125nM and 15.625nM was recorded in real time.

The direct comparison between the systems proposed and the commercial reader shows all of them exhibit almost the same sensitivity in the analysed range of ATP concentrations. It should be reminded that the proposed system is much cheaper and more compact with respect to the commercial one and allows real time measurements versus time.

Finally, the ability of the system based on 3D printed microfluidic chip to perform continuous flow monitoring of bioluminescence reaction was demonstrated, opening the possibility to fabricate and commercialize SiPM based detection systems for bioluminescence detection. The combination of SiPM with 3D printed microfluidic chips provides a means of creating compact, sensitive and potentially low-cost bioluminescence detection systems with wide-ranging applications in chemical and biological analysis and clinical diagnostics.

Conclusion

The SiPM produced by the R&D of STMicroelectronics in Catania was used to detect low fluorescence and bioluminescence signals, allowing the design and fabrication of easy-to-use optical system for biomedical applications.

Multichip characterization allowed defining the 5x5 pixels with trenches SiPM as the most suitable device for the biosensing applications discussed in this thesis, since it had the lowest DC and cross-talk probability. Pulsed measurements showed as SiPM can be used as photon counter also for biosensing applications.

Two different experimental setups for lifetime measurements, suitable for fast and slow fluorophores, were developed. They were used to study the photochemical properties of CY5 and $Ru(bpy)_3^{2+}$, for optical sensing applications. The analysis showed that this last molecule is a viable alternative to the conventional fluorophore CY5 for target gene labelling in optical DNA-chip application. In fact, $Ru(bpy)_3^{2+}$ reduces the risk of fluorescence self-absorption, thanks to the large distance between the absorption/emission peaks, and allows using a simple electronics for the fluorescence analysis, thanks to the long lifetime.

The measurements showed a cooperative effect of the molecules by increasing their density after drying of sample. This caused the red shift of the absorption peaks at 310 nm and 470 nm and the appearance of a dominant emission peak at 590 nm in dried samples. These samples exhibit an additional faster component in the lifetime of ~100ns, in addition to the 350 ns lifetime value measured in dissolved samples.

Moreover, the ability of SiPM, to replace traditional detection system for DNA microarray applications was demonstrated and some interesting results were carried out. First, the system based on SiPM technology provides a quantitative output signal. This feature simplifies considerably the output signal analysis with respect to traditional systems. In fact, optical readers provide an image as output and an offline analysis is required to quantify the results.

From the analysis performed on five different concentrations of DNA labelled with CY5, GAPDHCy5, emerged that as the sample concentration increases, the emitted fluorescence increases as well. The current signal value at each concentration is roughly constant in the measurement angular range chosen, confirming the isotropic emission of fluorescence and the signal linearity in the range 1 nM - 1 μM.

The direct comparison between traditional optical reader and SiPM showed that, thanks to its high sensitivity, SiPM is able to measure also the small signal difference between two concentration values

very close, that are indistinguishable with a commercial optical reader. Finally, the high SiPM sensitivity allows detecting very low fluorescence signals (1 nM), not visible with the commercial reader used for comparison.

In this work, the potentialities of SiPM to replace traditional detection system for Real Time PCR applications were demonstrated as well. The analysis performed on FAM and CY5, indicate that the system, based on SiPM technology, is able to detect very low fluorophore concentrations (500 fM for FAM and 100 fM for CY5). Moreover, when the sample concentration increases, the emitted fluorescence increases as well. In particular, both fluorophores exhibit a nonlinear increase of the luminescence signal with dye concentration. It occurs because when the dye concentration in the sample increases, the probability of interaction between molecules increases accordingly. It is known that CY5 aggregation causes a decrease of the emitted fluorescence for a fixed concentration, since, probably, non-radiative de-excitation paths form [86; 87]. Therefore, an increase of the concentration will produce an increase in the luminescence signal only as long as no interaction occur. The aggregates do not emit any fluorescence; hence, the florescence characteristics in terms of lifetime and emission spectrum does not change. In our samples, the aggregate presence can be inferred by the non-linearity of the signal as a function of the concentration.

Finally, the potentialities of SiPM to replace traditional detection systems for bioluminescence measurements were demonstrated. The analysis performed on ATP dissolved samples indicate that increasing the ATP concentration, the bioluminescence signal increases and, at high ATP concentration (1μM), a different behaviour during the measuring time is observed. A fast partial quenching is detected in the first seconds, then, the signal decreases exponentially down to a steady state emission. In fact, due to the reaction nature, when the ATP concentration is high, a lot of product is available and it is released immediately in the form of light. Moreover, due to the large amount of ATP with respect to the other reagents, a quenching due to the other reagents consumption occurs. It is more evident as the ATP concentration is increased.

The direct comparison between a PerkinElmer Victor 2030 bioluminescent reader, a traditional system, and the innovative system using glass tubes showed that, thanks to its high sensitivity, SiPM is able to detect very low emitted bioluminescence signals (15.625 nM), as well as very expensive instrument commonly used. Furthermore, it allows monitoring the reaction kinetics in real time and in a continuous mode. In fact, with the PerkinElmer Victor 2030 bioluminescent reader it was not possible to acquire in continuous mode the signal during the reaction time, hence only four time points were selected. This limit was overcome by the innovative system based on SiPM technology, which allows monitoring the bioluminescence current in real time and in a continuous mode.

In order to design the best structure for the 3D printed microfluidic chip, that will allow a continuous flow monitoring of the bioluminescence signals, PDMS chambers having sizes, hence different volume of solution, were tested. The analysis performed showed that the best operating conditions are: 100μl of sample solution and 6 mm of chamber diameter size.

However, to demonstrate the potentialities of the 3D microfluidic chip the ATP bioluminescence as a function of the reaction time for three different concentrations of ATP, 1uM, 125nM and 15.625nM, was recorded in real time.

The direct comparison between three different systems shows as the commercial reader and the optical system with glass tube exhibit almost the same sensitivity in the analysed range of ATP concentrations. It should be reminded that the proposed system is much cheaper and more compact with respect to the commercial one and allows real time measurements versus time.

The evolution of the glass tube system is the system based on 3D printed microfluidic chip. It exhibits almost the same sensitivity of its predecessor when detecting medium and high ATP concentrations, but, at low ATP concentrations, it is more sensitive than the previous one.

Finally, the ability of the system based on 3D printed microfluidic chip to perform continuous flow monitoring of bioluminescent signal was demonstrated, opening the possibility to fabricate and commercialize SiPM based detection systems for bioluminescence detection. The combination of SiPM with 3D printed microfluidic chips provides a means of creating compact, sensitive and potentially low-cost bioluminescence detection systems with wide-ranging applications in chemical and biological analysis and clinical diagnostics.

Appendix A

List of Publications

B.1 Journal papers

M.F. Santangelo, E.L.Sciuto, S. Lombardo, A.C.Busacca, S.Petralia, S. Conoci, S. Libertino, "Si photomultipliers for bio-sensing applications", IEEE Journal of Selected Topics in Quantum Electronics, vol. 22, n. 3, 2016; ISSN: 1077-260X, DOI: 10.1109/JSTQE.2015.2504979.

M.F. Santangelo, E.L.Sciuto, A.C.Busacca, S.Petralia, S. Conoci, S. Libertino, "SiPM as miniaturized optical biosensor in DNA-microarray applications", Sensing and Biosensing research, vol. 6, pp. 95-98, December 2015.

E.L.Sciuto, **M.F. Santangelo**, G. Villaggio, F. Sinatra, C. Bongiorno, G. Nicotra, S. Libertino, "Photo-physical characterization of fluorophore $Ru(bpy)_3^{2+}$ for optical biosensing applications", Sensing and Biosensing research,vol.6, pp. 65-71, December 2015.

G. Nicotra, E.L. Sciuto, **M.F. Santangelo**, G. Villaggio, F. Sinatra, C. Bongiorno, S. Libertino, "Single Atom Detection Through HAADF-STEM and EELS/EDX Characterization of Fluorophore Ru (bpy) $_3^{2+}$ for Optical DNA-Chip Applications", Microscopy and Microanalysis, vol. 21, n. S3, pp. 1429-1430, August 2015 (DOI: http://dx.doi.org/10.1017/S1431927615007928).

S. Libertino, S. Conoci, **M.F. Santangelo**, R. Pagano, E.L. Sciuto, F. Sinatra, D. Sanfilippo, G. Fallica and S. Lombardo. "Optical and Electrical Si-Based Biosensors: Fabrication and Trasduction Issues", J Anal Bioanal Tech, S12: 007, February 2014. (doi: 10.4172/2155-9872.S12-007)

B.2 International conference papers

M.F. Santangelo, S. La Cono, P. Vasquez, G. Fallica, S. Conoci, A.C. Busacca, R. Pagano, E.L. Sciuto, S. Lombardo, S. Libertino, "CY5 fluorescence measured with Silicon photomultipliers", IEEE Biomedical Circuits and Systems Conference (BioCAS), pp. 284-287, 2014 (DOI: 10.1109/BioCAS.2014.6981718)

M.F. Santangelo, R. Pagano, S. Lombardo, E.L. Sciuto, D. Sanfilippo, G. Fallica, F. Sinatra, S. Libertino, "Silicon photomultipliers applications to biosensors", Paper no. 8990-0T, Photonics West 2014 - Silicon Photonics IX, Feb. 5, 2014, San Francisco, USA

B.3   National conference paper

M.F. Santangelo, R. Pagano, S. Lombardo, E.L. Sciuto, A.C. Busacca, D.N. Sanfilippo, P.G. Fallica, F. Sinatra, S. Libertino, "SiPM as novel Optical Biosensor-Transduction and applications", Photonics Technologies, 2014 Fotonica AEIT Italian Conference, pp. 1-4, Naples, 12-14 May 2014. ISBN: 978-8-8872-3718-4

B.4   International conferences

M.F. Santangelo, E. L. Sciuto, S. A. Lombardo, A. C. Busacca, S. Petralia, S. Conoci, S. Libertino (oral), "Bioluminescence detection system based on Silicon Photomultiplier" Micro-Nano-Bio-ICT Convergence conference, Otranto (Italy), 25-29 June 2016.

M.F. Santangelo (poster)**,** E.L.Sciuto, A.C.Busacca, S.Petralia, S.Conoci, S.Libertino, " Silicon photomultipliers application to gene analysis ", Biosensors 2016, Gothenburg (Sweden), 25-27 May 2016.

R. Pagano (poster), E.L. Sciuto, **M.F. Santangelo**, S. Libertino, A. Parisi, G. Adamo, A. Busacca, P.G. Fallica, G. Ferla, C. Giaconia, A. Merla, S. Lombardo, "Continuous Wave fNIRs with Silicon Photomultiplier", 37th Annual International Conference of the IEEE Engineering in Medicine and Biology Society of the IEEE Engineering in Medicine and Biology Society in MiCo, Milano Conference Center, Milano, Italy during August 25-29, 2015.

M.F. Santangelo, E.L. Sciuto, A. Busacca, S. Petralia, S. Conoci, and S. Libertino (oral), "DNA-chip platform based on SiPM technology"*,* Micro-Nano-Bio-ICT Convergence conference, Otranto (Italy), 13-15 July 2015.

M.F. Santangelo (oral), E.L. Sciuto, A. C. Busacca, S. Petralia, S. Conoci, and S. Libertino, "SiPM as miniaturised optical biosensor for DNA microarray applications", Spring Meeting EMRS 2015, European Materials Research Society conference 2015, Lille (Francia), 11-15 May 2015.

E.L.Sciuto (poster), **M.F. Santangelo**, G. Villaggio, F. Sinatra, C. Bongiorno, G. Nicotra, S. Libertino, "Photo-physical characterization of fluorophore $Ru(bpy)_3^{2+}$ for optical biosensing applications", 4th International Conference on Bio-Sensing Technology, May 2015.

M.F. Santangelo (poster), R.Pagano, E.L.Sciuto, A.C.Busacca, S.La Cono, P. Vasquez, P.G.Fallica, S. Conoci, S.Lombardo and S.Libertino, "CY5 Fluorescence measured with Silicon Photomultipliers", Biomedical Circuits and Systems Conference (BioCAS), 2014 IEEE, pp. 284 - 287, Lausanne, Switzerland, 22-24 Oct. 2014.

S. Libertino(invited), **M.F. Santangelo**, S. Conoci, R. Pagano, E.L. Sciuto, F. Sinatra, M. Renis, A. Busacca, D. Sanfilippo, G. Fallica and S. Lombardo "Optical and electrical Si-based biosensors: first results" 5th International Conference and Exhibition on Analytical & Bioanalytical Techniques, Beijing (China) from the 18th to the 20th of August 2014.

M.F. Santangelo (oral), R. Pagano, S. Lombardo, E.L. Sciuto, D.N. Sanfilippo, P.G. Fallica, F. Sinatra and S. Libertino, "Silicon Photomultipliers application to biosensors", Photonics West 2014, San Francisco, California, United States, February 2014.

B.5   National conferences

E.L. Sciuto (oral), S. Petralia, T. Cosentino, M. Favetta, **M.F. Santangelo**, F. Sinatra, P. Fiorenza, C. Bongiorno, S. Conoci, S. Libertino, " Comparison between thermal Silicon Oxide and silicon Nitride surfaces for Biosensing applications", Materials.it 2016, Catania, 12-16 December, 2016.

M.F. Santangelo (poster), E.L.Sciuto, S. Lombardo, A.C.Busacca, S.Petralia, S. Conoci, S. Libertino, " Silicon Photomultipliers for DNA microarray applications", GE 2015, Brescia, June 2016.

M.F. Santangelo (oral), R. Pagano, S. Lombardo, E.L. Sciuto, A.C. Busacca, D.N. Sanfilippo, P.G. Fallica, F. Sinatra, S. Libertino, "Real Time PCR platform based on SiPM technology", 2016 Fotonica Convegno Italiano delle Tecnologie Fotoniche, Rome, 6-8 June 2016.

M.F. Santangelo (oral), E.L. Sciuto, A. Busacca, S. Petralia, S. Conoci, and S. Libertino, "Silicon photomultipliers as transducers for DNA hybridization detection", presentato alla Italian National Conference on Condensed Matter Physics conference (FisMat) 2015, Palermo, 28 Settembre – 2 October 2015;

M.F. Santangelo, E.L. Sciuto, A. Busacca, S. Petralia, S. Conoci, and S. Libertino (oral), "Silicon photomultipliers application to biosensors", 6th EOS Topical Meeting on Optical Microsystems, Capri (Italy), 17-19 September 2015.

M.F. Santangelo (poster), E.L.Sciuto, S. Lombardo, A.C.Busacca, S.Petralia, S. Conoci, S. Libertino, "Real Time PCR platform based on SiPM technology", GE 2015, Siena, June 2015.

M.F. Santangelo (oral), R.Pagano, E.L.Sciuto, A.C.Busacca, F.Sinatra, D.N.Sanfilippo, P.G. Fallica, S.Lombardo and S.Libertino, "SiPM as novel Optical Biosensor", GE 2014, Cagliari, June 2014.

M.F. Santangelo (oral), R. Pagano, S. Lombardo, E.L. Sciuto, A.C. Busacca, D.N. Sanfilippo, P.G. Fallica, F. Sinatra, S. Libertino, "SiPM as novel Optical Biosensor-Transduction and applications", 2014 Fotonica AEIT Italian Conference, Naples, 12-14 May 2014.

Bibliography

[1]   H. Hertz: Ann. Physik, 31, 983 (1887).

[2]   W. Hallwachs: Ann. Physik, 33, 301 (1888).

[3]   J. Elster and H. Geitel: Ann. Physik, 38, 497 (1889).

[4]   A. Einstein: Ann. Physik, 17, 132 (1905).

[5]   V.K. Zworykin, G.A. Morton, and L. Malter: Proc. IRE, 24, 351 (1936).

[6]   Hamamatsu Photonics K.K., 2006.

[7]   B. Dolgoshein et al., Status report on silicon photomultiplier development and its applications. Nuclear Instrum. Methods Phys.Res. A, Accel., Spectrometers, Detectors Assoc. Equip., 563(2):368, 2006.

[8]   J. F. Cox. Fundamentals of linear electronics: integrated and discrete. Cengage Learning, page 91, 2004.

[9]   D. Renker. Geiger-mode avalanche photodiodes, history, properties and problems. Nucl. Instrum. Methods Phys. Res. A, 567(1):48, 2006.

[10]   H. Dautet, P. Deschamps, B. Dion, A. D. MacGregor, D. MacSween, R. J. McIntyre, C. Trottier, and P. P. Webb. Photon counting techniques with silicon avalanche photodiodes. Applied Optics, 35(12):1956, 1996.

[11]   Valeri Saveliev. Silicon photomultiplier - new era of photon detection. Advances in Optical and Photonic Devices, page 352, 2010.

[12]   F. Zappa, S. Tisa, S. Cova, P. Maccagnani, R. Saletti, R. Roncella, F. Baronti, D. Bonaccini Calia, A. Silber, G. Bonanno, and M. Belluso. Photon counting arrays for astrophysics. J. Mod. Opt., 54:163{190, 2007.

[13]   I. Rech, A. Gulinatti, F. Zappa, M. Ghioni, and S. Cova. High-performance silicon single-photon avalanche diode array. In Proc. of SPIE, pages 73200H-173200-H-12, 2009.

[14]   Z. Sadygov, Russian Patent #2102820, priority of 10.10.1996.

[15]   F. Zappa, S. Tisa, A. Tosi, S. Cova, Sensors Actuators A 140 (2007) 103.

[16]   M. Mazzillo, G. Condorelli, D. Sanfilippo, G. Valvo, B. Carbone, G. Fallica, S. Billotta, M. Belluso, G. Bonanno, L. Cosentino, A. Pappalardo, and P. Finocchiaro. Silicon photomultiplier technology at stmicroelectronics. s.l. : IEEE Trans. Nucl. Sci., 56(4):2434, 2009.

[17]   W.G. Oldham et al., "Triggering phenomena in avalanche diodes", IEEE Trans. Electron. Dev. 19 (1972) 1056.

[18]   A. Lacaita, et al., IEEE TED 40 (3) (1993) 577.

[19] J. Briare et al., "Principles of Substrate Crosstalk generation in CMOS circuits", IEEE Trans. Comp. Des. And Sys.,19 (2000) 645-653.

[20] Fan Ji et al. "Evaluation of electrical crosstalk in high-density photodiode arrays for X-rays imagin application", Nucl. Instr. Meth. A, 610 (2009) 28-30.

[21] N. Otte et all., "A test of silicon photomultiplier as a readout for pet", Nucl. Instrum. Meth. A, 545 (2005) 705-715.

[22] M. Mazzillo et al., . Timing performances of large area silicon photomultipliers fabricated at stmicroelectronics. IEEE Trans. Nuclear Sci., 57(4):2273, 2010.

[23] SenseLight., Introduction to the SPM-Technical Note. Available on line url: http://www.sensl.com/downloads/ds/TN%20-%20Intro%20to%20SPM%20Tech.pdf.

[24] thesis., R. Pagano. Operative parameters of Si Photomultipliers. PhD.

[25] M. Mazzillo et al., "Single-photon avalanche photodiodes with integrated quenching resistor", Nucl. Instrum. Meth. A, 591, (2008), 367-373.

[26] S. Libertino, D. Corso, M. Lisiansky, Y. Roizin, F. Palumbo, F. Principato, C. Pace, P. Finocchiaro, and S. Lombardo, "Ionizing radiation effects on Non Volatile Read Only Memory cells", IEEE Trans. Nuclear Science, 59(6), pp. 3016-3020, 2012.

[27] R. Pagano, G. Valvo, D. Sanfilippo, S. Libertino, D. Corso, P.G. Fallica,S. Lombardo, "Silicon Photomultiplier Device Architecture with Dark Current Improved to the Ultimate Physical Limit,"Appl. Phys. Lett., Vol. 102, no. 18, p. 183502, 2013.

[28] M.F. Santangelo, E.L. Sciuto, S.A. Lombardo, A.C. Busacca, S. Petralia, S. Conoci, S. Libertino. Si Photomultipliers for Bio-Sensing Applications. IEEE J. Sel. Top. Quantum Electron.,vol.22,n.3, 2016.

[29] M. F. Santangelo et al., "SiPM as miniaturised optical biosensor for DNA-microarray applications," Sens. Biosens. Res., vol. 6, pp. 95-98, 2015.

[30] http://www.horiba.com/fileadmin/uploads/Scientific/Documents/Fluorescence/F-10.pdf), Application Notes F-10.Which Fluorescence Lifetime System is Best for You? Horiba (url:.

[31] R.A. Lampert, et al., Anal. Chem., 55:68–73, 1983.

[32] J.R. Lakowicz, et al., J. Fluor., 1(2):87–93, 1991.

[33] Waggoner, A.S., Ernst, L.A., Chen, C.H., Rechtenwald, D.J.,"PE-CY5," An. New York Acad. Scie., 677(1), 185–193(1993).

[34] M. F. Santangelo et al., "CY5 fluorescence measured with silicon photomultipliers",in Proc. IEEE Biomed. Circuits Syst. Conf., pp. 284–287, 2014.

[35] 2015, Available: http://www.lumiprobe.com/p/cy5-nhs-ester.

[36] J.N. Demas, B.A. DeGraff, Design and applications of higly luminescent transition metal complexes, Anal. Chem. 63 (1991) 829A–837A.

[37] K. Kalyanasundaram, Photophysics, photochemistry and solar energy conversion with tris(bipyridyl)ruthenium(II) and its analogues, Coord. Chem. Rev. 46 (1982) 159–244.

[38] T. Kajiwara, K. Haslmoto, T. Kawai, T. Sakata, Dynamics of luminescence from Ru(bpy)3Cl2 adsorbed on semiconductor surfaces, J. Phys. Chem. 86 (1982), 4516–4522.

[39] E.L. Sciuto et al., Photo-physical characterization of fluorophore Ru(bpy)3 2+ for optical biosensing applications, Sens. Biosens. Res., vol. 6, pp. 67-71, 2015.

[40] T. Kajiwara, K. Haslmoto, T. Kawai, T. Sakata, Dynamics of luminescence from Ru(bpy)3Cl2 adsorbed on semiconductor surfaces, J. Phys. Chem. 86 (1982) 4516–4522.

[41] V. D. Kovaltchouk, G. J. Lolos, Z. Papandreou, and K. Wolbaum. Comparison of a silicon photomultiplier to a traditional vacuum photomultiplier. Nucl. Instrum. Methods Phys. Res. A, 538(1):408, 2005.

[42] Lakowicz, J. R. , "Principles of Fluorescence Spectroscopy", 3rd Edition, Springer Science+Business Media, New York, 2006.

[43] O'Connor, D.V.O., Phillips, D., "Time-correlated Single Photon Counting", Academic Press, London, 1984.

[44] Nick Bertone, Musadi Wabuyele & Team, Achilles Kapanidis & Team, Henri Dautet, Murray Davies.Single Photon Counting with a focus On Biomedical Applications. 2003 (url:http://www.excelitas.com/downloads/app_spcmpaperforpittcon2003_feb28.pdf).

[45] M. F. Santangelo et al., "SiPM as novel Optical Biosensor: transduction and applications", Photonics Technologies, 2014 Fotonica AEIT Italian Conference,pp. 1-4, May 2014. (ISBN: 978-8-8872-3718-4).

[46] S. Libertino, S. Conoci, M.F. Santangelo, R. Pagano, E.L. Sciuto, F. Sinatra, D. Sanfilippo, G. Fallica, S. Lombardo. "Optical and Electrical Si-Based Biosensors: Fabrication and Trasduction Issues", J Anal Bioanal Tech, S12 (2014), pp. 1-6, February 2014.

[47] G. Heap et al, Complex nature of snp genotype effects on gene expression in primary human leucocytes, BMC Med. Genom. 2 (1) (2009) 1.

[48] M.J. Heller. Annu. Rev. Biomed. Eng., 4:129, 2002.

[49] Heller MJ, Tu E, Holmsen A, Sosnowski RG, O'Connell JP. 1999. Active microelectronic arrays for DNA hybridization analysis. See Ref. 85, 9:167–85.

[50] Schena M, Davis RW. 1999. Genes, genomes, and chips. See Ref. 85, 1:1–15.

[51] 18(5):427–31, Schena M. 1996. Genome analysis with gene expression microarrays. Bioessays.

[52] Schena M. Heller RA, Theriault TP, Konrad K, Lachenmeier E, Davis RW. 1998. Microarrays: biotechnology's discovery platform for functional genomics. Trends Biotechnol. 16(7):301–6.

[53] Schena M, Shalon D, Heller R, Chai A, Brown PO, Davis RW. 1996. Parallel human genome analysis: microarray-based expression monitoring of 1000 genes. Proc. Natl. Acad. Sci. USA 93:10614–19.

[54] Theriault TP, Winder SC, Gamble RC. 1999. Application of ink-jet printing technology to the manufacture of molecular arrays. See Ref. 85, 6:101–19.

[55] Cooley P, et al. 2001. Ink-jet deposited microarrays of DNA and other bioactive molecules. See Ref. 86, 7:117–30.

[56]   Marshall A, Hodgson J. 1998.DNAchips:an array of possibilities. Nat. Biotechnol. 16:27–31.

[57]   Fodor SP, Read JL, Pirrung MC, Stryer L, LuAT, Solas D. 1991. Light-directed, spatially addressable parallel chemical synthesis. Science 251:767–73.

[58]   Pease AC, Solas D, Sullivan EJ, Cronin MT, Holmes CP, Fodor SA. 1994. Lightgenerated oligonucleotide arrays for rapid DNAsequence analysis. Proc. Natl. Acad. Sci. USA 91: 5022–26.

[59]   McGall GH, Fidanza FA. 2001. Photolithographic synthesis of arrays. See Ref. 86, 170:71–101.

[60]   15:100–3, Heller MJ. 1996. An active microelectronics device for multiplex DNA analysis. IEEE Eng. Med. Biol.

[61]   Sosnowski R, Tu E, Butler W, O'Connell J, Heller MJ. 1997. Rapid determination of single base mismatch mutations in DNA hybrids by direct electric field control. Proc. Natl. Acad. Sci. 94:1119–23.

[62]   Y. Huang, D. Hodko, D. Smolko, G. Lidgard. Electronic Microarray Technology and Applications in Genomics and Proteomics. BioMEMS and Biomedical Nanotechnology, pp. 3-21. 2007.

[63]   M.J. Heller, E. Tu, R. Martinsons, R.R. Anderson, C. Gurtner, A.H. Forster, and R. Sosnowski. In M.J. Heller and A. Guttman (ed.), Integrated Microfabricated Biodevices. Marcel Dekker, New York, p. 223, 2002.

[64]   M. Heller, A.H. Forster, and E. Tu. Electrophoresis, 21:157, 2000.

[65]   M.J. Heller, E. Tu. U.S. Patent # 5,605,662 Nanogen, Inc., San Diego, CA, 1997.

[66]   C.F. Edman, D.E. Raymond, D.J. Wu, E. Tu, R.G. Sosnowski, W.F. Butler, M. Nerenberg, and M.J. Heller. Nucleic Acids Res., 25:4907, 1997.

[67]   S. Conoci et al., Fast and Efficient Nucleic Acid Testing by ST's In-CheckTM Lab-on-Chip Platform. NSTI-Nanotech 2006, www.nsti.org, ISBN 0-9767985-7-3 Vol. 2, 2006.

[68]   S. Petralia et al., In-Check system: A highly integrated silicon Lab-on-Chip for sample preparation, PCR amplification and microarray detection of nucleic acids directly from biological samples. Sensors and Actuators B, vol. 187, pp. 99-105. 2013.

[69]   S. Pernagallo et al., Novel Biochip Platform for Nucleic Acid Analysis. Sensors 2012, 12, 8100-8111 e doi:10.3390/s120608100.

[70]   http://www.news-medical.net/news/20110623/Veredus-Labs-develops-e28098Lab-on-Chipe28099-to-detect-and-differentiate-several-food-borne-pathogens-including-Escherichia-coli.aspx, Available on line at URL:.

[71]   N. Sabri, S. A. Aljunid, M. S. Salim, R. B. Ahmad, and R. Kamaruddin, Toward optical sensors: Review and applications. J. Phys., Conf. Series, vol. 423, art. no. 012064, pp. 1–7, 2013.

[72]   http://imagej.nih.gov/ij/.2012., [Online]. Available:.

[73]   K.B. Mullis and F.A. Faloona, Methods Enzymol. 155:355-350, 1987.

[74]   www.eurogentec.com., Eurogentec qPCR guide. Url:

[75] Kubista M., Andrade JM., Bengtsson M., Forootan A., Jonak J., Lind K., Sindelka R., Sjoback R., Sjogreen B., Strombom L., Stahlberg A., Zoric N., "The real-time polymerase chain reaction", Mol Aspects Med. 27(2-3):95-125, 2006.

[76] lifetechnologies.com., Real-time PCR handbook. Url:.

[77] Heid, C.A., J. Stevens, K.J. Livak, and P.M. Williams. Real time quantitative PCR. Genome Res. 6:986-994. 1996.

[78] Tichopad, A., M. Dilger, G. Schwarz, and M.W. Pfaffl. Standardized determination of real-time PCR efficiency from a single reaction set-up. Nucleic Acids Res. 31:e122.2003.

[79] von Ahsen et al., Rapid detection of prothrombotic mutations of prothrombin (G20210A), factor V (G1691A), and methylenetetrahydrofolate reductase (C677T) by real-time fluorescence PCR with the LightCycler.Clin. Chem. 45:694-696.1999.

[80] Bustin, S.A. Absolute quantification of mRNA using real-time reverse transcription polymerase chain reaction assays. J. Mol. Endocrinol. 25:169-193.2000.

[81] http://www.bio-rad.com/it-it/applications-technologies/introduction-qpcr-instrumentation., Introduction to qPCR Instrumentation. Url:.

[82] S. Petralia, M.E. Castagna, M.O. Spata, M.G. Amore, S. Conoci.A Point of Care Real Time PCR Platform Based on Silicon Technology. Biosens J 5: 136. doi:10.4172/2090-4967.1000136. 2016.

[83] Lazzara A, Castagna ME, Giuffrida R, Conoci S. Miniaturised LabonChip for Bio-Chem Analysis. 2015.

[84] M.O. Spata, M.E. Castagna, S. Conoci. Image data analysis in qPCR: A method for smart analysis of DNA amplification. Sens. Bios. Res., vol.6, pp.79-84.2015.

[85] R. Narayanaswamy and O. S.Wolfbeis, Optical Sensors: Industrial Environmental Diagnostic Applications (Springer Series on Chemical Sensors and Biosensors). New York, NY, USA: Springer, 2004.

[86] J. E. Berlier et al., Quantitative comparison of long-wavelength alexa fluor dyes to Cy dyes: Fluorescence of the dyes and their bioconjugates. J. Histochem. Cytochem., vol. 51, no. 12, pp. 1699–1712, 2003.

[87] J. B. Randolph andA. S.Waggoner. Stability, specificity and fluorescence brightness of multiply-labeled fluorescent DNA probes. Nucleic Acids Res., vol. 25, no. 14, pp. 2923–2929, 1997.

[88] Xiong, Yan Q,. "Real-Time in Vivo Bioluminescent Imaging for Evaluating the Efficacy of Antibiotics in a Rat Staphylococcus aureus Endocarditis Model". Antimicrobial Agents and Chemotherapy 49 (1): 380–7. doi:10.1128/AAC.49.1.380-387.2005.

[89] G. Di Rocco et al., "Analysis of biodistribution and engraftment into the liver of genetically modified mesenchymal stromal cells derived from adipose tissue". Cell Transplantation 21 (9): 1997–2008.

[90] Rautlin de la Roy Y. et al. Kinetics of bactericidal activity of antibiotics measured by luciferin-luciferase assay. J Biolumin Chemilumin 6, 193 (1991).

[91] Garewal HS et al., ATP assay: ability to distinguish cytostatic from cytocidal anticancer drug effects. J Natl Cancer Inst 77, 1039 (1986).

[92] X-F Sun et al., Prognostic significance of cytoplasmic p53 oncoprotein in colorectal adenocarcinoma. Lancet, 1992, 340, 1369.

[93] L. Yang, et al., Biological function and prognostic significance of peroxisome proliferator-activated receptor δ in rectal cancer. Clin Cancer Res, 2011, 17, 3760.

[94] G. Gnosa et al., AEG 1 expression is an independent prognostic factor in rectal cancer patients with preoperative radiotherapy–A study in a Swedish clinical trial. Bri J Cancer, (2014), 111, 166–173 (doi: 10.1038/bjc.2014.250).

[95] Available online, url: https://burningscience.wordpress.com/atp-adenosine-triphosphate/.

[96] Campbell, Neil A., Williamson, Brad e Heyden, Robin J. (2006). Biology: Exploring Life. Boston, MA: Pearson Prentice Hall. ISBN 0-13-250882-6.

[97] Souslova V, Cesare P, Ding Y, et al. Warm-coding deficits and aberrant inflammatory pain in mice lacking P2X 3 receptors. Nature. 2000 e 407(6807):1015-1017.

[98] Gourine AV, Llaudet E, Dale N, et al. ATP is a mediator of chemosensory transduction in the central nervous system. Nature. 2005 e 108-111., 436(7047):.

[99] Vlaskovska M, Kasakov L, Rong W, et al. P2X3 knock-out mice reveal a major sensory role for urothelially released ATP. J Neurosci. 2001 e 5670-5677., 21(15):.

[100] Kinnamon SC, Finger TE. A taste for ATP: neurotransmission in taste buds. ATP-gated P2X receptors in health and disease. Front Cell Neurosci. 2013 e 7:264.

[101] Finger TE, Danilova V, Barrows J, et al. ATP signaling is crucial for communication from taste buds to gustatory nerves. Science. 2005 e 310(5753):1495-1499.

[102] 102. 2005., Molecular Probes Product Information. ATP Determination Kit (A22066).

[103] 2008., PerkinElmer 2030. Instrument Manual. 2030-9020-01 March.

[104] Available online, url: http://4ti.co.uk/microplates/black-clear-bottom/96-well.

[105] Comina, G.,Suska,A.,Filippini,D.,2014b.LabChip14,424–430.

[106] G. Comina, A. Suska, D. Filippini,Towards autonomous lab-on-a-chip devices for cell phone biosensing, Biosensors and Bioelectronics 77 (2016), 1153–1167.

[107] Available online, url: http://formlabs.com/3d-printers/form-1-plus/.

[108] Available online, url: http://www.syringepump.com/NE-1000.php#NE-1010.